Investigating Adsorption and Diffusion of Gas Mixtures in Zeolite-like Nanoporous Materials Using Computational Techniques

by

Erhan Atcı

A Thesis Submitted to the
Graduate School of Engineering
in Partial Fulfillment of the Requirements for
the Degree of

Master of Science
in
Chemical and Biological Engineering

Koc University

July 2012

Koc University

Graduate School of Sciences and Engineering

This is to certify that I have examined this copy of a master's thesis by

Erhan Atcı

and have found that it is complete and satisfactory in all respects,
and that any and all revisions required by the final
examining committee have been made.

Committee Members:

_____

Seda Keskin, Ph. D. (Advisor)

_____

Seda Kızılel, Ph. D.

_____

Murat Sözer, Ph. D.

Date: _____

ABSTRACT

A new group of nanoporous materials, zeolite imidazolate frameworks (ZIFs), has been recently discovered. Their properties such as tunable pore sizes, large surface areas, high pore volumes, good thermal and mechanical stabilities made them promising materials for gas separation applications. Although there are hundreds of different ZIFs, performances of ZIFs in membrane-based gas separations were studied only for a few selected ZIFs. In this thesis, atomically detailed calculations were used to predict the performance of thirteen different ZIF materials both in adsorption-based and membrane-based separations of CH_4/H_2, CO_2/CH_4 and CO_2/H_2 mixtures. Adsorption-based selectivity, working capacity, membrane-based selectivity and gas permeability of ZIFs were predicted and compared with available experimental data. Results showed that several ZIFs can outperform traditional zeolite membranes in CH_4/H_2, CO_2/CH_4 and CO_2/H_2 separations. The accuracy of the mixing theories estimating mixture adsorption and diffusion based on single component data was also examined. Finally, performances of ZIF/polymer composite membranes were investigated for H_2/CO_2 mixture. It was observed that selectivity and permeability of polymer membranes can be improved by adding ZIFs as filler particles into polymer matrices.

ÖZET

Yakın geçmişte yeni bir nanogözenekli malzeme grubu olan zeolit imidazolat yapılar (ZIF) sentezlendi. Ayarlanabilir gözenek boyutu, büyük yüzey alanı, yüksek gözenek hacmi, ısıl ve mekanik dayanıklılık gibi özellikler bu malzemelerin gaz ayırma uygulamalarında gelecek vadeden malzemeler olabileceğini göstermektedir. Literatürde rapor edilmiş yüzlerce değişik ZIF çeşidi bulunmasına rağmen, membran bazlı gaz ayırma işlemleri için çalışılmış ZIF sayısı çok sınırlıdır. Bu tez çalışmasında, on üç farklı ZIF malzemesinin CH_4/H_2, CO_2/CH_4 ve CO_2/H_2 karışımlarını adsorpsiyon ve membran bazlı ayırma performansları detaylı atomik hesaplamalar kullanılarak tahmin edilmiştir. Adsorpsiyon seçiciliği, çalışma kapasitesi, membrane seçiçiliği ve gaz geçirgenliği her malzeme için tahmin edilmiştir ve mevcut deneysel data ile karşılaştırılmıştır. Sonuçlar birkaç ZIF malzemesinin CH_4/H_2, CO_2/CH_4 ve CO_2/H_2 gaz ayırımlarında zeolitlerden daha iyi olduğunu göstermiştir. Tek gaz sistemi datası kullanarak ikili gaz sistemlerinin adsorpsiyon ve difüzyonunu tahmin edebilen karışım teorilerinin doğruluğu incelenmiştir. Son olarak, ZIF/polimer membranların H_2/CO_2 karışımlarındaki performansı araştırılmıştır. ZIFlerin polimerler içine dolgu parçacıkları olarak kullanılmasının polimer membranların seçiciliğini ve geçirgenliğini arttırdığı gözlemlenmiştir.

ACKNOWLEDGEMENTS

I would like to express my sincere gratitude to my advisor, Assist.Prof.Dr. Seda Keskin for her supervision, support, encouragement, advice and comments in all steps of this thesis. I am also indebted to her due to providing me opportunitiy to do a PhD at Georgia Tech.

I would like to thank gratefully my committee members Assist. Prof. Dr. Seda Kızılel and Assoc. Prof. Dr. E. Murat Sözer for serving in my thesis committee.

My warmest thanks go to my mum Ayten Atcı, my dad Selçuk Atcı and my sister Özge Atcı for their endless support, patience, helps and encouragement during my whole life.

I express my special thanks to my friends Ilknur Erucar, Caner Nazli, Ibrahim Hocaoglu and Hasan Sildir for their help, friendship and support during my MS study.

I gratefully acknowledge the financial support provided by TUBITAK BIDEB 2228 scholarship program during my master of science.

In addition, I acknowledge Koc University for the opportunity to be able to complete this study.

TABLE OF CONTENTS

LIST OF TABLES

LIST OF FIGURES

NOMENCLATURE

σ_{ij}	collision diameter for i and j pairwise
ε_{ij}	well depth of the interaction between i and j atoms
ε_o	the dielectric constant
$Đ_i$	single component corrected diffusivity
$Đ_{ii}^{corr}$,$Đ_{ij}^{corr}$	self-exchange and binary-exchange diffusivities
$\Theta_{i,sat}$	the saturation loading of species i
Δq	delta loading
ϕ	fractional pore volume
∇c	the concentration gradient
Δp	pressure drop
ϕ	the volume fraction of ZIF particles
λ_{dm}	the permeability ratio (P_d/P_m)
a_i, b_i, c_i, d_i	fitting parameters of species i
c_i	the concentration of species i at the upstream face of the membrane
C_i	the adsorbed amount
$D_{i,\,self}$	self diffusivity of species i
$D_{i,o}$	corrected diffusivity of species i
D_t	transport diffusivity
$E_{coulomb}$	coulombic interaction
E_{vdW}	van der Waals energy
f_i	the bulk phase fugacity of the species i
J_i, J_j	single component fluxes of i and j species
L	membrane thickness

N	the number of molecules
P	fugacity
P	the permeability in polymer/ZIF composite membrane
P_i	the permeability of the species i
P_d	the permeability of dispersed phase (ZIF)
P_m	the permeability of continuous phase (polymers)
P_r	relative permeability
$q_{i,}\ q_j$	partial point charges of i and j
$r_{il}(t)$	the three dimensional position vector of molecule l of species i at time t
r_{ij}	distance between particles
$S_{adsorption}$	adsorption selectivity
S_{diff}	diffusion selectivity
S_{ideal}	ideal selectivity
$S_{permeation}$	permeation selectivity
$x_i,\ x_j$	the molar fraction of adsorbed phase i and j
$y_i,\ y_j$	molar fraction of the bulk phase i and j

Chapter 1

INTRODUCTION

Selective and economical gas separation is an important process in industry. A large part of gas separation includes purification of noncondensable gases such as nitrogen from air (air purification); nitrogen and carbon dioxide from methane (natural gas purification); and hydrogen from carbon dioxide, nitrogen or methane (hydrogen recovery) [1]. The most common methods for separation of these mixtures are amine absorption and cryogenic distillation. For example, separation of carbon dioxide and nitrogen from natural gas is performed using amine absorption or cryogenic distillation, respectively [2]. Amine absorption process includes two stages: the first stage is absorber where CO_2 reacts with the solvent at 40-60°C, and second stage is stripper where CO_2-rich solvent was cleaned out with steam at 100-140°C [3]. In cryogenic distillation process, gaseous mixture of nitrogen and methane is compressed and cooled below the boiling point of methane and above the boiling point of nitrogen (-123°C to -130°C). Thereafter, methane and nitrogen mixture with a distillative aid (ethane, propane, isobutane, etc.) is sent to a cryogenic distillation column. Mixture of liquid methane and distillative aid is withdrawn from the bottom and sent to regenerator which heats and separates liquid methane and distillative aid by methane evaporation at -150°C [4]. Since both methods require high energy for regeneration of solvent and operation of cryogenic distillation column, they are not economical. Usage of highly corrosive solvents such as monoethanolamine (MEA), diethanolamine (DEA), methyldiethanolamine (MDEA) in amine absorption [3] is another

disadvantage. Unlike these traditional gas separation methods, adsorption-based and membrane-based gas separations offer great potential due to significant reductions in energy consumption and absence of corrosive organic solvents.

Adsorption-based gas separations can be classified as pressure swing adsorption (PSA), vacuum swing adsorption (VSA) and temperature swing adsorption (TSA). Advantages of adsorption-based process such as physical adsorption by adsorbent and operation at ambient temperature reduce high energy requirement compared to traditional methods [5]. In a PSA process, adsorption pressure is at high pressure, whereas desorption pressure is at ambient. In a VSA process, adsorption is performed at ambient pressure, whereas desorption is at vacuum [6]. Finally, a TSA process requires ambient temperature for adsorption and higher temperature for desorption [7]. Adsorption and desorption pressures and temperatures may change depending on the type of adsorbates and adsorbents due to difference in the affinity of adsorbents for specific gas molecules. PSA, VSA (TSA) units are set to certain pressure and temperature where adsorbent achieves high working capacity, the difference in the adsorption amounts at adsorption and desorption pressure (temperature). In addition to high working capacity, high gas selectivity is desired for effective adsorption-based gas separations.

One of the advantages of membrane-based separation over adsorption-based separation is continuous separation of gas mixtures. Generally, permeate side of membranes is at ambient pressure, whereas feed side pressure is relatively higher than the ambient pressure. Membranes can be classified into three groups: polymeric membranes, inorganic membranes and composite membranes (combination of polymeric and inorganic membranes). Polymeric membranes have been commercially used from the beginning of the industrial membrane applications [1]. Currently, several polymeric membranes are commercially used in industrial applications. High gas selectivity and permeability is desired in membrane-based separations. However, there is a trade-off between gas

selectivity and permeability in polymeric membranes [8]. Inorganic membranes are metals (platinum etc.), ceramics and zeolites. They can operate at high temperatures and wide pH ranges compared to polymeric membranes. For example, porous glass, one of the materials used in inorganic membrane fabrication, can operate at 700°C and 1-9 pH range, whereas polyimide (a polymeric membrane material) can operate at 40°C and 2-8 pH range [9]. Inorganic membranes made up of nanoporous zeolites are also able to avoid trade-off between selectivity and permeability [10]. Zeolite membranes have emerged as an alternative to polymeric membranes and have been efficiently used in gas separation applications [11]. Zeolite imidazolate frameworks (ZIFs) are a new subclass of nanoporous materials resembling zeolites with tetrahedral networks and transition metals linked by imidazolate ligands [12, 13]. ZIFs are considered as promising materials for adsorption-based and membrane-based gas separation applications due to their properties such as tunable pore sizes, large surface areas, high pore volumes, good thermal and mechanical stabilities. However, potential of ZIFs as adsorbents and membranes was not investigated in detail in the literature.

In this thesis, atomically detailed models were used to assess adsorption-based and membrane-based gas separation (CH_4/H_2, CO_2/CH_4, CO_2/H_2) performances of ZIF materials. Atomically detailed models were used to predict adsorption selectivity, working capacity, permeation selectivity, and permeability of ZIF-1, ZIF-2, ZIF-3, ZIF-4, ZIF-6, ZIF-8, ZIF-10, ZIF-60, ZIF-65, ZIF-67, ZIF-69, ZIF-79, ZIF-81 and ZIF-90 materials. Chapter 2 provides background and literature survey on ZIFs and reviews studies on adsorption-based separations and membrane-based separations done with ZIFs. Chapter 3 describes calculation details, Grand Canonical Monte Carlo (GCMC) and Equilibrium Molecular Dynamics (EMD) simulations, prediction of adsorption selectivity, permeation selectivity, ideal selectivity and permeability. Chapter 4 compares the predictions of simulations with the available experimental data to validate accuracy of simulations for

membrane applications, evaluates adsorption-based and membrane-based separation performances of ZIFs, compares the performances of ZIFs with traditional materials for gas separation applications and examines mixing theory estimations for ZIF-2 material and gives discussion of findings and future studies. Chapter 5 compares the predictions of simulations and models with the available experimental data to validate the accuracy of calculations for composite membrane applications of ZIF-90 membrane, evaluates selectivities, permeability and composite membrane performances of ZIF-90 and ZIF-65 membranes.

Chapter 2

LITERATURE REVIEW

2.1 Overview

Since the discovery of natural zeolite, porous compounds have been widely studied to be used for drying and separation of gases and liquids, softening of hard water, treatment of sewage, melioration of soils, and catalysis [14]. Porous materials can be classified in terms of pore size, pore shape, material and production method. Classification based on pore size (aperture) is useful for applications of porous materials. There are three groups of porous compounds classified according to the pore sizes: microporous (pore diameter < 2 nm), mesoporous (pore diameter of 2-50 nm), and macroporous (pore diameter > 50 nm) [15]. Examples of microporous/meso/macroporous materials are zeolites and ZIFs/, M41S, MCM-41 and SBA-15/,some types of titanium, silicon and zirconium oxides, respectively [14, 15]. Materials for specific applications can be selected in terms of pore characteristics. For example, mesoporous M41S material series were synthesized by Mobil [16] as a substitute of microporous ZSM-5 zeolite which have diffusion limitations in catalytic applications. On the other hand, microporous materials such as zeolites and ZIFs can be utilized for selective gas separation applications due to their microporous nature. Newly synthesized ZIFs are considered as a subclass of nanoporous materials. ZIFs have attracted significant attention due to their adjustable and open framework structures. ZIFs are composed of tetrahedral networks that resemble those of zeolites with transition metals

connected by imidazolate ligands [12, 13]. Zeolites are known with the $Al(Si)O_2$ unit formula whereas ZIFs are recognized by $M(Im)_2$ where M is the transition metal (zinc, cobalt, copper, iron etc.) and Im is the imidazolate type linker. Figure 2.1 shows the basic structure of zeolites and ZIFs.

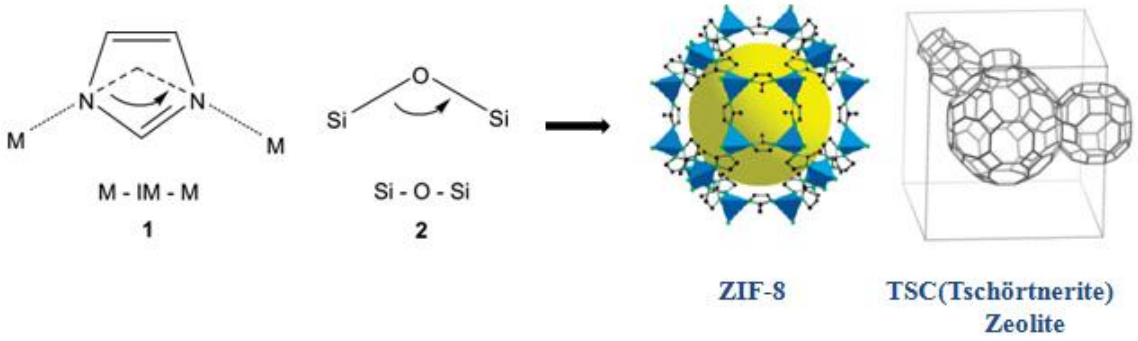

Figure 2.1: Schematic representations of zeolite and ZIF structures [12, 17, 18]

Advantageous properties of ZIFs such as wide range of pore sizes, large surface areas, porosities can be modified by switching metal center and type of organic linker. For example, adaptation in the organic linkers of ZIFs can increase the framework's affinity to the gas molecules. Liu et al. [19], Liu&Smit [20] and Hou et al. [21] showed that ZIF-69 which has chlorine atoms in cbIM linkers instead of hydrogen as in ZIF-68 performed selective CO_2 separation in CO_2/CH_4 and CO_2/N_2 mixtures due to strong electrostatic interaction between chlorine atom and CO_2 molecules. Several experimental studies showed that ZIF materials have remarkable chemical resistance (to boiling alkaline water and organic solvents) and thermal stability (up to 550°C) compared to zeolites. These features make ZIFs promising for various applications [12, 22]. Recently, a large number of ZIFs were synthesized in powder form [12, 13, 22-26]. However, experiments and

simulation studies investigated performances of a few selected ZIFs in adsorption-based and membrane-based gas separation applications.

2.2. Adsorption-based Separation of Gas Mixtures

Although a large number of ZIFs was synthesized, adsorption-based separation performances of a few selected ZIFs were experimentally investigated. Banerjee et al. [22] synthesized a large group of ZIFs (ZIF-2 to ZIF-77) and investigated adsorption of CO_2/CO mixture in ZIF-68, ZIF-69 and ZIF-70. All three ZIFs were found to have high affinity for CO_2 molecules. Gas separation selectivity of ZIF-68, ZIF-69 and ZIF-70 in CO_2/CO mixtures was measured as 19.2, 20.9 and 37.8 at room temperature, respectively, which outperform selectivity of widely used industrial BPL carbon (7.5). In a later study, Banerjee et al. [23] synthesized ZIF-68, ZIF-69, ZIF-70, ZIF-78, ZIF-79, ZIF-80, ZIF-81, ZIF-82 and investigated CO_2/CH_4, CO_2/N_2 and CO_2/O_2 separations in these materials. ZIF-78 exhibited the highest selectivity for all three mixtures compared to ZIF-68, ZIF-69, ZIF-70, ZIF-79, ZIF-81, ZIF-82 and BPL carbon. All ZIFs exhibited higher selectivity than BPL carbon for CO_2/CH_4, CO_2/N_2 and CO_2/O_2 mixtures except CO_2/O_2 and CO_2/N_2 mixtures in ZIF-70 and CO_2/O_2 mixture in ZIF-69. Both experimental studies of Banerjee et al. [22, 23] showed that ZIFs are promising candidates for various gas separation applications.

Molecular simulations have been recently used to assess the performance of ZIFs in adsorption based separation applications. Guo et al. [27] reported adsorption selectivity of ZIF-3, ZIF-8, ZIF-10, ZIF-60 and ZIF-67 for CH_4/H_2 mixtures. ZIF-3 exhibited the highest CH_4/H_2 selectivity at three different gas compositions (CH_4/H_2:0.05/0.95, 0.5/0.5, 0.95/0.05) and 300 K. Liu and Smit [20] studied adsorption selectivity of ZIF-68 and ZIF-69 for CO_2/N_2, CO_2/CH_4 and CH_4/N_2 mixtures and showed that adsorption selectivities of

ZIF-68 and ZIF-69 are comparable to well known zeolites such as MFI, DDR and FAU. Furthermore, ZIF-69 exhibited higher CO_2 selectivity for mixtures involving CO_2 (CO_2/N_2 and CO_2/CH_4) because chlorine functional groups existing in ZIF-69 increase CO_2 adsorption amount due to strong electrostatic interactions between Cl functional groups and CO_2. However, ZIF-68 outperformed ZIF-69 for CH_4 selectivity in CH_4/N_2 separation. This was attributed to chlorine functional groups in ZIF-69 which shows higher affinity to N_2 molecules in CH_4/N_2 mixture and yields smaller adsorption selectivity for CH_4.

Li and co-workers [28] calculated CO_2 adsorption selectivity of ZIF-78 and ZIF-79 for CO_2/CH_4 and CO_2/N_2 mixtures. The presence of nbIM linkers and oxygen atoms in ZIF-78 instead of MebIM linkers and hydrogen atoms as in ZIF-79 increases affinity of ZIF-78 to CO_2 molecules. Therefore, ZIF-78 exhibited higher CO_2 selectivity in CO_2/CH_4 and CO_2/N_2 mixtures compared to ZIF-79.

Wu et al. [29] recently studied ZIF-1, ZIF-2, ZIF-3, ZIF-6, ZIF-8, ZIF-10, ZIF-11, ZIF-60, ZIF-67, ZIF-68, ZIF-69, ZIF-70, ZIF-71, ZIF-78, ZIF-79, ZIF-80 and ZIF-81 for adsorption-based separation of CH_4/H_2 mixtures. Among ZIFs studied in this work, ZIF-1 showed the highest CH_4 adsorption selectivity (76.2) at 1 bar and 298 K. Wu et al. [29] also calculated zero pressure limiting selectivity of CH_4 (working capacity) for ZIF-11 and ZIF-67 as 38.09 (0.572 mol/L) and 14.5 (0.508 mol/L) and then compared these values with traditional materials. For example, limiting selectivities (working capacities) of 5A zeolite, silica gel and activated alumina for CH_4 are 37.9 (0.580 mol/L), 14.3 (0.200 mol/L) and 13 (0.120 mol/L), which showed that performance of ZIFs is comparable to zeolites and better than activated alumina and silica gel for adsorption-based separations. Krishna and van Baten [10] calculated adsorption selectivity and working capacity of CO_2 in CO_2/CH_4, CO_2 in CO_2/N_2, CO_2 in CO_2/H_2 and CH_4 in CH_4/H_2 mixtures in traditional zeolites, ZIF-8 and selected nanoporous materials. For calculation of working capacity, adsorption and desorption pressure was set to 10 bar and 1 bar, respectively. The results showed that ZIF-8

has higher adsorption selectivity and working capacity than traditional zeolites such as ITQ-29, TSC, BEA, ISV, FAU and LTA.

2.3. Membrane-based Separation of Gas Mixtures

Several experimental and molecular simulation studies focused on adsorption-based separations. There is very little known about the membrane-based performances of ZIFs. Huang et al. [30] fabricated ZIF-22 membrane, measured mixture gas permeances of H_2/CO_2, H_2/O_2, H_2/CH_4, H_2/N_2 and calculated mixture separation factor. ZIF-22 was found to be a H_2 selective membrane due to its pore size. Mixed gas separation factors of ZIF-22 for equimolar H_2/CO_2, H_2/O_2, H_2/CH_4 and H_2/N_2 mixtures were computed as 7.2, 6.4, 6.4 and 5.2 at 1 bar and 323 K, respectively. ZIF-22 membrane has higher mixed gas separation factor compared to some nanoporous materials. For example, gas selectivity of NaA membrane for H_2/CO_2, H_2/O_2, H_2/N_2 and H_2/CH_4 mixtures is 5.3, 4.4, 4.2 and 3.6, respectively. Thermal stability of ZIF-22 membrane was also tested increasing the temperature from 323 to 423 K. Huang et al. [30] observed that with increased temperature H_2 permeance increased, whereas selectivity decreased from 7.2 to 6.5. Thermal stability of ZIF-22 membrane was tested during one week at 323 K and its separation performance was unchanged.

In a later study, Huang et al. [31] fabricated ZIF-90 membrane using novel covalent functionalization method and measured mixture gas permeances for H_2/CO_2, H_2/N_2, H_2/CH_4 and H_2/C_2H_4. Similar to ZIF-22, ZIF-90 acts as a H_2 selective membrane and mixed gas separation factors of H_2 were calculated for equimolar H_2/CO_2, H_2/N_2, H_2/CH_4 and H_2/C_2H_4 mixtures as 7.3, 11.7, 15.3 and 62.8, respectively at 200°C and 1 bar. Highly H_2 selective ZIF-90 membrane was fabricated and a support surface with a continuous layer was obtained. While temperature was increased from 25 to 225°C, mixed gas

separation factor increased from 7 to 16. On the other hand, hydrothermal stability test with 3 mol % steam was carried out at 200°C and 1 bar. Both H_2 permeance and H_2/CH_4 selectivity was not changed during 24 hours, which is the indication of very good hydrothermal stability. In the other study of Huang et al. [32], ZIF-90 membrane was fabricated with covalent post-functionalization method by ethanol-amine to improve hydrogen selectivity. It is known that polycrystalline and intercrystalline defects spoil membrane selectivity. Post-functionalization method eliminates invisible incrystalline defects of the ZIF-90 layer, which increases molecular sieving performance of membrane. In this method, ZIF-90 membrane was synthesized with the same method of their previous study and it was treated in a solution of methanol and ethanolamine and refluxed for 10 h and at 60°C. Hydrogen selectivity of ZIF-90 membrane with post-functionalization [32] (w/o post-functionalization [31]) for equimolar H_2/CO_2, H_2/N_2 and H_2/CH_4 was calculated as 15.3 (7.3), 15.8 (11.7) and 18.9 (15.3) at 200°C and 1 bar. Comparison with the results of the previous study showed that post-functionalization of ZIF-90 membrane increases H_2 selectivity. Significant increase in H_2 selectivity for H_2/CO_2 mixture (62.5) was observed for longer post-functionalization (24 h at 60^oC) of the ZIF-90 membrane. Similar to previous study, ZIF-90 membrane with covalent post-functionalization was tested in H_2/CO_2 mixture for hydrothermal stability (in 3 vol % steam at 200°C for 48 h) and thermal stability (325°C for 24 h). Test results showed high thermal and hydrothermal stability of the ZIF-90 membrane.

Liu et al. [33] prepared first ZIF-69 membrane on porous α-alumina support using *in situ* solvothermal synthesis procedure. Permeances of CO_2/CO mixture were measured and permeation selectivity of CO_2 was calculated as 3.5 at room temperature and ambient pressure. In addition to good thermal stability, chemical stability in boiling methanol, boiling benzene and supercritical CO_2 was observed. However, it was reported that stability in boiling water should be improved. In a later study, Liu et al. [34] measured permeances

of CO_2/N_2, CO_2/CH_4 and CO_2/CO mixtures through ZIF-69 membranes. It was found that ZIF-69 was found to be a CO_2 selective membrane and mixed gas separation factors for equimolar mixtures of CO_2/N_2, CO_2/CH_4 and CO_2/CO were calculated as 6.3, 5.0 and 4.6, respectively at 298 K and 1 atm.

Li and co-workers [35] studied permeances of H_2/CO_2, H_2/N_2 and H_2/CH_4 mixtures through ZIF-7 membrane. Mixed gas separation factors for equimolar H_2/CO_2, H_2/N_2 and H_2/CH_4 mixtures were measured as 6.48, 7.74 and 5.92, respectively at 200°C and 1 bar. Furthermore, ZIF-7 membrane avoided the trade-off between selectivity and permeability and it was located above the Robeson upper bound [36]. In a later study, Li et al. [37] measured permeances of H_2/CO_2, H_2/N_2 and H_2/CH_4 mixtures through ZIF-7 membrane with minor changes in experimental methods. Higher mixed gas separation factors were achieved for equimolar H_2/CO_2 (13.6), H_2/N_2 (18.0) and H_2/CH_4 (14.0) mixtures at 220°C and 1 bar compared to the previous study. Both studies showed that ZIF-7 has good thermal and hydrothermal stability.

Several research groups fabricated ZIF-8 membranes and studied H_2/CH_4 [38], CO_2/CH_4 [39, 40], C_2H_6/C_2H_4 [41] permeances. Bux et al. [38] fabricated ZIF-8 by microwave-assisted solvothermal synthesis and measured permeance and mixed gas separation factor for equimolar H_2/CH_4 mixture (11.2) through ZIF-8 membrane at 298 K and 1 bar. Venna et al. [39] fabricated ZIF-8 membranes with four different thicknesses (5-9 μm) on α-Al_2O_3 porous support. Gas permeances and mixture gas separation factors (CO_2/CH_4: 4.1-7) for equimolar CO_2/CH_4 mixtures were measured at 295 K and 1.4 bar. In the other study for ZIF-8, Bux et al. [40] measured permeation selectivity and permeance of CO_2/CH_4 mixture through ZIF-8 membrane both experiments and combined Grand Canonical Monte Carlo(GCMC)–Infrared Microscopy(IRM) approach. Permeation selectivity from experimental measurements for equimolar CO_2/CH_4 mixture was calculated as 3.4, 2.0 and 1.7 at 298, 373 and 423 K, respectively. Good agreement

between experimental measurements and GCMC-IRM predictions for gas permeance was also validated. Chmelik et al. [41] measured gas permeance and gas mixture separation factor of C_2H_4/C_2H_6 mixtures (~2.6 at 298 K and 1 bar) through ZIF-8 membrane with different feed side pressures.

ZIFs have attracted significant attention as filler particles in polymers to make composite membranes. Several experimental studies investigated performance of ZIF/polymer composite membranes. Similar to pure ZIF membranes, number of studies on ZIF/polymer composite membranes is limited. Liu and co-workers [42] incorporated ZIF-8 nanoparticles into a polymer matrix to provide preferential pathways for the separation of organic compounds. Yang et al. [43] synthesized ZIF-7/polybenzimidazole (PBI) composite membranes which showed enhanced H_2 permeability and H_2/CO_2 permeation selectivity, surpassing those of PBI membranes. Zhang et al. [44] fabricated ZIF-8/6FDA-DAM polyimide membranes and showed that both propylene selectivity and permeability increase as the amount of ZIF-8 increases in the polymer matrix.

Considering the large number of available ZIFs, experimental fabrication and testing of new ZIF membranes is very time consuming and the number of studies on ZIF membranes limited to these five ZIFs (ZIF-7, ZIF-8, ZIF-22, ZIF-69 and ZIF-90) since fabrication and testing of thin films of non-polymeric membranes are very challenging and requires significant effort. An alternative approach is to use molecular simulations to screen large number of materials and narrow down the number of candidates to a handful of promising materials that can be subjected to more detailed experimental investigations [45-47].

Molecular simulation studies on predicting membrane-based separation performances are limited compared to the studies on predicting adsorption-based separation performances. Keskin [48] reported permeation selectivity of ZIF-3 and ZIF-10 membranes for CH_4/H_2, CO_2/CH_4 and CO_2/H_2 mixtures at 10 bar feed side pressure and 298 K and compared them with well known zeolites. Gas selectivity and permeability of ZIF-3 and

ZIF-10 for CH_4/H_2, CO_2/CH_4 and CO_2/H_2 mixtures are comparable to traditional zeolites such as MFI, CHA, DDR and LTA. Liu et al. [49] studied permeation-based separation of CH_4/H_2 and CO_2/CH_4 mixtures in ZIF-68 and ZIF-70 membranes. Membrane selectivity of ZIF-68 and ZIF-70 for CH_4/H_2 mixtures was calculated as 3 and 1, respectively at 10 bar and 298 K. On the other hand, membrane selectivity for CO_2/CH_4 mixture in ZIF-68 and ZIF-70 was calculated as 4.5 and 2.5, respectively at 10 bar and 298 K.

Krishna and Van Baten [10] studied ZIF-8 membrane for separation of CO_2/H_2 and CH_4/H_2 mixtures. ZIF-8 membrane was found to be a H_2 selective membrane for CO_2/H_2 and CH_4/H_2 separations. For CH_4/H_2 mixture, ZIF-8 exhibited similar gas permeability compared to LTA-Si, ITQ-29 and CHA, whereas permeation selectivity is slightly greater than those of zeolite membranes. Battisti et al. [50] predicted permeation selectivities of ZIF-2, ZIF-4 and ZIF-8 for CO_2/H_2, CH_4/H_2, CO_2/CH_4, CO_2/N_2 and CH_4/N_2 mixtures at zero-pressure limit. ZIF-4 showed significant performance for CO_2/N_2 separation with a separation factor of 10.4. Besides CO_2/N_2 mixture, ZIF-4 has the highest separation factor for CO_2/H_2 (3.2), CO_2/CH_4 (3.82) and CH_4/N_2 (2.71) separations. For CH_4/H_2 mixture, ZIF-2 has the highest gas separation factor of 1.42 compared to ZIF-4 (0.84) and ZIF-8 (0.30).

Atci and Keskin [51] described molecular simulation methods to model pure ZIF-90 and ZIF-65 membranes in addition to the composite membranes composed of various polymers, ZIF-90 and ZIF-65. Similar to ZIF-8, ZIF-90 and ZIF-65 were found to be H_2 selective membranes. It was found that addition of ZIF-90 into liquid crystalline polyester, polyaniline (redoped) and polyimide (1.1 GFDA-DMA) to fabricate composite membranes enhances H_2 permeability of both ZIF-90 and ZIF-65 membrane. Addition of ZIF-90 into poly (trimethylsilylpropyne) polymer enhances both H_2 selectivity and permeability. As can be seen from this literature review, most of the molecular simulations have focused on a few specific ZIFs and information about the potential of several ZIFs as adsorbents and

membranes is lacking. The aim of this thesis is to evaluate adsorption-based and membrane-based separation performances of ZIFs as adsorbents and membranes by considering adsorption selectivity, working capacity, permeation selectivity and permeability.

Chapter 3

COMPUTATIONAL DETAILS

3.1 Modeling of ZIFs and Adsorbates

Thirteen different ZIFs, ZIF-1, ZIF-2, ZIF-3, ZIF-6, ZIF-8, ZIF-10, ZIF-60, ZIF-65, ZIF-67, ZIF-69, ZIF-79, ZIF-81 and ZIF-90 were studied in this thesis. Experimental X-ray diffraction (XRD) data of Morris et al. [25] and Banerjee et al. [22] were used to assign atomic positions of ZIFs, and solvent-free, rigid structures were used in all molecular simulations. The structural properties of ZIFs are tabulated in Table 3.1. Data for ZIF-68 and ZIF-70 which was not studied in this thesis were taken from the study of Liu et al. [49] for comparison. Unit cell representations of ZIFs are given in Appendix-A. Universal force field (UFF) [52] was used to perform all molecular simulations. Well known force fields such as MM2 [53], MMP2 [54], MM3 [55] are well defined models for the prediction of organic structures and energies. Experimental accuracy is usually obtained using these force fields in molecular simulation of organic molecules, whereas these standard force fields define limited number of atoms and unable to describe the dynamics of inorganic materials such as zeolites. Therefore, Rappe et al. [52] described a full periodic table force field based on hybridization dependent atomic bond radii, hybridization angles, van der Waals parameters, torsional and inversion barriers and a set of effective nuclear charges. Simulation inputs in this thesis such as atomic radius and energy parameters were taken from reported bond radii and nonbond energy values of Rappe et al. [52]. UFF fully defines

the interatomic potentials needed for all ZIF atoms and several previous molecular simulation studies have used UFF for ZIFs [19, 27, 48, 56-59]. Liu et al. [19] showed that simulated CO_2 adsorption isotherms employing UFF force field agreed well with the experimental results of ZIF-68 and ZIF-69 [19, 22]. Guo et al. [27] reported that CH_4 and H_2 adsorption amount computed using UFF agreed well with the experimental results of ZIF-8 [60]. Atci and Keskin [51] showed that predictions of molecular simulations employing UFF were consistent with experimental measurements of gas permeances for single component gases (CH_4, CO_2, H_2 and N_2) and binary gas mixtures (H_2/CO_2, H_2/N_2, H_2/CH_4) in ZIF-90. Several research groups refined force field parameters or used DREDING force field in their simulations to reproduce experimental results [20, 50, 61]. Mayo et al. [62] reported DREIDING force field for the estimation of structures and dynamics of organic, biological and main-group inorganic molecules. In contrast to UFF, DREIDING force field parameters were computed with general force constants and geometry parameters depending on simple hybridization considerations. Parameters for some atoms were not defined in DREIDING force field. For example, force field parameters of cobalt which is the metal of ZIF-65 were not included in DREIDING [62].

In order to examine the effect of using different force fields on the simulation results, DREIDING force field was used for selected ZIFs in this thesis. ZIF crystal structures were the only experimental input of the molecular simulations and no parameter refinement was done. Refining force field parameters to match the results of molecular simulations with the experimentally measured gas adsorption isotherms is not a well developed strategy because the accuracy of the experiments can be significantly affected by the defects of as-synthesized ZIFs or trapped residual solvent molecules present in the samples. For example, Venna et al. [39] and Perez-Pellitero[61] reported different gas adsorption isotherms for ZIF-8.

Spherical Lennard-Jones (LJ) 12-6 potentials were used to model H_2 and CH_4 molecules [63, 64]. This approximation increases the computational efficiency and provides single center of interaction. In the united atom approximation both H_2 and CH_4 molecules can be represented as single spheres. For example, H atoms connected to C atom in CH_4 are not considered explicitly in the calculations. Contribution of H atoms to the CH_4 molecule is modeled expanding van der Waals radius of C atom as size of H atoms [65]. The CO_2 molecule was modeled as a three-site rigid linear molecule which is an all-atom LJ potential with atomic charges to approximate CO_2's quadrupole moment [66]. The accuracy of this model was tested by reproducing vapor-liquid equilibria (VLE) of the pure CO_2 and the ternary mixture of CO_2/N_2/propane [66]. The N_2 molecule was represented as a three site model with two sites located at two N atoms and the third one located at its center of mass (COM) with partial point charges [67]. This model was also tested to reproduce adsorption isotherm of N_2 in H-ZSM-5 zeolite and results showed that simulations results employing this N_2 model exhibited good agreement with the experimental results at 77 K.

There are two types of nonbonded interactions that need to be considered in molecular simulations: van der Waals interactions and electrostatic interactions. Van der Waals interactions acting on each adsorbate molecules and atoms of ZIFs as dispersive and repulsive forces were calculated using Lennard-Jones 12-6 equation. Pairwise interactions between adsorbates and each atom in ZIFs were used to model interaction between adsorbate molecules and the atoms of ZIFs. Lorenz-Berthelot mixing rules and Lennard-Jones 12-6 formula to describe the interactions between different pairs of particles are given in equation 3.1 and 3.2., respectively.

$$\sigma_{ij} = \frac{(\sigma_i + \sigma_j)}{2} \qquad (3.1)$$

$$\varepsilon_{ij} = \sqrt{\varepsilon_i \times \varepsilon_j}$$

$$E_{vdW}(r) = \sum_{i>j} 4\varepsilon_{ij}\left[\left(\frac{\sigma_{ij}}{r_{ij}}\right)^{12} - \left(\frac{\sigma_{ij}}{r_{ij}}\right)^{6}\right] \quad (3.2)$$

The van der Waals energy (E_{vdW}) for i and j pairwise was calculated using collision diameter (σ_{ij}), well depth of the interaction between atoms (ε_{ij}) which were calculated from pure σ (σ_i,σ_j) and ε (ε_i,ε_j) values using equation 3.1, and distance between particles (r_{ij}) [68].

Electrostatic interactions between adsorbate molecules and ZIF atoms were calculated using Coulomb's law in equation 3.3.

$$E_{coulomb}(r) = \sum_i \sum_j \frac{q_i q_j}{4\pi\varepsilon_o r_{ij}} \quad (3.3)$$

q_i, q_j, r_{ij} and ε_o defines partial point charges of i and j, distance between particles and the dielectric constant [68]. In simulations, partial point charges were defined for each ZIF atoms and CO_2, N_2 adsorbate molecules. The atomic partial charges for all ZIFs except ZIF-90 were assigned using the connectivity-based atom contribution method (CBAC) [69] which assumes that the partial charge of an atom in a framework is determined by its bonding connectivity and the atoms with the same connectivity have identical charges. Xu and Zhong [69] tested this approach on 43nanoporous materials including ZIFs and showed that CBAC charges give nearly identical results to those from the quantum mechanical (QM) calculations as well as good reproduction of the experimental isotherm data. Keskin [48] also showed that adsorption isotherms computed using CBAC method are very similar to the ones computed using QM methods based on the ChelpG [70] density functional theory (DFT) calculations. Since CBAC method does not include partial point charges for

some ZIF-90 atoms, the atomic partial charges of ZIF-90 were defined using REPEAT charges of Watanabe et al. [71]. Atci and Keskin [51] showed that simulation results employing REPEAT charges for ZIF-90 were consistent with the experimental results of permeances for single component CO_2 and H_2/CO_2, H_2/N_2 mixtures which have electrostatic potential to ZIF atoms.

Table 3.1: Structural properties of ZIFs

Material	Composition	Porosity (%) [29, 50, 72]	Density (g/cm^3)	Pore size (Å) [17, 73]	Volume (Å)	Cell Dimensions (a, b, c) (Å) Cell Angles (α, β, γ) (^{o})	Topology
ZIF-1	$Zn(Im)_2$	55.75	1.194	3.00/6.94	2221	9.7405×15.266×14.936 90, 98.62, 90	BCT
ZIF-2	$Zn_2(Im)_4$	49.20	0.929	6.4/6.9	5707	9.679×24.114×24.450 90, 90, 90	BCT
ZIF-3	$Zn_2(Im)_4$	57.80	0.880	4.6/6	6024	18.9701×18.9701×16.740 90, 90, 90	DFT
ZIF-6	$Zn(Im)_2$	62.70	0.764	8.2/8.8	6940	18.515×18.515×20.245 90, 90, 90	GIS
ZIF-8	$Zn(mIm)_2$	43.30	0.924	3.4/11.6	4905	16.9910×16.9910×16.9910 90, 90, 90	SOD
ZIF-10	$Zn(Im)_2$	65.00	0.746	8.2/12.12	14210	27.0608, 27.0608,19.406 90, 90, 90	MER
ZIF-60	$Zn_2(Im)_3(mIm)$	70.82	0.769	7.2/9.4	14270	27.2448×27.2448×19.2254 90, 90, 90	MER
ZIF-65	$Co(nIm)_2$	67.90	1.095	3.4/10.4	5152	17.2715×17.2715×17.2715 90, 90, 90	SOD
ZIF-67	$Co(nIm)_2$	62.27	0.904	3.4/11.6	4877	16.9589×16.9589×16.9589 90, 90, 90	SOD
ZIF-68	Zn(cbIm)(nIm)	60.69	1.033	7.5/10.3	11364	26.6407×26.6407×18.4882 90, 90, 120	GME
ZIF-69	Zn(cbIm)(nIm)	57.41	1.145	4.4/7.8	11436	26.0840×26.0840×19.4082 90, 90, 120	GME
ZIF-70	$Zn(Im)_{1.13}(nIm)_{0.87}$	72.09	0.854	13.1/15.9	11387	27.0111×27.0111×18.0208 90, 90, 120	GME
ZIF-79	Zn(mbIm)(nIm)	56.87	1.075	4.0/7.5	11441	25.9263×25.9263×19.6532 90, 90, 120	GME
ZIF-81	Zn(brbIm)(nIm)	56.65	1.292	3.9/7.4	11527	25.9929×25.9929×19.6997 90, 90, 120	GME
ZIF-90	$Zn(Ica)_2$	60.40	0.974	3.5/11.2	5233	17.3612×17.3612×17.3612 90, 90, 90	SOD

3.2. Grand Canonical Monte Carlo Simulations

Single component and binary mixture adsorption isotherms of gases in ZIFs were computed using conventional grand canonical Monte Carlo (GCMC) simulations. Grand-canonical ensemble (μ,V,T ensemble) was used in the adsorption calculations. By fixing the temperature, volume and chemical potential, the number of particles fluctuates during the simulation and the number of adsorbed molecules was calculated at equilibrium. For pure components, four types of trial moves, attempts to translate a molecule, attempts to rotate a molecule, attempts to create a new molecule and attempts to delete an existing molecule were included. For gas mixtures, in order to speed up the equilibrium, an additional type of trial, attempts to exchange molecular identity, was also included. Detailed information about GCMC can be obtained from Frenkel and Smit [74]. A cut-off radius was used to speed up GCMC simulations. Cut-off radius is selected equal or smaller than the half of unit cell dimension [74]. Van der Waals and electrostatic energy of particles are assumed to be zero if distance between two atoms is greater than cut-off radius. Energy grids of adsorbate-ZIF interaction in the cut-off radius were computed not to calculate interaction energy at each step. During simulations, interaction energies of adsorbate-ZIF pairs were interpolated using energy grids [75]. A cut-off distance of 13 Å was used for LJ interactions and 25 Å was used for electrostatic interactions. Periodic boundary conditions which are used for simulation of bulk materials using a reasonable number of atoms were applied in all simulations. The size of the simulation box was increased up to 7×7×7 unit cells in cases to accommodate enough adsorbates to guarantee the simulation accuracy at the lowest loadings. Simulations at the lowest fugacity for each system were started from an empty ZIF matrix and each subsequent simulation at higher fugacity was started from the final configuration of the previous run. Simulations included minimum 1.5×10^7 cycle equilibration period followed by a 1.5×10^7 cycle production run.

3.3. Equilibrium Molecular Dynamics Simulations

Equilibrium molecular dynamics simulation is a technique to calculate equilibrium and transport properties of many body systems. In this thesis, single component and mixture diffusivities were computed using equilibrium molecular dynamics (EMD) simulations in the canonical ensemble with a Nose-Hoover thermostat [74]. In canonical ensemble (N,V,T ensemble), the number of particles, volume and temperature is constant. A short grand canonical Monte Carlo (GCMC) simulation was performed for initial configuration of particles. Initial velocities for each particle were assigned using Maxwell-Boltzmann velocity distribution. Before taking data, NVT-MD simulation was carried out to equilibrate the system for about 20 ps. When the system was equilibrated, final positions of the particles were calculated by integrating Newton's equation of motion. During NVT-MD simulations, temperature was kept at desired value using Nose-Hoover thermostat algorithm. Diffusion coefficients of molecules were calculated using final and initial positions of particles with Einstein relation [76]. Detailed information about Einstein relation will be given in the next section.

In order to apply mixing theory for diffusion, both single component self and corrected diffusivities were calculated. For the single component corrected (self) diffusivities 20 (10) independent EMD simulations were performed since using a large number of independent trajectories is vital in order to accurately compute the corrected diffusivities. Mixture self diffusivities of each species were computed directly at the adsorbed concentrations calculated from binary mixture GCMC simulations. The details of using EMD simulations to obtain various diffusion coefficients have been described in previous studies. For example, Sanborn and Snurr [77] measured diffusion of binary mixtures CF_4 and n-alkanes in faujasite zeolite. Ackerman et al. [78] measured diffusivities of argon and neon in carbon

nanotubes. Keskin [48] measured mixture diffusivities of CH_4/H_2, CO_2/CH_4 and CO_2/H_2 in ZIF-3 and ZIF-10.

3.4. Calculation of Self Diffusivity, Corrected Diffusivity and Transport Diffusivity

Single component self diffusivities, single component corrected diffusivities and mixture self diffusivities of each species were calculated using EMD simulations. The self diffusivity, $D_{i,\ self}$ describes the motion of individual tagged particles and in an isotropic three dimensional material it is related to the mean-squared displacement of tagged particles by the Einstein relation,

$$D_{i,self} = \lim_{t\to\infty} \frac{1}{6t} \left\langle \frac{1}{N_t} \sum_{l=1}^{N_i} \left[r_{il}(t) - r_{il}(0) \right]^2 \right\rangle \tag{3.4}$$

where N is the number of molecules, $r_{il}(t)$ is the three dimensional position vector of molecule l of species i at time t and the angular brackets denote the ensemble average [79]. The corrected diffusivity includes information on the collective motion of multiple adsorbed molecules that is relevant to the net mass transport and can be calculated using the following expression [79, 80]:

$$D_{i,o} = \lim_{t\to\infty} \frac{1}{6Nt} \left\langle \left(\sum_{l=1}^{N_i} \left[r_{il}(t) - r_{il}(0) \right] \right)^2 \right\rangle \tag{3.5}$$

EMD simulations provided the loading dependent corrected diffusivities (D_o) which are required to compute permeance of single gases in ZIF membranes. The transport diffusivity (D_t) is then defined without any approximation in terms of corrected diffusivity and a

thermodynamic correction factor, a partial derivative relating the adsorbate concentration, c and bulk gas phase fugacity, f [80]:

$$D_t(c) = D_o(c) \cdot \frac{\partial \ln f}{\partial \ln c} \tag{3.6}$$

The thermodynamic correction factor is fully defined once the single component adsorption isotherm is known.

3.5. Application of Mixing Theories

The prediction of adsorption and transport properties of mixtures from data taken from single component studies has been a long-standing goal in describing equilibrium and mass transport in nanoporous materials. The validation of methods for this task can have great practical significance, but this type of validation can only be considered when high quality mixture adsorption and diffusion data is available. GCMC and EMD data from binary mixtures in some ZIFs were used to test the validity of the mixing theories that have been proposed to predict mixture properties from single component data.

For adsorption, Ideal Adsorbed Solution Theory (IAST) [81] was tested, which is well-known to give accurate predictions for mixture adsorption isotherms based on adsorption data of pure gases in many nanoporous materials except in materials characterized by strong energetic or geometric heterogeneity [82]. In order to apply IAST, single component adsorption isotherms of CH_4 and H_2 (CO_2) were fitted to (a)dual site Langmuir ((b)Freundlich-Langmuir) models given in equation 3.7.

$$\text{(a)}\ \ C_i = \frac{a_i P}{b_i + P} + \frac{c_i P}{d_i + P}\ ,\ \text{(b)}\ C_i = \frac{a_i P^{c_i}}{b_i + P^{c_i}} \tag{3.7}$$

In these models, C_i is the adsorbed amount (molecules/unit cell), P is the fugacity (bar), a_i, b_i, c_i, d_i are fitting parameters of species i (CO_2, CH_4, H_2).

For diffusion, Krishna and Paschek (KP) [83] approach was used which predicts the self diffusion coefficients of species in a binary mixture using the following correlations:

$$D_{i,self} = \frac{1}{\frac{1}{Đ_i} + \frac{\theta_i}{Đ_{ii}^{corr}} + \frac{\theta_j}{Đ_{ij}^{corr}}}, \quad D_{j,self} = \frac{1}{\frac{1}{Đ_j} + \frac{\theta_i}{Đ_{ji}^{corr}} + \frac{\theta_j}{Đ_{jj}^{corr}}} \tag{3.8}$$

In these correlations, $D_{i,self}$ is the self diffusivity of species i in a binary mixture with species j, $Đ_i$ is the single component corrected diffusivity, $Đ_{ii}^{corr}$ and $Đ_{ij}^{corr}$ are the self-exchange and binary-exchange diffusivities, respectively, which reflect the correlation effects in a mixture and θ_i is the fractional loading of species i. In order to use Equation 3.8, single component self diffusivities, $D_{i,self}(\theta)$ and corrected diffusivities, $Đ_i(\theta)$ of pure gases were fitted to continuous functions and then these diffusivities were evaluated at the total fractional loading for mixtures. The self-exchange diffusivities and binary-exchange diffusivities were calculated using equation 3.9 and 3.10,

$$D_{i,self}(\theta) = \frac{1}{\frac{1}{Đ_i(\theta)} + \frac{\theta_i}{Đ_{ii}^{corr}(\theta)}} \tag{3.9}$$

$$\Theta_{j,sat} Đ_{ij}^{corr}(\theta) = \left[\Theta_{j,sat} Đ_{ii}^{corr}(\theta)\right]^{\theta_i/\theta_i+\theta_j} \left[\Theta_{i,sat} Đ_{jj}^{corr}(\theta)\right]^{\theta_j/\theta_i+\theta_j} \tag{3.10}$$

where $\Theta_{i,sat}$ defines the saturation loading of species i, respectively. The KP approach has been tested in the past for carbon nanotubes (CNTs) [84], MFI, [85] CuBTC [86] and the predictions were found to be in good agreement with EMD simulations.

3.6. Prediction of Adsorption-Based and Membrane-Based Separation Performances

Adsorption-based separation performances of ZIFs were evaluated considering adsorption selectivity and working capacity (Δq, delta loading). The adsorption selectivity of component i from component j was calculated using equation 3.11,

$$S_{adsorption(i/j)} = \frac{x_i / x_j}{y_i / y_j} \tag{3.11}$$

where x is the molar fraction of adsorbed phase obtained from mixture GCMC simulations, y is the molar fraction of the bulk phase. Besides adsorption selectivity, delta loading is an important parameter for the determination of the economy of the process. Delta loading in PSA units for selected component (i) was calculated using equation 3.12 [10],

$$\Delta q = c_i(10\ \text{bar}) - c_i(1\ \text{bar}) \tag{3.12}$$

where c_i (10 bar) is the loading at adsorption pressure , c_i (1 bar) is the loading at desorption pressure.

Membrane-based separation performances of ZIFs were evaluated considering permeation selectivity and gas permeability. The permeation selectivity can be calculated as the multiplication of adsorption selectivity and diffusion selectivity [87] as in equation

3.13. Krishna and van Baten [88] derived this equation for the permeation selectivity of zeolite membranes under conditions where the permeate side is under vacuum. In their model, adsorbed loadings from GCMC simulations were calculated for equimolar bulk gas mixtures and self-diffusivities from MD simulations were determined for equimolar adsorbed mixtures. However, equation of Krishna and van Baten [88] cannot give accurate predictions for different bulk gas compositions due to equimolar bulk gas composition assumption. Recently, Keskin and Sholl [87] modified this equation to be able to use it for arbitrary bulk gas compositions. Self-diffusivities from MD were directly evaluated at the adsorbed compositions using equation 3.13.

$$S_{permeation(i/j)} = S_{ads(i/j)} \cdot S_{dif(i/j)} = \frac{x_i / x_j}{y_i / y_j} \cdot \frac{D_{i,self}(x_i, x_j)}{D_{j,self}(x_i, x_j)} \qquad (3.13)$$

In this expression, x is the molar fractions of the adsorbed phase calculated from mixture GCMC simulations and y is the molar fractions of the bulk phase, $D_{i,self}$ is the mixture self diffusivity of component i evaluated directly at the corresponding adsorbed compositions of the mixture from GCMC simulations. Permeability of gases in a binary mixture through a ZIF membrane was defined by Krishna and van Baten [89] as in equation 3.14,

$$P_i = \frac{\phi \cdot D_{i,self} \cdot c_i}{f_i} \qquad (3.14)$$

where P_i is the permeability of the species i (mol/m/s/Pa), ϕ is the fractional pore volume of the membrane material, c_i is the concentration of species i at the upstream face of the membrane (mol/m^3) and f_i is the bulk phase fugacity of the species i (Pa).

3.7. Prediction of ZIF/Polymer Composite Membrane Performances

Among ZIFs studied in this thesis, ZIF-90/polymer composite membrane was studied since it was experimentally fabricated and tested for gas separation. In ZIF/polymer composite membranes, calculation of selectivity and permeability is slightly different. Steady state fluxes of each gas across a single ZIF crystal was calculated by Fick's law [90] which relates the flux of each species with the concentration gradient (∇c) through transport diffusivities:

$$J = -D_t(c) \cdot \nabla c \tag{3.15}$$

The concentration gradient of the adsorbed species was calculated based on the difference between the feed and permeate side pressures of the membrane. Shell description of the membrane which calculates the transport diffusivity at the mean concentration was used to calculate steady state fluxes [91]. More details of the methods used to calculate single component fluxes based on atomistic simulations and shell model were described in earlier studies of Keskin and Sholl [92, 93]. The gas flux in ZIF membrane was then converted to single component gas permeability, P, using pressure drop (Δp), and membrane thickness, L, by [94]:

$$P = \frac{J}{\Delta p / L} \tag{3.16}$$

Once the single component steady state fluxes through a ZIF membrane are known, ideal selectivity of the ZIF membrane is simply defined by the ratio of the single component fluxes of each species:

$$S_{ideal(i/j)} = \frac{J_i}{J_j} \tag{3.17}$$

Designing a composite membrane-based gas separation process requires knowledge of the permeability of gases through the continuous phase (the polymer matrix) and the dispersed phase (the filler particles, ZIFs). In this thesis, Maxwell model [95] was used to predict gas permeabilities through polymer/ZIF composite membranes:

$$P_r = \frac{P}{P_m} = \left[\frac{2(1-\phi) + (1+2\phi)\lambda_{dm}}{(2+\phi) + (1-\phi)\lambda_{dm}} \right] \tag{3.18}$$

In this model, λ_{dm} is the permeability ratio (P_d/P_m), P_d is the permeability of dispersed phase (ZIF), P_m is the permeability of continuous phase (polymers), P_r is the relative permeability, P is the permeability in polymer/ZIF composite membrane and ϕ is the volume fraction of ZIF particles. Maxwell model is valid for low to moderate values of volume fractions ($0<\phi<0.2$) since it assumes that nearby particles do not affect the streamlines around particles. This model does not consider packing limit of particles, the effect of particle size distribution, particle shape and aggregation of particles. The experimental data for gas permeability through polymers, Matrimid and Ultem, was taken from the work of Bae et al. [72] Gas permeabilities through ZIFs were predicted by molecular simulations using equation 3.16. Molecular simulations for ZIFs (ZIF-90 and ZIF-65) were performed at 308 K and at 4.5 bar feed pressure to be consistent with the

experimental data of Matrimid and Ultem polymers. Gas permeabilities (P) through ZIF/polymer composite membranes were calculated using gas permeability (P_d) through ZIF membrane and experimentally measured gas permeability (P_m) of polymer. Ideal selectivity of ZIF/polymer composite membranes is computed as the ratio of permeabilities (P) for each species using equation 3.19.

$$S_{ideal(i/j)} = \frac{P_i}{P_j} \tag{3.19}$$

Chapter 4

ADSORPTION-BASED AND MEMBRANE-BASED GAS SEPARATIONS WITH ZIFS

4.1. Validation of Simulations with Experimental Data of ZIF Membranes

Among the ZIFs considered in this thesis, thin film membranes were made for two of them: ZIF-69 and ZIF-90. Figure 4.1 compares the predictions of molecular simulations for the permeance of mixed gases (CO_2/H_2, N_2/H_2, CH_4/H_2, CO_2/CH_4, CO_2/H_2) with the experimental measurements of Huang et al. [31] and Liu et al. [34] through ZIF-90 and ZIF-69 membranes. There is a reasonable agreement between theoretical predictions from molecular simulations and experimental measurements for mixed gas permeance through ZIF membranes considering the fact that the only experimental input of simulations in this thesis is the XRD structures of the ZIFs. The predictions for mixed gas permeance of H_2 and CO_2 in ZIF-90 membranes were remarkably well. Lower CO_2 permeances were predicted for CO_2/CH_4 and CO_2/N_2 mixtures in ZIF-69 membrane. In fact, Liu et al. [34] reported that measured CO_2 diffusion in their experiments was exceptionally higher than Knudsen diffusion rate and CO_2 permeance in mixtures was higher than single component permeance. Predictions for mixed gas permeances of CH_4 and N_2 through narrow pore membranes were less than the experimental measurements due to the rigid framework assumption of molecular simulations. Since the narrow pore sizes of ZIF-90 (3.5 Å) and ZIF-69 (4.4 Å) are close to kinetic diameter of CH_4 (3.8 Å) and N_2 (3.6 Å), diffusion rate of these molecules can be affected by the lattice flexibility.

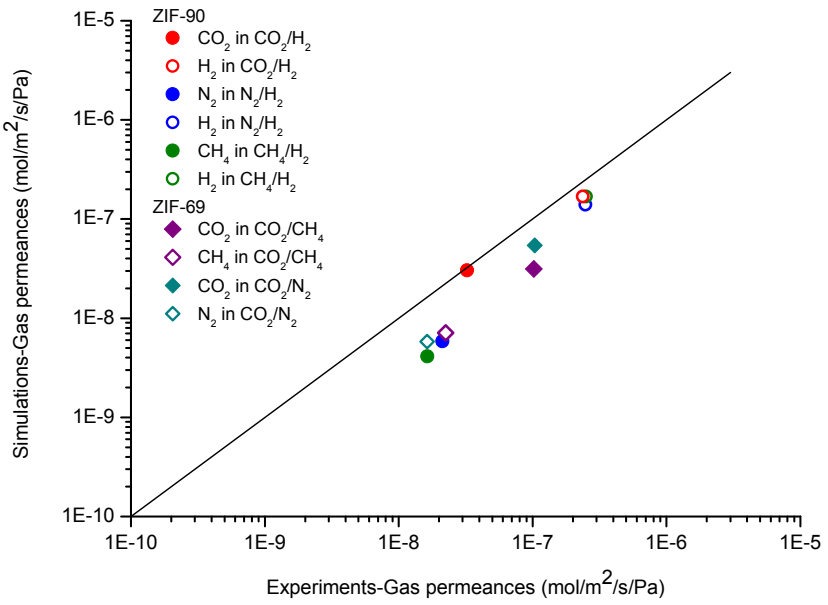

Figure 4.1: Comparison of the experimental data [31, 34] with the predictions of molecular simulations of this thesis for permeation of mixed gases through ZIF-90 (circles) and ZIF-69 (diamond) membranes at 473 K and 298 K, respectively. The mixed gases are at 1 bar and equimolar in composition.

One important point to mention is that although ZIF-8 membrane was fabricated and tested for separation of CH_4/H_2 and CO_2/CH_4 mixtures [38-41, 96, 97], no prediction can be made for separation of these mixtures in ZIF-8 by molecular simulations of this thesis. This is because molecular simulations showed that CH_4 experiences a large energy barrier (~45 kJ/mol) in the narrow pore windows of ZIF-8 (3.4 Å) and diffusion coefficient of CH_4 is far too slow to be directly observed with EMD [98]. This situation was previously observed and discussed by Haldoupis et al. [99] who used computational methods and predicted extremely high H_2/CH_4 selectivities for ZIF-8 due to very slow diffusion of CH_4. They concluded that the high discrepancy between their predicted CH_4 selectivity (~10^7) and the experimentally reported one [38] (11.2) is mostly associated with defects in the microstructure of the intergrown thin films of ZIF-8 membrane, where defects associated

with grain boundaries can allow significant fluxes of CH_4 through the membrane. More detailed modeling studies are required to assess the contribution of fluxes through microstructural defects to solve this discrepancy [100].

4.2. Adsorption-based Separation Performances of ZIFs

In order to predict membrane-based separation performances, adsorption selectivity of ZIFs should be evaluated. Therefore, binary mixture adsorption equilibria of gases were calculated in all ZIFs to compute adsorption-based separation performance of ZIFs for CH_4/H_2, CO_2/CH_4 and CO_2/H_2 mixtures. As an example, adsorption isotherms for CH_4/H_2, CO_2/CH_4 and CO_2/H_2 mixtures in ZIF-1 and ZIF-2 at 298 K are shown in Figure 4.2. Adsorption of CO_2 is strongly favored over CH_4 (H_2) in CO_2/CH_4 (CO_2/H_2) mixtures due to the electrostatic interactions of CO_2 molecules with the ZIF atoms. Adsorption of CH_4 is preferred over H_2 in CH_4/H_2 mixtures since H_2 has weaker interactions with ZIFs. IAST was also used to predict the mixture adsorption isotherms based on pure gas adsorption data. There is a good agreement between IAST predictions and GCMC simulations for all mixtures suggesting that IAST can be used to get accurate predictions for binary adsorption equilibria of CO_2, CH_4, H_2 gases in ZIFs.

Adsorption-based separation performances of ZIFs were examined by computing the adsorption selectivity ($S_{adsorption}$) using equation 3.11. Figure 4.3a shows adsorption selectivity of ZIFs as a function of fugacity for CH_4/H_2 mixtures. All ZIFs are CH_4 selective and selectivity generally shows a slight decrease at high pressures. This can be explained by the interplay of energetic and size effects. At low pressures, energetic effects favor CH_4 adsorption whereas at high loadings, small H_2 molecules can find adsorptions sites in the pores due to entropic effects. Materials having narrow pore apertures and small cavities such as ZIF-1, ZIF-79, ZIF-81 exhibit high adsorption selectivities (>40) because the degree of confinement of CH_4 molecules in these narrow pores is much stronger compared to the small H_2 molecules. Result for high CH_4 selectivity of ZIF-1 (71) in this

thesis is in agreement with the result of recent molecular simulation study of Wu et al. [29] who computed CH_4 adsorption selectivity of ZIF-1 as 76 at 1 bar. Materials having large cages connected with narrow windows such as ZIF-65, ZIF-67 and ZIF-90 exhibit mediocre CH_4 selectivity (15-20) since adsorbate molecules are not very strongly confined in the large cages. The two ZIFs with large cavities, ZIF-10 and ZIF-60, exhibit the lowest CH_4 selectivity (~10).

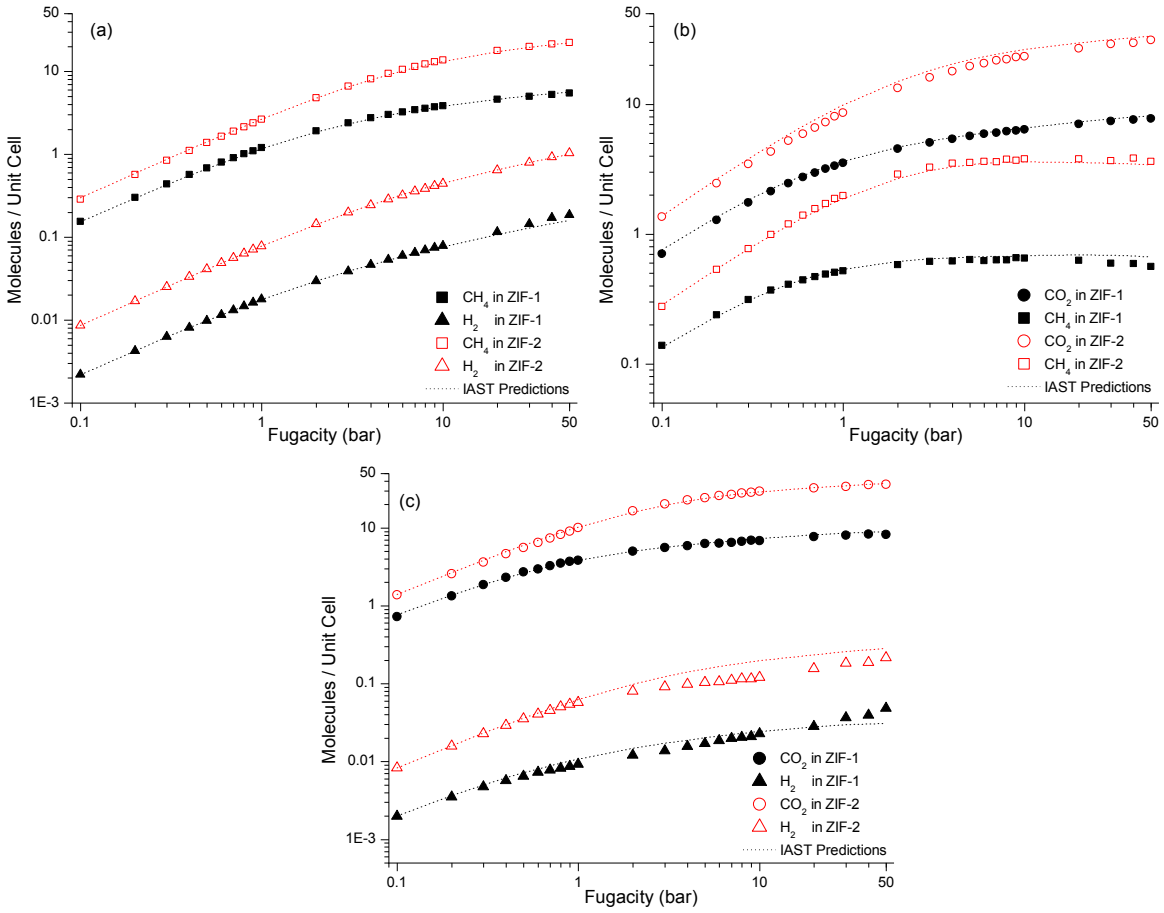

Figure 4.2: Equimolar mixture adsorption isotherms of (a)CH_4/H_2 (b)CO_2/CH_4 and (c)CO_2/H_2 in ZIF-1 and ZIF-2 at 298 K. Symbols are the results of mixture GCMC simulations, dotted lines represent the predictions of IAST.

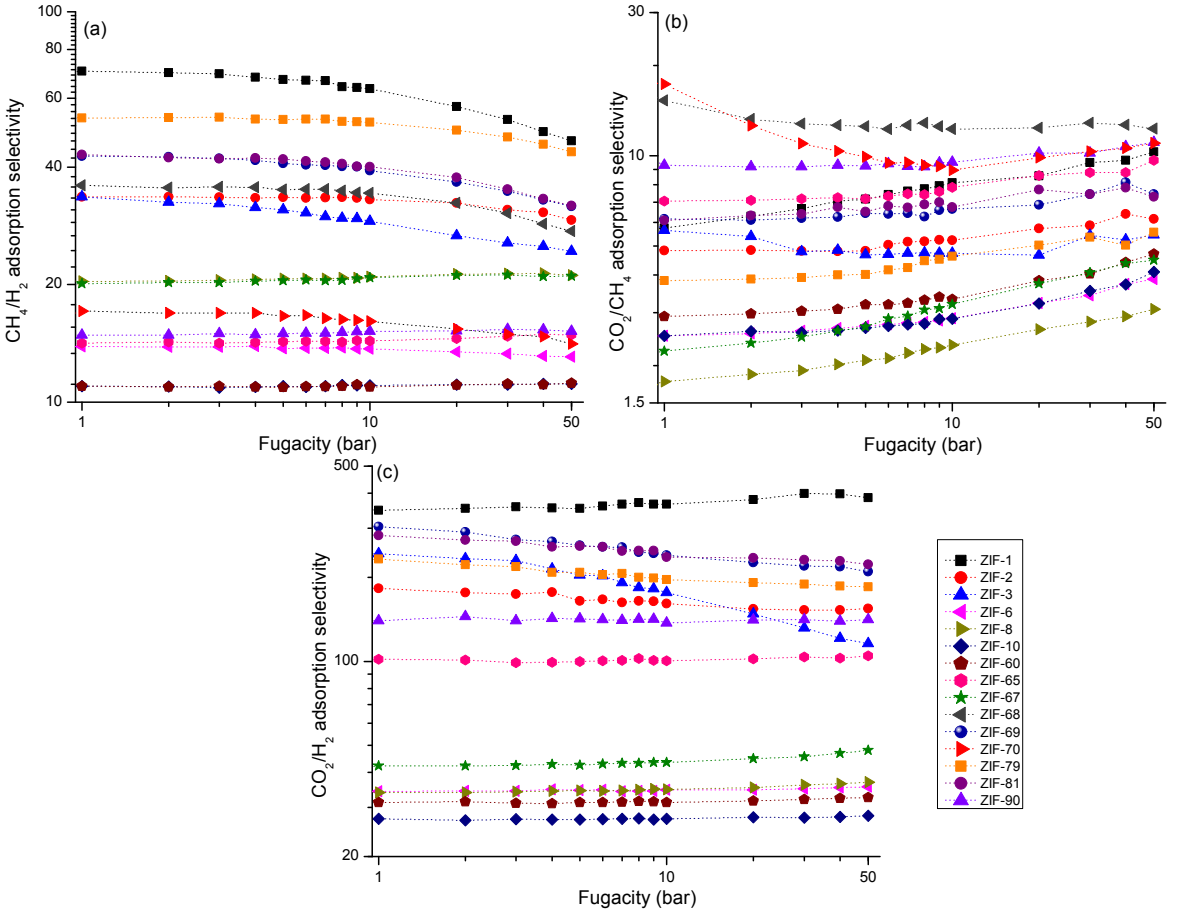

Figure 4.3: Predicted adsorption selectivity of ZIFs for (a)CH_4/H_2 (b)CO_2/CH_4 and (c)CO_2/H_2 mixtures at 298 K. Compositions of the bulk gas mixtures are CH_4/H_2:10/90, CO_2/CH_4:10/90 and CO_2/H_2:1/99. The first species in the label represents the selected component. Data for CO_2/CH_4 selectivity of ZIF-68 and ZIF-70 was taken from calculations of Liu et al. [49].

Predictions for CH_4/H_2 adsorption selectivity of ZIFs in this thesis are in a good agreement with the predictions of Wu et al. [29] and Guo et al. [27] who employed DREIDING and UFF force fields in their molecular simulations, respectively. For example, CH_4 selectivities of 14, 21, 11, 21 and 40 were predicted for ZIF-6, ZIF-8, ZIF-60, ZIF-67 and ZIF-81, respectively in this thesis whereas Wu et al. computed selectivities as 12, 18, 10, 15 and 35 at 10 bar, 298 K for the same materials.

Adsorption selectivities of ZIFs for CO_2/CH_4 mixtures are shown in Figure 4.3b. The CO_2 selectivities are not very high (2-12) due to the competitive adsorption between CO_2 and CH_4 molecules in the ZIF pores. There is a slight increase in CO_2 selectivity at high pressures which can be attributed to the collective interaction of CO_2 molecules at high loadings. CO_2 selectivity was calculated as 6.6 (5) in ZIF-69 (ZIF-79) for a CO_2/CH_4:10/90 mixture in this thesis which agrees with the value of 5.6 (7.3) calculated by Liu and Smit [20] (Li et al. [28]) for equimolar mixtures at 10 bar, 298 K. As can be seen from Figure 4.3c, CO_2/H_2 selectivities are significantly higher than CO_2/CH_4 selectivities since CO_2 is strongly selected over H_2 due to weak interactions of H_2 with ZIFs. Similar to the previous discussion, ZIFs with narrow pores (ZIF-1, ZIF-69, ZIF-79, ZIF-81) provide stronger confinement hence show higher selectivity (200-400) for CO_2 whereas ZIFs with large cavities like ZIF-6, ZIF-10 and ZIF-60 are less promising materials for CO_2/H_2 separations. One striking feature of Figure 4.3c is that ZIFs having the same topology (ZIF-8, ZIF-65, ZIF-67, ZIF-90) exhibit different CO_2/H_2 selectivities ~35, 102, 43, 137, respectively. Although adsorbed H_2 amount in these materials are similar, CO_2 adsorption amounts are different in each material. This can be attributed to the complex interplay of several material properties such as available free volume, pore shape, type of metal sites and organic linkers forming the pores. For example, the type of imidazolate linkers in ZIF-90 ($Zn(Ica)_2$) is different from the ones in ZIF-8, ZIF-65 and ZIF-67 ($Zn(mIm)_2$, $Co(nIm)_2$ and $Co(mIm)_2$, respectively) which causes differences in electrostatic and dispersion interactions of CO_2 with the pore walls of the materials.

Adsorption selectivity and working capacity are the two important factors determining the efficiency of an adsorption-based separation process. Working capacity also known as delta loading was calculated as the difference of the adsorbed loadings at adsorption pressure (10 bar) and desorption pressure (1 bar) [10]. Figure 4.4 compares adsorption selectivities and delta loadings of ZIFs considered in this study for separation of CH_4/H_2, CO_2/CH_4 and CO_2/H_2 mixtures at 10 bar and room temperature. In order to assess the performance of ZIFs, data for zeolites and other nanoporous materials were taken from the

study of Krishna and van Baten [10] is shown in Figure 4.4. The best adsorbent candidates are expected to be in the upper right corner of Figure 4.4, exhibiting high selectivity and high working capacities. Figure 4.4a shows that ZIF-1, ZIF-2, ZIF-3, ZIF-68, ZIF-69, ZIF-79, ZIF-81 are promising materials for CH_4/H_2 separation because they have higher selectivities than traditional zeolites CHA, ITQ-29, LTA-Si and their working capacities are similar to zeolites. The remaining ZIFs have mediocre selectivities but their working capacities are low due to smaller pore volumes. As discussed previously, more open nanoporous structures with high pore volumes and high surface areas such as IRMOF-1, CuBTC, MOF-177, ZnMOF-74, MgMOF-74 tend to yield high working capacities than zeolites and ZIFs [10, 89].

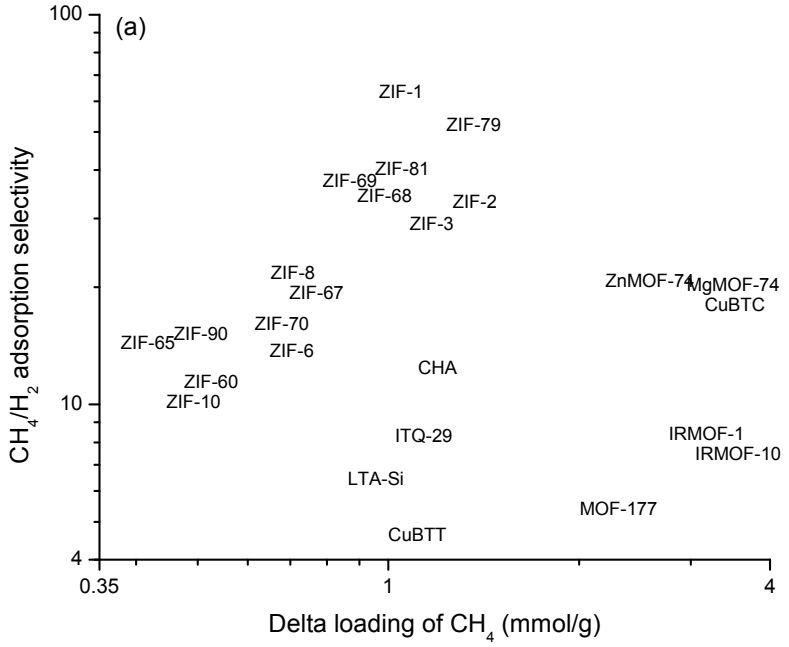

Figure 4.4: a) Adsorption-based separation performance of ZIFs for CH_4/H_2 mixture. The composition of the bulk gas mixture is 10/90 for ZIFs at 298 K, 50/50 for zeolites at 300 K.

The performance of ZIF adsorbents for CO_2/CH_4 separation is similar to that of zeolites DDR, MFI, ITQ-29. The CO_2 selectivities are around 10 and the CO_2 working capacities are in the range of 1-2.4 mmol/g. It is obvious from Figure 4.4b that NaX and NaY have high CO_2 selectivities due to the strong electrostatic interaction between CO_2 and non-framework cations (Na^+) [101]. However, molecular simulations clearly demonstrated the drawbacks of these commonly used adsorbents; very low working capacities [10]. These zeolites are also among the best candidates for CO_2/H_2 separations as shown in Figure 4.4c. A significant portion of the ZIFs examined in this thesis have greater CO_2/H_2 adsorption selectivities than the widely studied MFI, CHA, DDR and CuBTC but none of the ZIFs considered in this thesis can outperform MgMOF-74 which offers the best combination of adsorption selectivity and working capacity for CO_2/H_2 separations.

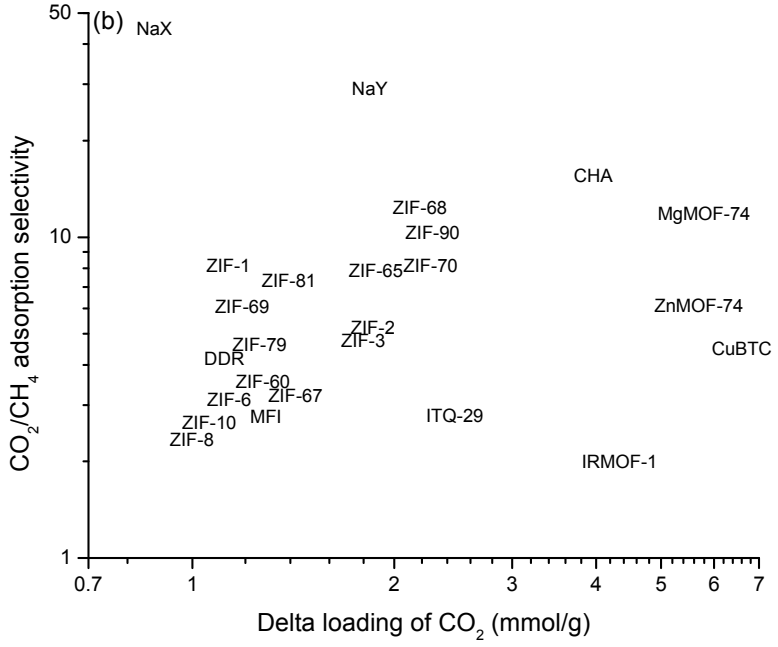

Figure 4.4: b) Adsorption-based separation performance of ZIFs for CO_2/CH_4 mixture. The composition of the bulk gas mixture is 10/90 for ZIFs at 298 K, 50/50 for zeolites at 300 K.

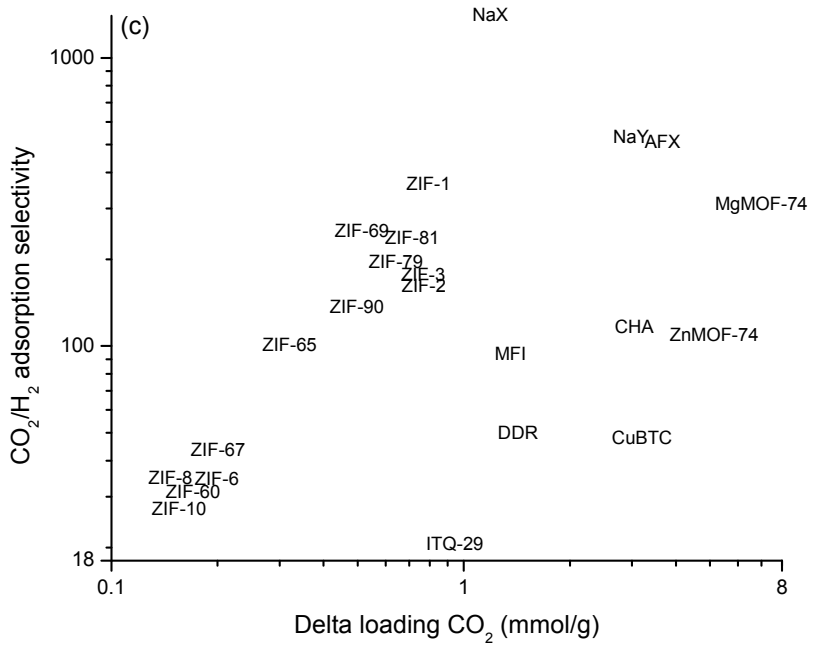

Figure 4.4: c) Adsorption-based separation performance of ZIFs for CO_2/H_2 mixture. The composition of the bulk gas mixture is 1/99 for ZIFs at 298 K, 15/85 for zeolites at 300 K.

4.3. Diffusion of Gas Mixtures in ZIFs

Membrane-based separations intrinsically rely on both adsorption and diffusion, therefore knowledge of how species in adsorbed mixtures diffuse is a prerequisite for considering new materials like ZIFs in these applications [92]. Kinetic-based separations are widely done industrially with established nanoporous adsorbents [102] and these kinds of processes cannot be evaluated for ZIFs without information on diffusion rates. In order to assess the performance of ZIFs as membranes for gas separation applications, the mixture self diffusivities of each species were computed using EMD simulations in addition to the single component self diffusivities. Both single component self diffusivities and mixture self diffusivities of gases in all ZIFs are given in Appendix-B.

Theoretical methods that can predict multi-component diffusion coefficients from single component data can be extremely useful in modeling of new membrane materials if these methods are known to be accurate. The accuracy of KP approach for a ZIF material was tested in this thesis. Since ZIF-2 has the best membrane-based separation performance and the highest diffusion-based selectivity for CH_4/H_2 and CO_2/H_2 separations, as will be discussed in the next section, KP theory was tested for this material. Figure 4.5 shows the self diffusivities of CH_4/H_2 mixtures in ZIF-2 computed by EMD simulations and predicted by KP theory at three different adsorbed compositions. There is a good agreement between theory predictions and MD simulations. The self diffusivities of both CH_4 and H_2 decrease as the total adsorbed loading increases due to steric hindrance. Theory predictions get better for diagonal composition (50/50) whereas the diffusivity of H_2 (CH_4) was underestimated for a non-diagonal adsorbed composition of CH_4/H_2:75/25 (25/75) as previously discussed by Keskin et al. [86]. Single component self-diffusivities of CH_4 and H_2 were also shown in Figure 4.5. As expected, when the fraction of H_2 (CH_4) in the mixture increases, the increase (decrease) of CH_4 (H_2) diffusivities is more profound.

The application of KP theory for diffusion of CH_4/H_2 mixtures in ZIF-2 suggested that it is possible to make accurate predictions for the diffusivity of adsorbed gas mixtures in ZIFs by using the single component diffusion data. Similar levels of agreement can be expected for CH_4/H_2 mixtures in other ZIFs because ZIF-2 does not have any structural characteristics that differ greatly from other ZIFs. In fact, this idea is already supported by the observation that qualitative aspects of molecular diffusion in ZIFs have been found to be similar to diffusion in zeolites and other nanoporous materials and the same correlations that have been tested here were shown to work well in a variety of non-cationic zeolites, CuBTC, IRMOF-1 and COFs [85, 86, 103]. The other aspect to think is how well these correlations can perform for a more chemically complex adsorbed mixtures in ZIFs. Previous tests of this method for CO_2/CH_4 mixture diffusion in ZIF-68 [49] gave good results and it can be said that the similar outcomes will be found for other ZIFs.

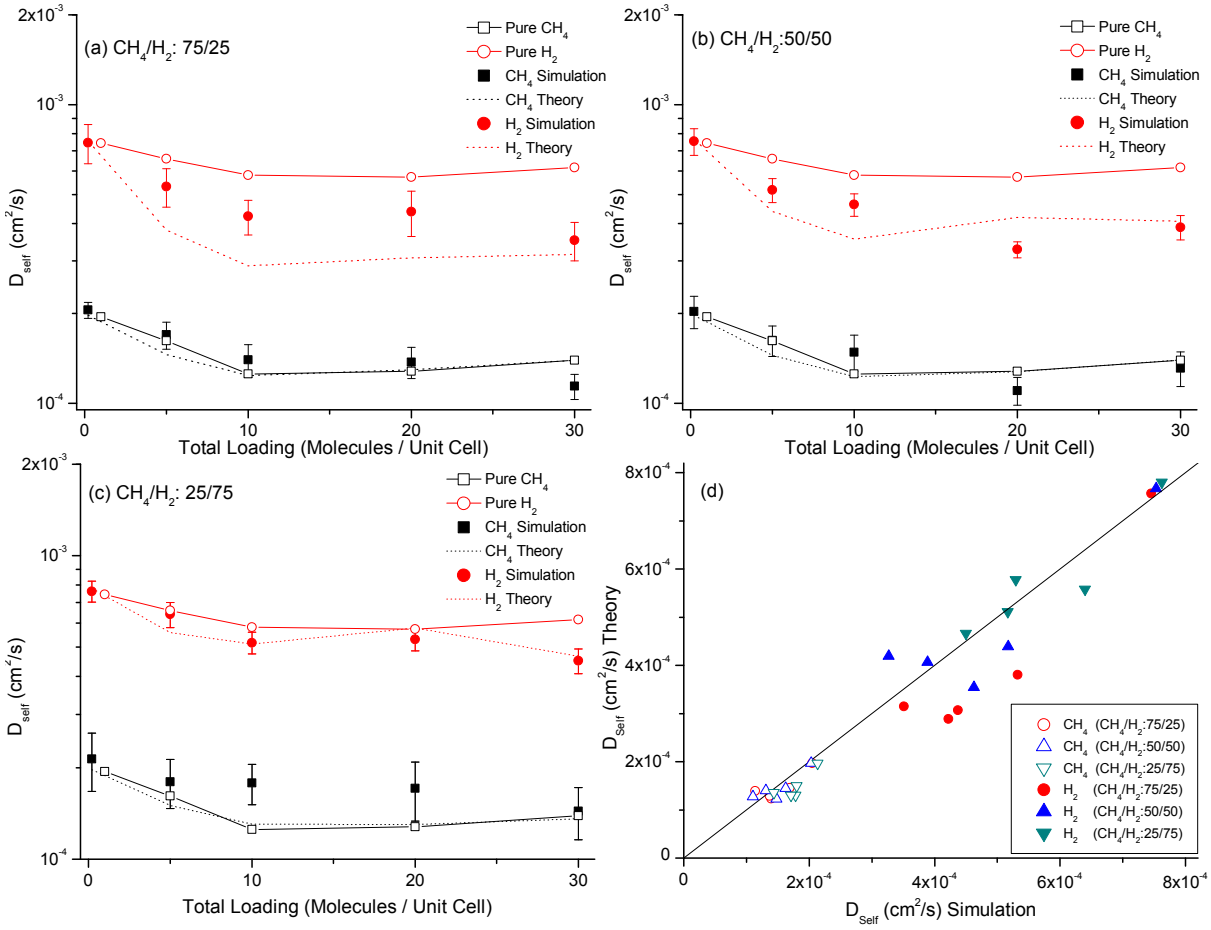

Figure 4.5: Self-diffusivities of (a)CH_4/H_2:75/25, (b)CH_4/H_2:50/50 and (c)CH_4/H_2:75/25 mixtures in ZIF-2 at 298 K. Symbols (dotted lines) represent the results of EMD simulations (predictions of KP theory). (d)Comparison of theory predictions with the EMD simulations at various loadings.

4.4. Membrane-based Separation Performances of ZIFs

Once adsorption and diffusion-based selectivities of ZIFs are computed, membrane-based selectivities can be predicted using Equation 3.13. Data for adsorption selectivity, diffusion selectivity and permeation selectivity of all ZIFs for CH_4/H_2, CO_2/CH_4 and CO_2/H_2 mixtures are given in Table C1, C2, and C3 of Appendix-C. Figure 4.6 shows permeation selectivity of ZIFs as a function of pressure for CH_4/H_2, CO_2/CH_4 and CO_2/H_2 mixtures. Here the abscissa of the figures can be considered as the feed pressure of the membrane since the permeate side is assumed to be vacuum. Figure 4.6a shows that ZIF-2 and ZIF-79 exhibit the highest permeation selectivities for CH_4 (~10). The adsorption selectivity of ZIF-79 for CH_4 (~50) was higher than ZIF-2 (~30) however, the diffusion selectivity is higher in ZIF-2 (~0.30) due to faster diffusion of CH_4 in the broader pores of ZIF-2 (6.4 Å) compared to ZIF-79 (4 Å). It is important to note that in contrast to other ZIF membranes, ZIF-65 and ZIF-90 act as H_2 selective membranes due to slow diffusion of CH_4 ($3\text{-}6\times10^{-7}$ cm^2/s) compared to H_2 ($\sim3\times10^{-4}$ cm^2/s). The difference in the transport rates of CH_4 and H_2 causes high diffusion selectivity towards H_2 and makes ZIF-65 and ZIF-90 weakly H_2 selective membranes. This is also true for CO_2/H_2 separations as shown in Figure 4.6c.

Figure 4.6b shows that ZIF-90 has the highest CO_2 selectivity in CO_2/CH_4 separations due to slow diffusion of CH_4. Both adsorption selectivity (9.54) and diffusion selectivity (2.34) favor CO_2 and equation 3.13 predicts a high CO_2 permeation selectivity (22.31) for ZIF-90 compared to other ZIFs. This is actually a rare situation because in most of the nanoporous materials high adsorption selectivities for CO_2 are compensated by low diffusion selectivities [48, 87]. For example, Figure 4.6c shows that permeation selectivities of ZIF-69 (4.1) and ZIF-79 (3.4) are low. The adsorption selectivities of these ZIFs (240 and 195, respectively) were high but lower diffusion selectivity towards CO_2 made them unpromising materials.

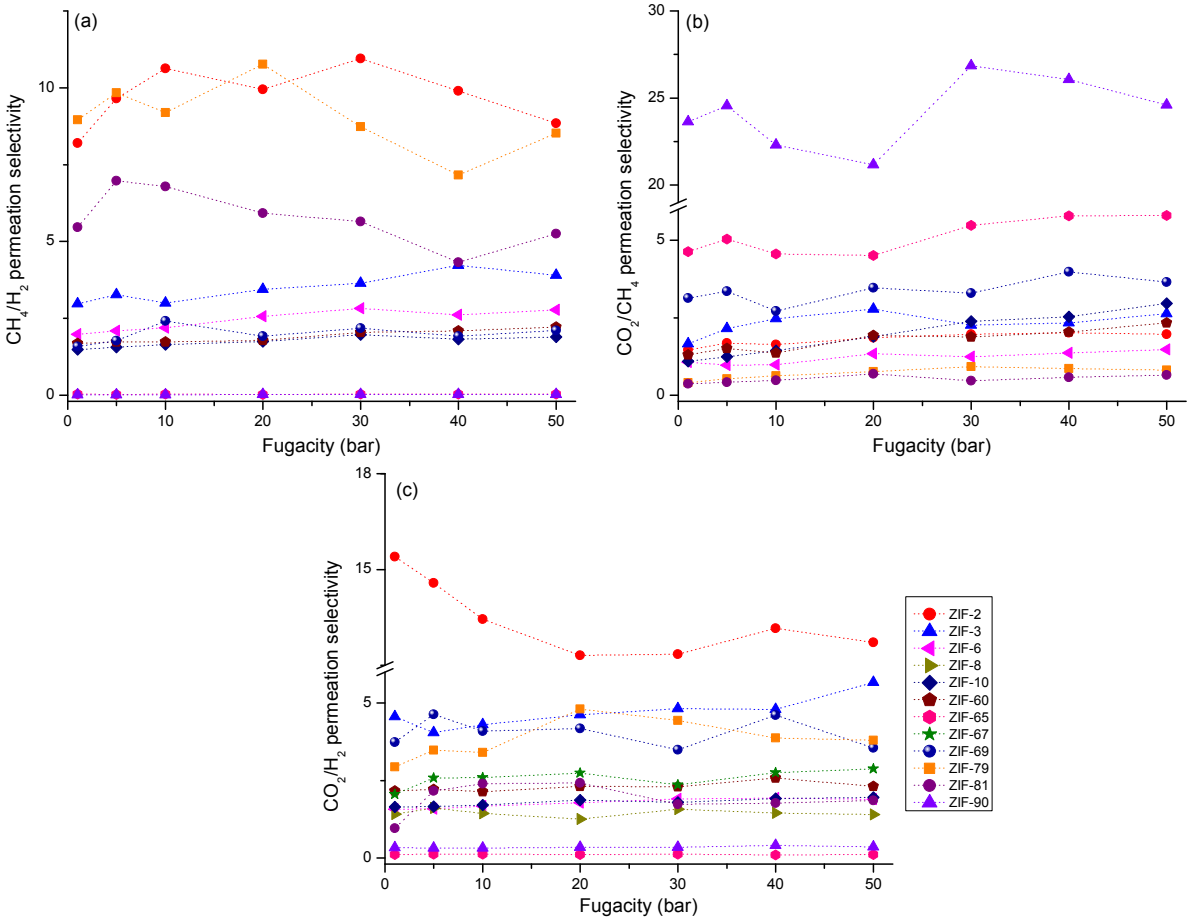

Figure 4.6: Predicted permeation selectivity of ZIFs for (a)CH_4/H_2, (b)CO_2/CH_4 and (c)CO_2/H_2 mixtures at 298 K. The composition of bulk gas mixtures are CH_4/H_2:10/90, CO_2/CH_4:10/90 and CO_2/H_2:1/99.

In addition to comparison of simulations with the available experimental data in section 4.1, permeation selectivities reported in this thesis compared with the other simulation studies which investigated membrane performances of ZIFs. For example, predictions for CO_2 selectivity (1.39) of ZIF-8 membrane from CO_2/H_2:1/99 mixture in this thesis agreed with the CO_2 selectivity (0.5) predicted by Krishna and van Baten [10] for CO_2/H_2:15/85

mixture and selectivity (0.96) predicted by Battisti et al. [50] In addition to ZIF-8, Battisti et al. also studied ZIF-2 and computed very low CO_2 and CH_4 permeation selectivities (~1.5) for CO_2/H_2 and CH_4/H_2 separations, respectively at zero pressure limit. Selectivities of 15.3 and 8.2 were predicted for the same mixtures at 1 bar in this thesis. The reason of this discrepancy can be discussed as follows: Firstly, Battisti et al. rescaled UFF parameters to match their simulation results to one of the experimentally reported CO_2 adsorption isotherm [61] for ZIF-8 and then used the same set of parameters for simulation of ZIF-2. Transferability of adjusted force field parameters has not been tested among different ZIFs. Secondly, they did not consider partial charges for ZIFs which is most likely the reason of their low CO_2/H_2 selectivities compared to results in this thesis. Recent work showed that partial framework charges are important in computing CO_2 adsorption and diffusion in ZIFs [56].

For an efficient membrane-based separation, both high selectivity and permeability are desired. Membranes having high selectivity and low permeability are not economic since they require large surface areas, high capital costs. In order to assess the performance of ZIF membranes for CH_4/H_2, CO_2/CH_4 and CO_2/H_2 separations, they were compared with well known zeolite and nanoporous membranes. Figure 4.7a shows that ZIF-90 and ZIF-65 are H_2 selective membranes for CH_4/H_2 separation similar to LTA and CHA because of their molecular sieving properties. Both selectivity and permeability performance of other ZIF membranes are similar to CuBTT and MOF-177 membranes. None of the ZIFs considered in this thesis can outperform CNTs which show the highest permeation selectivity and permeability for CH_4/H_2 mixtures due to their specific potential energy surface as reported by experiments and predicted by molecular simulations [104, 105]. Among the ZIFs studied in this thesis, ZIF-2 and ZIF-79 can be identified as the best candidates with high gas selectivity (10.63 and 9.19) and permeability (~3×10^5 and ~1.6×10^5 Barrer, respectively) compared to zeolite and other nanoporous membranes.

The CO_2/CH_4 permeation selectivity and CO_2 permeability of ZIFs, zeolites and other nanoporous membranes are shown in Figure 4.7b together with Robeson's upper bound

[36] established for CO_2/CH_4 separations using polymer membranes. Materials that can exceed this upper bound are highly promising candidates. All ZIFs except ZIF-90 are located below the Robeson's upper bound and the reason for high CO_2 permeation selectivity of ZIF-90 is that both adsorption and diffusion selectivity favor CO_2 (see Figures B10 and B33 in Appendix-B). This was also observed for DDR and CHA due to their narrow windows that control molecular transport inside the pores as evidenced by experiments and molecular simulations [106, 107].

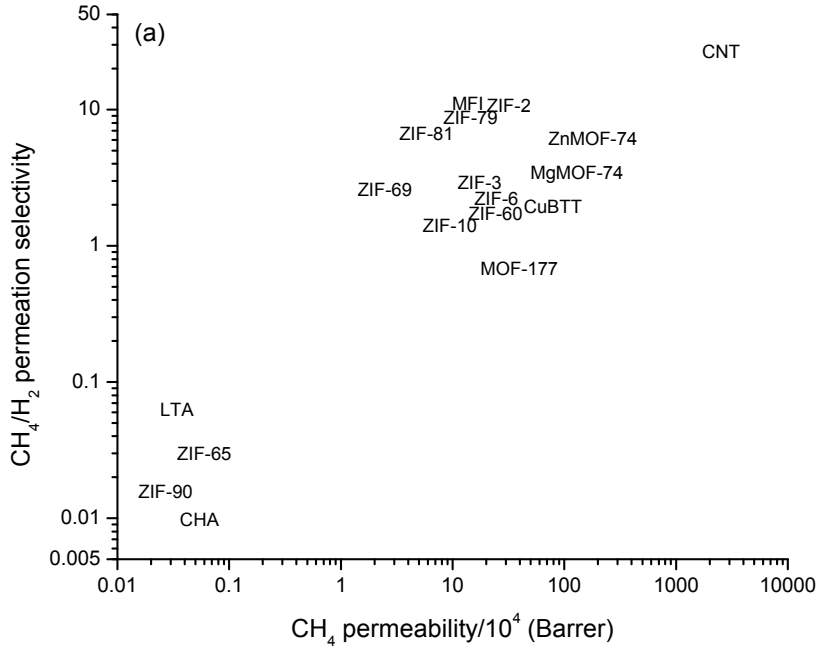

Figure 4.7: a) Permeation-based separation performance of ZIFs for CH_4/H_2 mixture. The bulk gas mixture is CH_4/H_2:10/90 for ZIFs at 298 K, 50/50 for zeolites at 300 K.

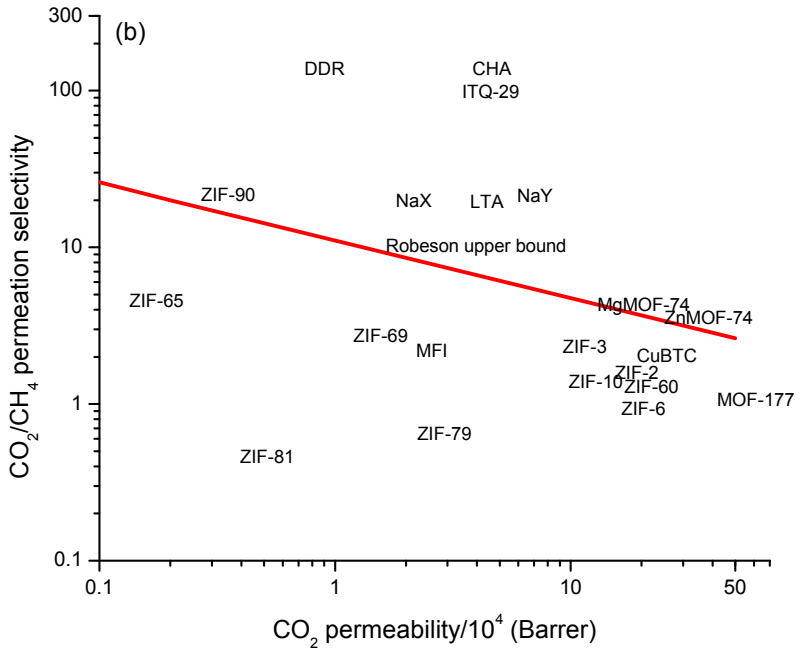

Figure 4.7: b) Permeation-based separation performance of ZIFs for CO_2/CH_4 mixture. The bulk gas mixture is CO_2/CH_4:10/90 for ZIFs at 298 K, 50/50 for zeolites at 300 K.

Figure 4.7c shows that ZIF-65 and ZIF-90 are H_2 selective membranes since high diffusion selectivities of these materials towards H_2 dominated the high adsorption selectivities towards CO_2. Gas permeability and permeation selectivity of ZIF-2 is significantly high compared to CHA, DDR, MFI, CuBTC, MOF-177 and other ZIFs. On the other hand, MgMOF-74 offers high permeation selectivity and permeability due to increased correlation effects within the one dimensional channels when there is a preponderance of CO_2 molecules [10].

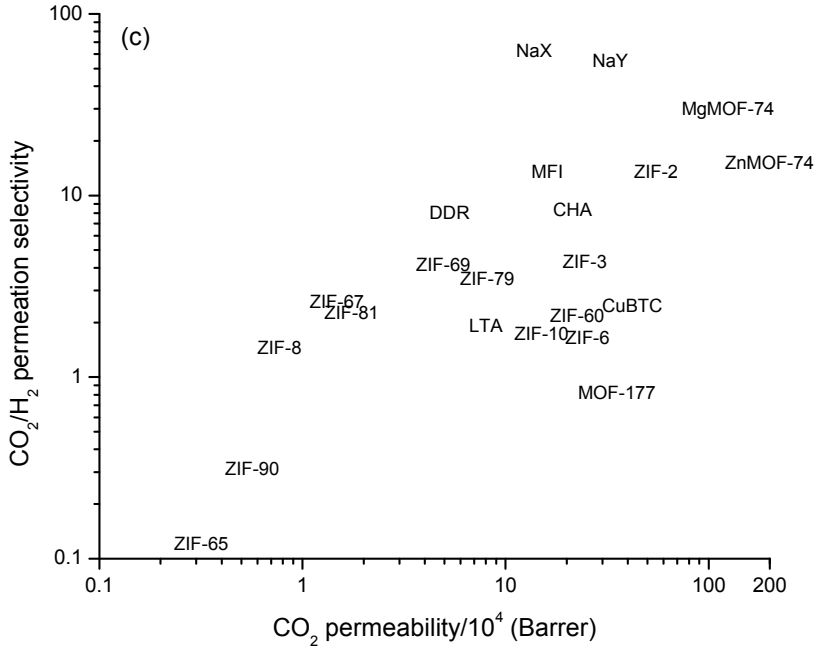

Figure 4.7: c) Permeation-based separation performance of ZIFs for CO_2/H_2 mixture. The bulk gas mixture is CO_2/CH_2:1/99 for ZIFs at 298 K, 15/85 for zeolites at 300 K.

In order to examine how the predictions of simulations would change if a different force field was used, GCMC and EMD simulations for selected ZIFs using DREIDING force field were carried out. Calculations were repeated specifically for ZIF-2, ZIF-69, ZIF-79, ZIF-81 and ZIF-90 since these materials were identified as the membrane candidates with the highest permeation selectivities for CH_4/H_2, CO_2/CH_4 and CO_2/H_2 mixtures. The results are shown in Figure 4.8 and the uncertainties of the calculations were included to show that the predictions of simulations employing different force fields are remarkably close to each other in terms of selectivity and permeability. The idea of this methodology is that the quantitative accuracy of the theoretical predictions must allow making confident judgments for separating promising and unpromising materials. It is obvious from Figure 4.8 that changing the force field of molecular simulations does not change the conclusion about the performance of a material. The largest change was observed for ZIF-90 and even for this

material both force fields suggest that ZIF-90 is a H_2 selective membrane for CH_4/H_2 (CO_2/H_2) separation with low CH_4 (CO_2) permeability.

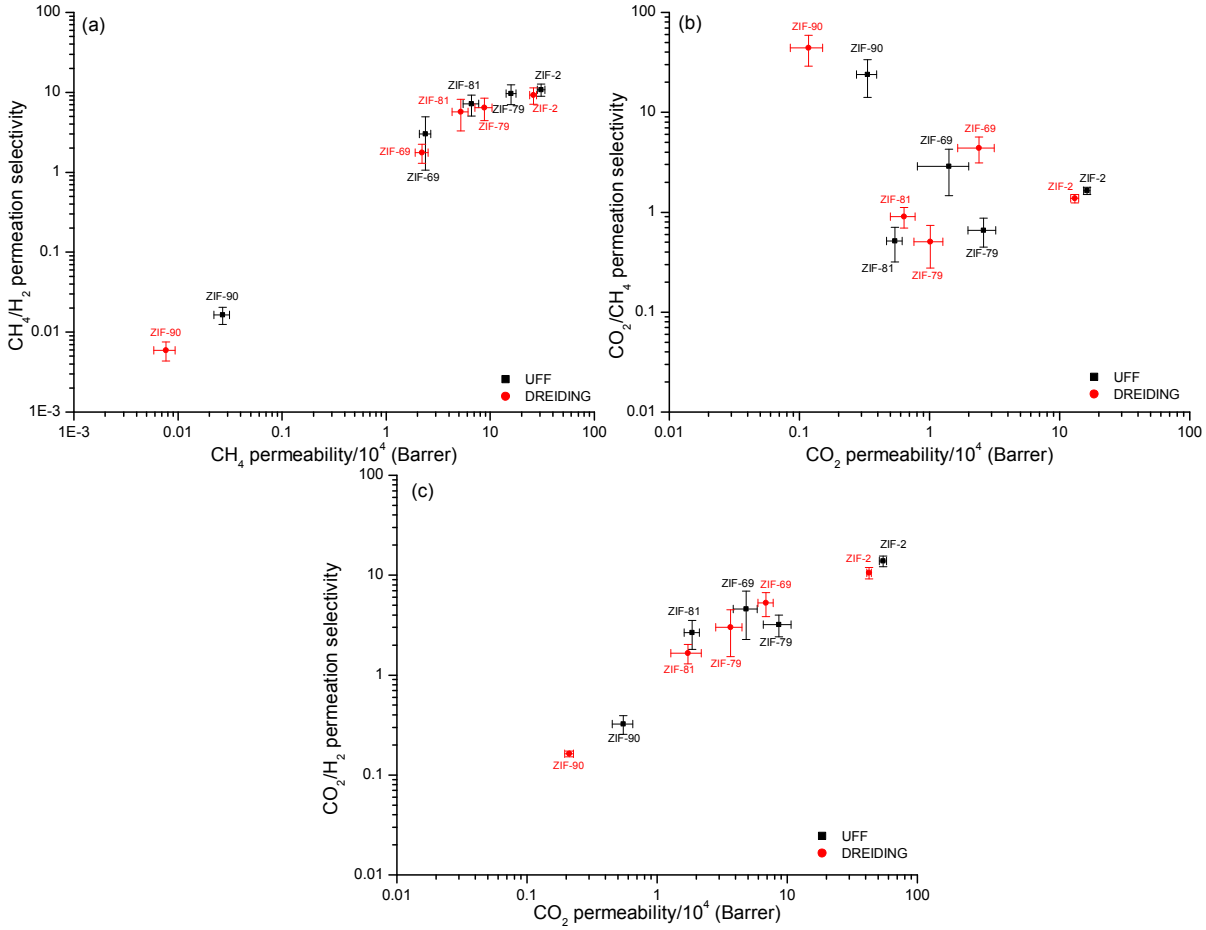

Figure 4.8: Predicted permeation selectivities of ZIFs based on molecular simulations employing UFF and DREIDING force fields for (a)CH_4/H_2, (b)CO_2/CH_4, and (c)CO_2/H_2 mixture separations at 298 K. The bulk gas mixtures are CH_4/H_2:10/90, CO_2/CH_4:10/90 and CO_2/H_2:1/99.

Chapter 5

ZIF/POLYMER COMPOSITE MEMBRANE PERFORMANCES

5.1. Validation of Simulations for ZIF/Polymer Composite Membranes

The aim of chapter 5 is to assess gas separation performances of ZIF/polymer composite membranes using atomically detailed simulations. Several composite membranes have been fabricated using ZIFs as filler particles [42-44]. Experiments observed that gas separation performance of a pure polymer can be improved with ZIF/polymer composite membranes. However, it is possible to design a large number of ZIF/polymer composite membrane with different combinations of ZIFs and polymers. In order to predict promising ZIF/polymer combinations, atomically detailed simulations that evaluate composite membrane performances by screening ZIFs as filler particles are of great importance. Bae et al. [72] fabricated ZIF-90/Ultem and ZIF-90/Matrimid composite membranes and investigated CO_2/CH_4 gas separation performance of these membranes. They showed that ZIF-based composite membranes present great promise for short-term commercial implementation because there is a good adhesion between ZIF-90 and polymers, ZIF-90 can be well dispersed in polymers and the performance of ZIF-90/polymer composites are better than the pure polymers. For example, pure ultem selectivity for CO_2/CH_4 separation was reported as 38.0, whereas ZIF-90/ultem composite membrane was found to have a selectivity of 39.1 under the same conditions. In order to validate the accuracy of atomic and continuum models which is described in section 3.7 for

modeling of ZIF-based composite membranes, theoretical predictions were compared with the available experimental data of CO_2/CH_4 permeation in ZIF-90/Ultem and ZIF-90/Matrimid [72]. Then, gas permeability and gas selectivity were calculated through several ZIF-90/polymer and ZIF-65/polymer membranes composed of different polymers. In addition to ZIF-90, ZIF-65 was selected to predict gas separation performances due to structural similarity with ZIF-90. Various selectivities such as adsorption selectivity, diffusion selectivity, permeation selectivity and ideal selectivity were calculated for both pure ZIF-90 and pure ZIF-65 membranes.

Figure 5.1 shows the performances of pure polymer membranes (Matrimid and Ultem), pure ZIF-90 membrane and ZIF-90/polymer composite membranes. The line on this figure represents the upper bound established for CO_2/CH_4 separations for pure polymer membranes. There is a very good agreement between theoretical predictions and experimental measurements for selectivity and permeability of polymer/ZIF-90 composite membranes. For example, experimental work measured that Ultem/ZIF-90 (Matrimid/ZIF-90) composite membrane has a CO_2 selectivity of 38.7 (34.7) and CO_2 permeability of 2.9 (12.1) Barrer, whereas CO_2 selectivity and permeability were predicted as 38 (35.1) and 2.4 (13.1) Barrer, respectively, in this thesis. Both predictions from molecular simulations and experiments suggested that adding ZIF-90 as filler particles into polymer matrices increases the permeability of CO_2 in polymers. In the case of Ultem, CO_2 permeability was increased from 1.4 to 2.4 Barrers, in Matrimid it was increased from 7.9 to 13.1 Barrers. Since the CO_2/CH_4 selectivity of pure ZIF-90 (8.7) is not as high as pure Matrimid (35.1) or Ultem (38) membranes, there is no significant change in ZIF-90/polymer composite membrane's selectivity relative to pure polymer membrane's selectivity.

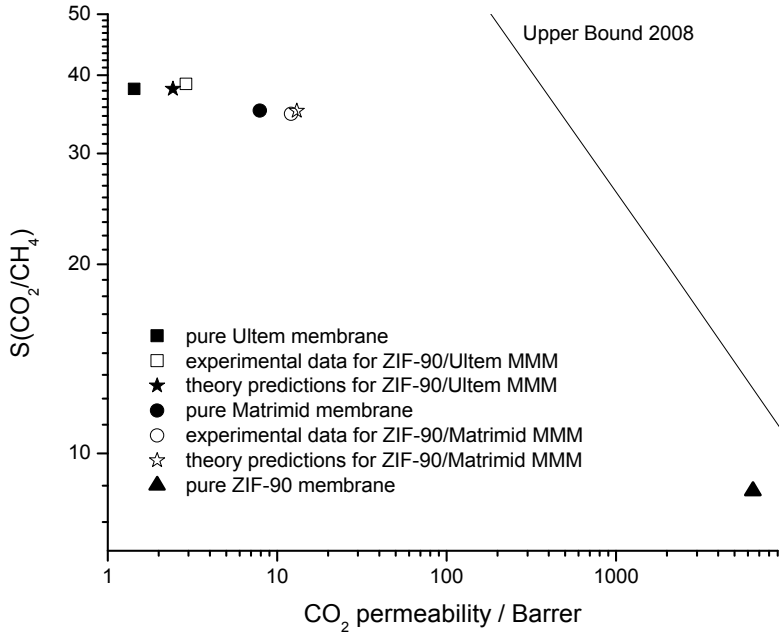

Figure 5.1: Comparison of experimental data [72] and theoretical predictions for ZIF-90/Matrimid and ZIF-90/Ultem composite membranes for CO_2/CH_4 separations.

5.2. H_2 Selectivity and Permeability of ZIF/Polymer Composite Membranes

Once atomistic and continuum models for two ZIF-90/polymer composite membranes were validated, these models were applied to assess the performances of composite membranes having ZIF-90 and ZIF-65 as filler particles for H_2/CO_2 separations. Figures 5.2a and 5.2b show H_2/CO_2 selectivity and H_2 permeability of liquid crystalline polyester, polyaniline, polyimide and poly(trimethylsilypropyne) (PTMSP). These polymers are the ones forming the upper bound (the line in Figure 5.2a,b) for separation of H_2 from CO_2.

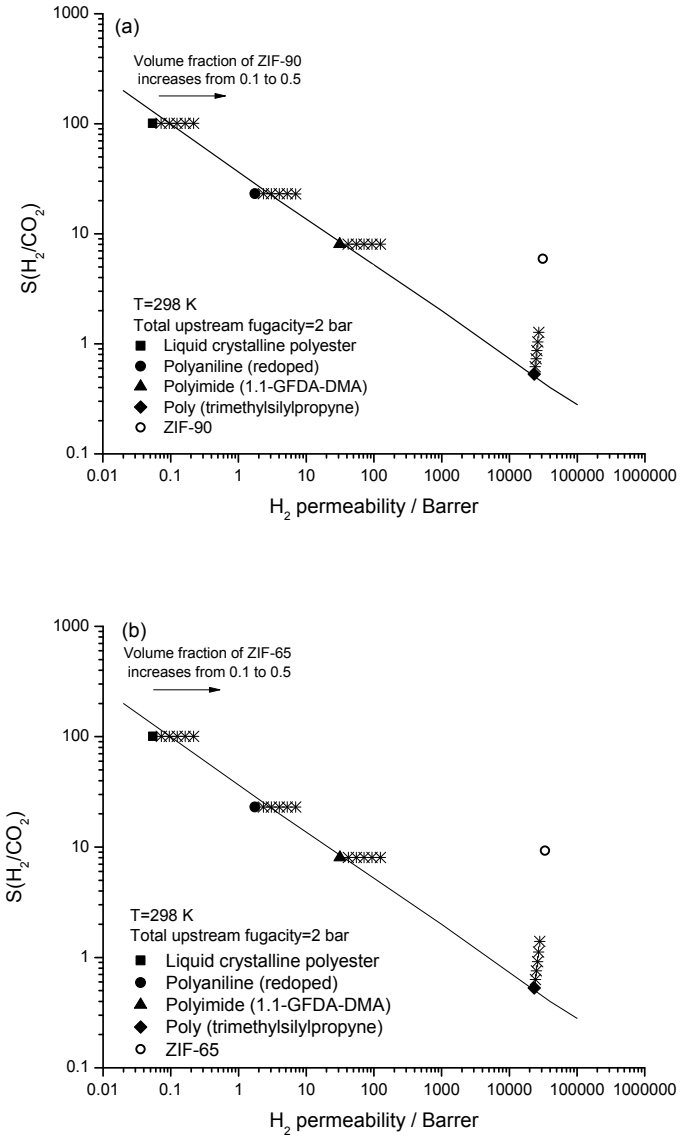

Figure 5.2: Predictions for H_2 selectivity and permeability of composite membranes composed of different types of polymers and a) ZIF-90 b)ZIF-65. In a (b), stars represent the predictions of Maxwell model for composite membranes having ZIF-90 (ZIF-65) with volume fractions varying from 0.1 to 0.5. The line represents present upper bounds established for H_2/CO_2 separations.

All the selectivity and permeability calculations for ZIF-90/polymer (ZIF-65/polymer) composite membranes were performed at a feed pressure of 2 bar and permeate pressure of vacuum to be consisted with the experimental data of pure polymers. Predictions of Maxwell model indicated that as the volume fraction of ZIF-65 and ZIF-90 increases in composite membranes, permeability of H_2 is significantly improved in case of polyester, polyaniline and polyimide. For example, increasing the volume fraction of ZIF-90 from 0 to 0.3 improves the permeability of H_2 from 31.4 to 71.6 Barrer in ZIF-90/polyimide membranes. Figures 5.2a and 5.2b show that liquid crystalline polyester, polyaniline and polyimide can exceed the Robeson's upper bound if the volume fraction of ZIF particles is higher than 0.2. Since the selectivity of these polymers is higher (or very close) than the ZIF-90 and ZIF-65, no selectivity improvement was observed. In contrast to these polymers, both the H_2 selectivity and H_2 permeability of PTMSP increased when ZIFs are used as filler particles. Pure PTMSP is highly permeable (23300 Barrer) with a low H_2 selectivity (0.53). Since ZIF-90 and ZIF-65 exhibit better H_2 selectivity under the same conditions (6 and 9, respectively), adding these as filler particles in PTMSP improved the selectivity. The H_2 permeabilities of PTMSP and ZIFs are very close (~24000), therefore a very slight permeability increase can be achieved.

5.3. Selectivity and Permeability of ZIF-90 and ZIF-65 Membranes

In order to calculate permeation selectivity of a ZIF membrane using equation 3.13, both adsorption and diffusion selectivities are required. To calculate adsorption selectivity, adsorption isotherms of H_2/CO_2 mixtures were computed using GCMC simulations. Figure 5.3 shows both single component adsorption isotherms and mixture isotherms of H_2/CO_2 for 50% and 85% H_2 in the bulk phase. As should be expected from the single component isotherms, adsorption strongly favors CO_2 over H_2 in the mixtures because the more strongly adsorbing CO_2 molecules exclude H_2 molecules in the pores.

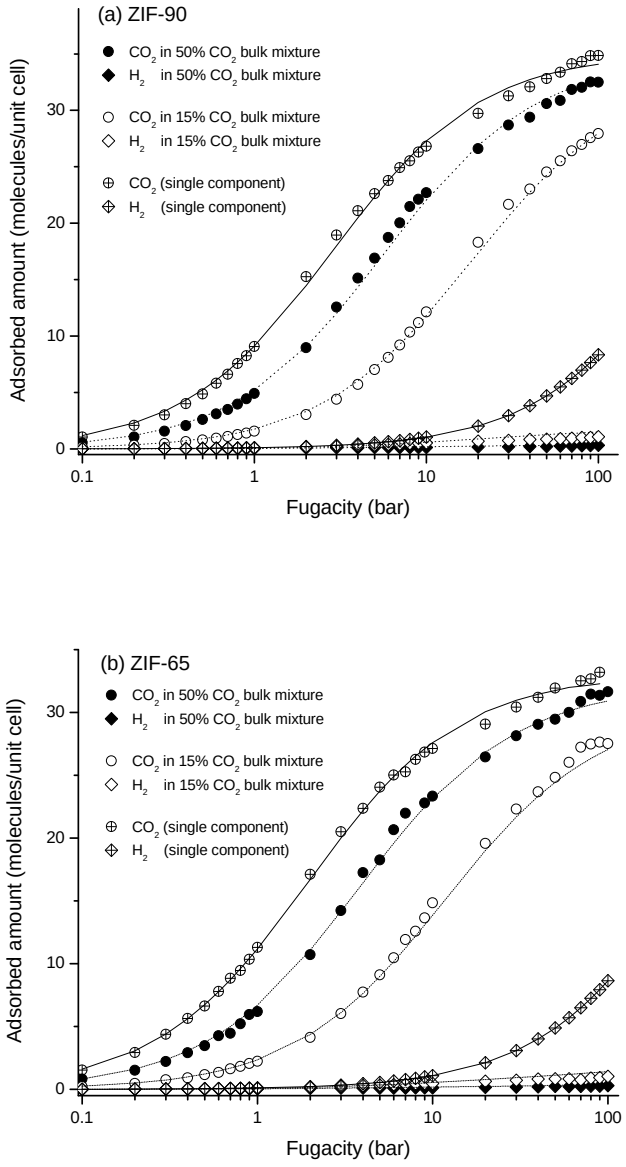

Figure 5.3: Single component and mixture adsorption isotherms for CO_2 and H_2 in a)ZIF-90 b)ZIF-65 at 25°C as computed from GCMC simulations. The composition of the bulk mixture is 50% and 85% H_2. Dotted (Continuous) lines represent the predictions of IAST for CO_2/H_2 mixture adsorption (single component adsorption isotherm fits).

Amount of adsorbed CO_2 (H_2) in the mixture increases (decreases) as the amount of CO_2 increases in the bulk phase. Single component isotherms of CO_2 and H_2 were fitted using a dual-site Langmuir isotherm to apply IAST and the predictions of IAST for mixtures with different compositions are also shown for ZIF-90 and ZIF-65 in Figure 5.3. Similar to the earlier results, there is a very good agreement between GCMC simulation results and IAST predictions for both ZIFs.

Figure 5.4 shows adsorption selectivity, diffusion selectivity, mixture selectivity and ideal selectivity of ZIF-90 and ZIF-65 membranes for separation of H_2/CO_2 mixtures at room temperature as a function of pressure. The selectivities greater (less) than 1 indicate that ZIF membrane is selective for H_2 (CO_2). As shown in Figure 5.3, adsorption favors CO_2 in a H_2/CO_2 mixture due to energetic effects and adsorption selectivities for H_2 (CO_2) are less than 0.01. Since ZIF-90 and ZIF-65 have the same topology (SOD), adsorption selectivities of ZIFs for H_2 are very similar, 0.007 for ZIF-90 and 0.009 for ZIF-65. Adsorption selectivities of both ZIFs was found to be higher than that of IRMOFs [93], similar to CuBTC [108] and Zn(bdc)(ted) [109] under the same conditions. Adsorption selectivities are not significantly affected by the composition of the gas mixtures. In contrast to adsorption selectivity, diffusion selectivity favors H_2 since the weakly adsorbed species (H_2) diffuse faster than the strongly adsorbed species (CO_2). The diffusion selectivity for H_2 over CO_2 is higher in ZIF-65 compared to ZIF-90. This can be explained by examining the self diffusivities of each component in a binary mixture. The degree of confinement of H_2 molecules in ZIF-90 and ZIF-65 pores is similar because H_2 molecule is very small relative to the pore sizes of ZIFs. The self diffusivities of H_2 molecules are ~2-3×10^{-4} cm^2/s in both ZIFs. On the other hand, the degree of confinement of larger CO_2 molecules depends on the pore sizes of the materials.

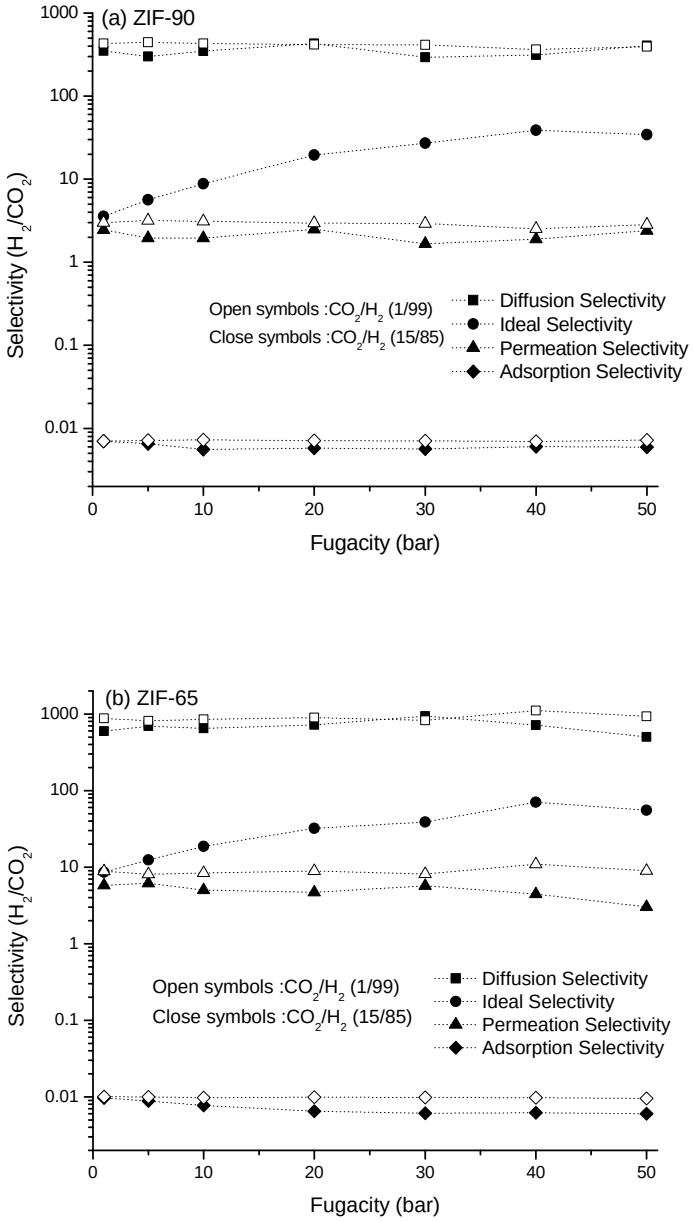

Figure 5.4: Different types of selectivities of a) ZIF-90 b)ZIF-65 membranes at 25°C as a function of fugacity.

Since ZIF-90 has larger pores than ZIF-65, the self diffusivities of CO_2 molecules in the less confined pores of ZIF-90 (6-7×10^{-7} cm^2/s) are slightly higher than the ones in ZIF-65 (4-5×10^{-7} cm^2/s). This difference resulted in higher H_2 diffusion selectivities for ZIF-65.

In examining the mixture selectivity results, the *x* axis of Figure 5.4 can be thought of as the feed pressure of the ZIF membrane because the permeate side is assumed to be at vacuum by equation 3.13. The mixture selectivity for H_2 is smaller than the diffusion selectivity for H_2 as the latter is compensated by the low adsorption selectivity. Mixture selectivities of ZIF-65 for H_2 (~5-6) are higher than those of ZIF-90 (~2) since diffusion selectivities are higher in the former. Past studies [48, 87, 93, 110] showed that several nanoporous membranes, ZIF-3 and ZIF-10 membranes are CO_2 selective. For example, mixture selectivities of ZIF-3 and ZIF-10 for CO_2 were predicted to be 4.3 and 1.7, respectively for CO_2/H_2:1/99 mixtures at 10 bar [48]. In this thesis, the mixture selectivities of ZIF-90 and ZIF-65 for H_2 were predicted to be 3.1 and 8.4, respectively. These results underlined the importance of choice of membrane material for a specific gas separation application. Large pore materials such as isoreticular nanoporous materials, ZIF-3, ZIF-10 are known to give CO_2 selective membranes because separation in these membranes are generally driven by the adsorption selectivities [87]. Materials having large cages connected with narrow pore openings like ZIF-90 and ZIF-65, on the other hand, are H_2 selective due to hindrance in transport of molecules that are larger than narrow pore diameter (CO_2 for H_2/CO_2 separation).

Previous studies showed that the ideal selectivity can be enormously different than mixture selectivity for nanoporous membranes [92, 110]. To see whether this is the case for ZIF membranes, ideal selectivity of ZIF membranes was predicted using shell model approach as described in chapter 3.7 and compared with the permeation selectivity. Figure 5.4 presents that at low pressures ideal and mixture selectivities are very similar but as the pressure increases the ideal selectivity becomes larger than the mixture selectivity. For

instance, at 50 bar the ideal selectivity of ZIF-65 (ZIF-90) membrane for H_2 is approximately 55 (35) meaning that ZIF membrane is very selective for H_2. Under the same conditions, the permeation selectivity of ZIF-65 (ZIF-90) is around 9 (3) indicating that ZIF-65 and ZIF-90 membranes are slightly H_2 selective for separation of H_2/CO_2 mixtures. The difference between ideal selectivity and mixture selectivity at high loadings can be attributed to the multi-component mixture effects [85, 92]. At high loadings strongly adsorbing gas component CO_2 reduces the concentration gradient of the weakly adsorbed gas component H_2 (see Figure 5.3). Furthermore, diffusion rate of the more mobile species, H_2 is decreased by the strongly adsorbing component, CO_2 (see Figure D1 and D2 in Appendix-D). As a result of these two effects, the mixture selectivities are lower than the ideal selectivities of the ZIF membranes.

Figure 5.4 shows that ideal selectivity of both ZIF membranes for H_2 increases as the fugacity increases. For example, the ideal selectivity of ZIF-90 (ZIF-65) is around 3.5 (9) at a feed pressure of 1 bar whereas this number increases up to 35 (55) for a feed pressure of 50 bar. This increase in ideal selectivity can be explained by the trends of single component gas fluxes as shown in Figure 5.5. As the fugacity increases CO_2 approaches saturation (see Figure 5.3) and its concentration gradient remains almost constant. Therefore, the flux of CO_2 is almost constant after the saturation loading (see Figure 5.5). In contrast to CO_2, H_2 is further away from saturation and as the fugacity increases its concentration gradient keeps increasing. Increasing H_2 flux and constant CO_2 flux resulted in an increasing H_2 ideal selectivity for ZIF membranes.

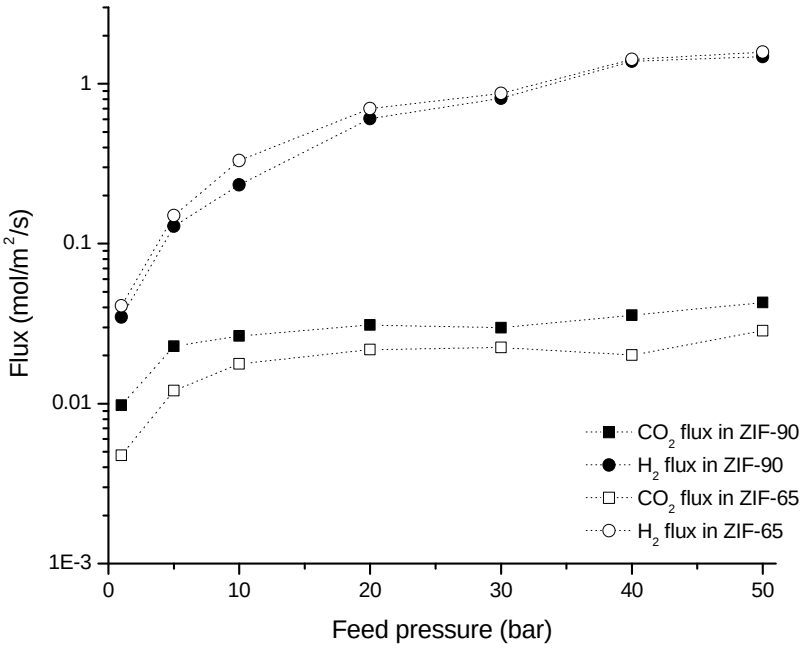

Figure 5.5: Single component gas fluxes in ZIF-90 and ZIF-65 membranes at 25°C as a function of feed pressure.

The two important factors determining the performance of membranes are selectivity and permeability. A highly selective membrane is useless if the permeability is very low since a membrane with low permeability requires high surface area, therefore large capital costs. Figure 5.6 compares the selectivity and permeability of ZIF-65 and ZIF-90 membranes with the widely studied zeolite and nanoporous membranes. Data for ZIF-3, ZIF-10, ZIF-65 and ZIF-90 membranes were calculated at 298 K and at a feed pressure of 10 bar for CO_2/H_2:1/99 composition. Data for other membranes were taken from the study of Krishna and Van Baten [89], in which molecular simulations were carried out at 300 K and 10 bar for CO_2/H_2:15/85 composition. Membranes located on the right hand side of Figure 5.6 are desired to achieve high CO_2 selectivity and high CO_2 permeability. Materials

such as DDR, MFI, CHA, ITQ-29, ZIF-3, ZIF-10, CuBTC, MOF-177, IRMOF-1 exhibit high CO_2 permeability (~10^5 Barrer) due to their large pore volumes. Except MOF-177 and IRMOF-1, these materials are moderately/highly CO_2 selective membranes with selectivities between 1.7 and 10. On the other hand, ZIF-8, ZIF-65, ZIF-90, IRMOF-1 and MOF-177 act as H_2 selective membranes. As discussed earlier, CO_2 permeability of ZIF membranes are very low due to their narrow pore openings compared to some nanoporous membranes.

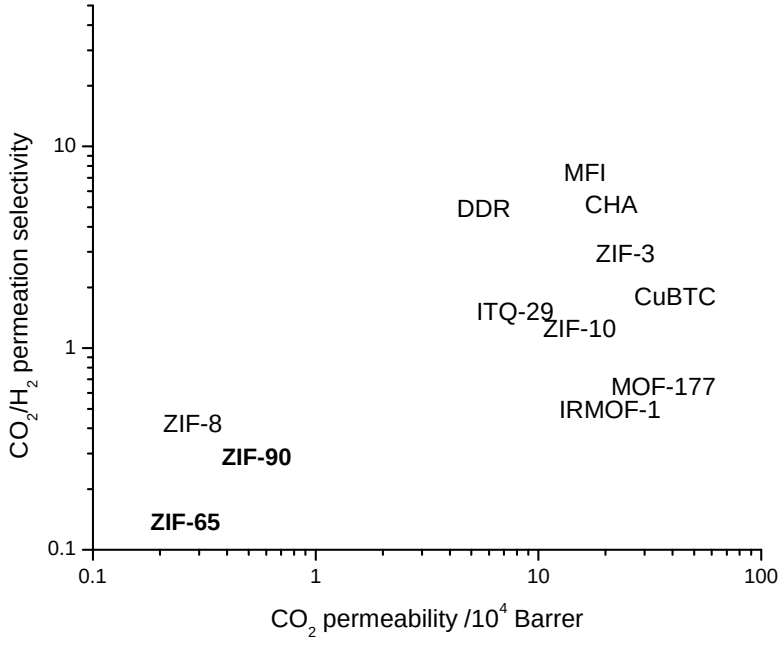

Figure 5.6: Comparison of gas selectivity and permeability of ZIF membranes with zeolite and selected nanoporous membranes.

Chapter 6

CONCLUSIONS

In this thesis, adsorption-based and membrane-based performances of a series of ZIF materials for CH_4/H_2, CO_2/CH_4 and CO_2/H_2 separations were assessed using atomically detailed simulations. Mixture gas permeances from molecular simulations showed good agreement with the experimental gas permeances through thin film membranes of ZIF-90 and ZIF-69, and that validated the accuracy of simulations. Results of calculations showed that several ZIF membranes (adsorbents) outperform widely studied zeolites due to higher selectivity and/or permeability (working capacity). For example, ZIF-2 was found to be very promising as a membrane for CH_4/H_2 and CO_2/H_2 separations, and ZIF-90 was the only membrane located above the Robeson upper bound for CO_2/CH_4 separation. As adsorbents, ZIF-1 and ZIF-79, ZIF-68 and ZIF-90, ZIF-1 were the best performing ones among the studied ZIFs for CH_4/H_2, CO_2/CH_4 and CO_2/H_2 gas separations, respectively. In addition to assessment of adsorption-based and membrane-based performances of ZIFs, ideal selectivity, permeation selectivity of pure ZIF-90 and ZIF-65 membranes were calculated. Performances of these ZIFs as filler particles in various polymers were investigated for H_2/CO_2 separation at different gas compositions. Results showed that both the H_2 selectivity and H_2 permeability of poly(trimethylsilypropyne) increase when ZIFs are used as filler particles.

The main assumption of the molecular simulations in this thesis was rigid ZIF structures. Besides simulations in this thesis, almost all of the molecular simulations for ZIFs and other nanoporous materials in the literature were performed with rigid framework

assumption to save computational time which makes assessment of materials possible in a shorter time period compared to experiments. However, rigid framework assumption cannot be thought as totally correct because structural changes for some nanoporous materials were observed by experiments with adsorption and heating [111]. Since framework flexibility was not considered in molecular simulation of this thesis, membrane selectivities could have been overestimated due to the fact that gas species larger than the material's pore size cannot pass through the membrane. Among ZIFs studied in this thesis, some ZIFs can exhibit framework flexibility. Using density functional theory (DFT) calculations for this type of materials will be appropriate to evaluate the performance of the material, especially for diffusion characteristics [98]. This thesis cannot provide information about the stability of ZIFs in the presence of water. Although several studies showed that ZIFs are stable in the presence of water, steam stability of ZIFs that are not studied experimentally should be tested. Many-body interactions and intramolecular interactions were neglected not to increase computational cost in the molecular simulations. In the literature, it is showed that calculation of two-body interactions can give accurate results without adding multi-body interactions [112]. In membrane calculations, transport diffusivity which describes macroscopic transport of matter needs to be considered for accurate modeling. However, recent calculations showed that self diffusivity can be used instead of transport diffusivity to estimate a membrane's selectivity and permeability with a good accuracy [87, 89].

Gas separation performance of ZIF membranes and ZIF/polymer composite membranes were investigated in this thesis. A large number of ZIFs synthesized in powder form, but have not been fabricated as membranes yet. Therefore, there is no information about the performance of pure ZIF membranes and composite membranes except a few selected ZIFs. This thesis provides information about gas separation performances of a large group

of ZIFs as membranes. As a future work, promising ZIFs that were suggested in thesis can be fabricated and detailed experimental investigations can be performed.

BIBLIOGRAPHY

1. Baker, R.W., Future Directions of Membrane Gas Separation Technology, Industrial & Engineering Chemistry Research, 41 (2002), 1393-1411.
2. Freeman, B. and Y. Yampolskii, Membrane Gas Separation John Wiley & Sons, (2011).
3. Aroussi, A. and F. Benyahia, Proceedings of the 3rd International Gas Processing Symposium, Qatar, Elsevier Science, March (2012).
4. Yao, J., J.J. Chen, and D.G. Elliot, Method and Apparatus for Purification of High Nitrogen Content Gas, (1986).
5. Cavenati, S., C.A. Grande, and A.E. Rodrigues, Adsorption Equilibrium of Methane, Carbon Dioxide, and Nitrogen on Zeolite 13X at High Pressures, Journal of Chemical & Engineering Data, 49 (2004), 1095-1101.
6. Ho, M.T., G.W. Allinson, and D.E. Wiley, Reducing the Cost of CO_2 Capture from Flue Gases Using Pressure Swing Adsorption, Industrial & Engineering Chemistry Research, 47 (2008), 4883-4890.
7. Park, S.J. and M.K. Seo, Interface Science and Composites, Elsevier Science, (2011).
8. Robeson, L.M., W.F. Burgoyne, M. Langsam, A.C. Savoca, and C.F. Tien, High performance polymers for membrane separation, Polymer, 35 (1994), 4970-4978.
9. Hsieh, H.P., Inorganic Membranes for Separation and Reaction, Elsevier, (1996).
10. Krishna, R. and J.M. van Baten, In silico screening of metal-organic frameworks in separation applications, Physical Chemistry Chemical Physics, 13 (2011), 10593.
11. Bose, A.C., Inorganic Membranes for Energy And Environmental Applications, Springer, (2008).
12. Park, K.S., Z. Ni, A.P. Cote, J.Y. Choi, R.D. Huang, F.J. Uribe-Romo, H.K. Chae, M. O'Keeffe, and O.M. Yaghi, Exceptional chemical and thermal stability of zeolitic imidazolate frameworks, Proceedings of the National Academy of Sciences of the United States of America, 103 (2006), 10186-10191.
13. Hayashi, H., A.P. Côté, H. Furukawa, M. O'Keeffe, and O.M. Yaghi, Zeolite A imidazolate frameworks, Nature Materials, 6 (2007), 501-506.
14. Xu, R., Chemistry of Zeolites and Related Porous Materials: Synthesis and Structure, John Wiley & Sons (Asia), (2007).
15. Ishizaki, K., S. Komarneni, and M. Nanko, Porous Materials: Process Technology and Applications, Kluwer Academic Publishers, (1998).
16. Bonneviot, L. and S. Kaliaguine, Zeolites: A Refined Tool for Designing Catalytic Sites: Proceedings of the International Zeolite Symposium, Québec, Canada, Elsevier, October 15-20 (1995).

17. Phan, A., C.J. Doonan, F.J. Uribe-Romo, C.B. Knobler, M. O'Keeffe, and O.M. Yaghi, Synthesis, Structure, and Carbon Dioxide Capture Properties of Zeolitic Imidazolate Frameworks, Accounts of Chemical Research, 43 (2009), 58-67.
18. Baerlocher, C., L.B. McCusker, D. Olson, and I.Z.A.S. Commission, Atlas of Zeolite Framework Types Elsevier, (2007).
19. Liu, D., C. Zheng, Q. Yang, and C. Zhong, Understanding the Adsorption and Diffusion of Carbon Dioxide in Zeolitic Imidazolate Frameworks: A Molecular Simulation Study, The Journal of Physical Chemistry C, 113 (2009), 5004-5009.
20. Liu, B. and B. Smit, Molecular Simulation Studies of Separation of CO_2/N_2, CO_2/CH_4, and CH_4/N_2 by ZIFs, The Journal of Physical Chemistry C, 114 (2010), 8515-8522.
21. Hou, X.-J. and H. Li, Unraveling the High Uptake and Selectivity of CO_2 in the Zeolitic Imidazolate Frameworks ZIF-68 and ZIF-69, The Journal of Physical Chemistry C, 114 (2010), 13501-13508.
22. Banerjee, R., A. Phan, B. Wang, C. Knobler, H. Furukawa, M. O'Keeffe, and O.M. Yaghi, High-Throughput Synthesis of Zeolitic Imidazolate Frameworks and Application to CO_2 Capture, Science, 319 (2008), 939-943.
23. Banerjee, R., H. Furukawa, D. Britt, C. Knobler, M. O'Keeffe, and O.M. Yaghi, Control of Pore Size and Functionality in Isoreticular Zeolitic Imidazolate Frameworks and their Carbon Dioxide Selective Capture Properties, Journal of the American Chemical Society, 131 (2009), 3875-3877.
24. Wang, B., A.P. Cote, H. Furukawa, M. O/'Keeffe, and O.M. Yaghi, Colossal cages in zeolitic imidazolate frameworks as selective carbon dioxide reservoirs, Nature, 453 (2008), 207-211.
25. Morris, W., C.J. Doonan, H. Furukawa, R. Banerjee, and O.M. Yaghi, Crystals as Molecules: Postsynthesis Covalent Functionalization of Zeolitic Imidazolate Frameworks, Journal of the American Chemical Society, 130 (2008), 12626-12627.
26. Huang, X., J. Zhang, and X. Chen, A metal-organic open-framework with sodalite topology, Chinese Science Bulletin, 48 (2003), 1531-1534.
27. Guo, H.-c., F. Shi, Z.-f. Ma, and X.-q. Liu, Molecular Simulation for Adsorption and Separation of CH_4/H_2 in Zeolitic Imidazolate Frameworks, The Journal of Physical Chemistry C, 114 (2010), 12158-12165.
28. Li, B., S. Wei, and L. Chen, Molecular simulation of CO_2, N_2 and CH_4 adsorption and separation in ZIF-78 and ZIF-79, Molecular Simulation, 37 (2011), 1131-1142.
29. Wu, D., C. Wang, B. Liu, D. Liu, Q. Yang, and C. Zhong, Large-scale computational screening of metal-organic frameworks for CH_4/H_2 separation, AIChE Journal, (2011), 58, 2078-2074.
30. Huang, A., H. Bux, F. Steinbach, and J. Caro, Molecular-Sieve Membrane with Hydrogen Permselectivity: ZIF-22 in LTA Topology Prepared with 3-

Aminopropyltriethoxysilane as Covalent Linker, Angewandte Chemie, 122 (2010), 5078-5081.

31. Huang, A., W. Dou, and J.r. Caro, Steam-Stable Zeolitic Imidazolate Framework ZIF-90 Membrane with Hydrogen Selectivity through Covalent Functionalization, Journal of the American Chemical Society, 132 (2010), 15562-15564.
32. Huang, A. and J. Caro, Covalent Post-Functionalization of Zeolitic Imidazolate Framework ZIF-90 Membrane for Enhanced Hydrogen Selectivity, Angewandte Chemie International Edition, 50 (2011), 4979-4982.
33. Liu, Y., E. Hu, E.A. Khan, and Z. Lai, Synthesis and characterization of ZIF-69 membranes and separation for CO_2/CO mixture, Journal of Membrane Science, 353 (2010), 36-40.
34. Liu, Y., G. Zeng, Y. Pan, and Z. Lai, Synthesis of highly c-oriented ZIF-69 membranes by secondary growth and their gas permeation properties, Journal of Membrane Science, 379 (2011), 46-51.
35. Li, Y.-S., F.-Y. Liang, H. Bux, A. Feldhoff, W.-S. Yang, and J. Caro, Molecular Sieve Membrane: Supported Metal–Organic Framework with High Hydrogen Selectivity, Angewandte Chemie, 122 (2010), 558-561.
36. Lloyd M, R., The upper bound revisited, Journal of Membrane Science, 320 (2008), 390-400.
37. Li, Y., F. Liang, H. Bux, W. Yang, and J. Caro, Zeolitic imidazolate framework ZIF-7 based molecular sieve membrane for hydrogen separation, Journal of Membrane Science, 354 (2010), 48-54.
38. Bux, H., F. Liang, Y. Li, J. Cravillon, M. Wiebcke, and J.r. Caro, Zeolitic Imidazolate Framework Membrane with Molecular Sieving Properties by Microwave-Assisted Solvothermal Synthesis, Journal of the American Chemical Society, 131 (2009), 16000-16001.
39. Venna, S.R. and M.A. Carreon, Highly Permeable Zeolite Imidazolate Framework-8 Membranes for CO_2/CH_4 Separation, Journal of the American Chemical Society, 132 (2009), 76-78.
40. Bux, H., C. Chmelik, J.M. van Baten, R. Krishna, and J. Caro, Novel MOF-Membrane for Molecular Sieving Predicted by IR-Diffusion Studies and Molecular Modeling, Advanced Materials, 22 (2010), 4741-4743.
41. Chmelik, C., H. Voß, H. Bux, and J. Caro, Adsorption and Diffusion – Basis for Molecular Understanding of Permeation through Molecular Sieve Membranes, Chemie Ingenieur Technik, 83 (2011), 104-112.
42. Liu, X.-L., Y.-S. Li, G.-Q. Zhu, Y.-J. Ban, L.-Y. Xu, and W.-S. Yang, An Organophilic Pervaporation Membrane Derived from Metal–Organic Framework Nanoparticles for Efficient Recovery of Bio-Alcohols, Angewandte Chemie International Edition, 50 (2011), 10636-10639.

43. Yang, T., Y. Xiao, and T.-S. Chung, Poly-/metal-benzimidazole nano-composite membranes for hydrogen purification, Energy & Environmental Science, 4 (2011), 4171-4180.
44. Zhang, C., Y. Dai, J.R. Johnson, O. Karvan, and W.J. Koros, High performance ZIF-8/6FDA-DAM mixed matrix membrane for propylene/propane separations, Journal of Membrane Science, 389 (2012), 34-42.
45. Getman, R.B., Y.-S. Bae, C.E. Wilmer, and R.Q. Snurr, Review and Analysis of Molecular Simulations of Methane, Hydrogen, and Acetylene Storage in Metal–Organic Frameworks, Chemical Reviews, 112 (2011), 703-723.
46. Duren, T., Y.-S. Bae, and R.Q. Snurr, Using molecular simulation to characterise metal-organic frameworks for adsorption applications, Chemical Society Reviews, 38 (2009), 1237-1247.
47. Haldoupis, E., S. Nair, and D.S. Sholl, Finding MOFs for Highly Selective CO_2/N_2 Adsorption Using Materials Screening Based on Efficient Assignment of Atomic Point Charges, Journal of the American Chemical Society, 134 (2012), 4313-4323.
48. Keskin, S., Atomistic Simulations for Adsorption, Diffusion, and Separation of Gas Mixtures in Zeolite Imidazolate Frameworks, The Journal of Physical Chemistry C, 115 (2010), 800-807.
49. Liu, J., S. Keskin, D.S. Sholl, and J.K. Johnson, Molecular Simulations and Theoretical Predictions for Adsorption and Diffusion of CH_4/H_2 and CO_2/CH_4 Mixtures in ZIFs, The Journal of Physical Chemistry C, 115 (2011), 12560-12566.
50. Battisti, A., S. Taioli, and G. Garberoglio, Zeolitic imidazolate frameworks for separation of binary mixtures of CO_2, CH_4, N_2 and H_2: A computer simulation investigation, Microporous and Mesoporous Materials, 143 (2011), 46-53.
51. Atci, E. and S. Keskin, Atomically Detailed Models for Transport of Gas Mixtures in ZIF Membranes and ZIF/Polymer Composite Membranes, Industrial & Engineering Chemistry Research, 51 (2012), 3091-3100.
52. Rappe, A.K., C.J. Casewit, K.S. Colwell, W.A. Goddard, and W.M. Skiff, UFF, a full periodic table force field for molecular mechanics and molecular dynamics simulations, Journal of the American Chemical Society, 114 (1992), 10024-10035.
53. Allinger, N.L., Conformational analysis. 130. MM2. A hydrocarbon force field utilizing V1 and V2 torsional terms, Journal of the American Chemical Society, 99 (1977), 8127-8134.
54. Sprague, J.T., J.C. Tai, Y. Yuh, and N.L. Allinger, The MMP2 calculational method, Journal of Computational Chemistry, 8 (1987), 581-603.
55. Allinger, N.L., Y.H. Yuh, and J.H. Lii, Molecular mechanics: The MM3 force field for hydrocarbons 1, Journal of the American Chemical Society, 111 (1989), 8551-8566.

56. Rankin, R.B., J. Liu, A.D. Kulkarni, and J.K. Johnson, Adsorption and Diffusion of Light Gases in ZIF-68 and ZIF-70: A Simulation Study, The Journal of Physical Chemistry C, 113 (2009), 16906-16914.
57. Sirjoosingh, A., S. Alavi, and T.K. Woo, Grand-Canonical Monte Carlo and Molecular-Dynamics Simulations of Carbon-Dioxide and Carbon-Monoxide Adsorption in Zeolitic Imidazolate Framework Materials, The Journal of Physical Chemistry C, 114 (2010), 2171-2178.
58. Morris, W., B. Leung, H. Furukawa, O.K. Yaghi, N. He, H. Hayashi, Y. Houndonougbo, M. Asta, B.B. Laird, and O.M. Yaghi, A Combined Experimental−Computational Investigation of Carbon Dioxide Capture in a Series of Isoreticular Zeolitic Imidazolate Frameworks, Journal of the American Chemical Society, 132 (2010), 11006-11008.
59. Amrouche, H., S. Aguado, J. Pérez-Pellitero, C.l. Chizallet, F. Siperstein, D. Farrusseng, N. Bats, and C. Nieto-Draghi, Experimental and Computational Study of Functionality Impact on Sodalite–Zeolitic Imidazolate Frameworks for CO_2 Separation, The Journal of Physical Chemistry C, 115 (2011), 16425-16432.
60. Zhou, W., H. Wu, M.R. Hartman, and T. Yildirim, Hydrogen and Methane Adsorption in Metal−Organic Frameworks: A High-Pressure Volumetric Study, The Journal of Physical Chemistry C, 111 (2007), 16131-16137.
61. Pérez-Pellitero, J., H. Amrouche, F.R. Siperstein, G. Pirngruber, C. Nieto-Draghi, G. Chaplais, A. Simon-Masseron, D. Bazer-Bachi, D. Peralta, and N. Bats, Adsorption of CO_2, CH_4, and N_2 on Zeolitic Imidazolate Frameworks: Experiments and Simulations, Chemistry – A European Journal, 16 (2010), 1560-1571.
62. Mayo, S.L., B.D. Olafson, and W.A. Goddard, DREIDING: a generic force field for molecular simulations, The Journal of Physical Chemistry, 94 (1990), 8897-8909.
63. Buch, V., Path integral simulations of mixed para-D2 and ortho-D2 clusters: The orientational effects, Journal of Chemical Physics, 100 (1994), 7610.
64. Martin, M.G. and J.I. Siepmann, Transferable Potentials for Phase Equilibria. 1. United-Atom Description of n-Alkanes, The Journal of Physical Chemistry B, 102 (1998), 2569-2577.
65. Rappé, A.K. and C.J. Casewit, Molecular Mechanics Across Chemistry University Science Books, (1997).
66. Potoff, J.J. and J.I. Siepmann, Vapor–liquid equilibria of mixtures containing alkanes, carbon dioxide, and nitrogen, AIChE Journal, 47 (2001), 1676-1682.
67. Makrodimitris, K., G.K. Papadopoulos, and D.N. Theodorou, Prediction of Permeation Properties of CO_2 and N_2 through Silicalite via Molecular Simulations, The Journal of Physical Chemistry B, 105 (2001), 777-788.
68. Leszczynski, J., Handbook of Computational Chemistry, Springer, (2012).

69. Xu, Q. and C. Zhong, A General Approach for Estimating Framework Charges in Metal−Organic Frameworks, The Journal of Physical Chemistry C, 114 (2010), 5035-5042.
70. Francl, M.M., C. Carey, L.E. Chirlian, and D.M. Gange, Charges Fit to Electrostatic Potentials. II. Can Atomic Charges Be Unambiguously Fit to Electrostatic Potentials?, Journal of Computational Chemistry, 17 (1996), 367.
71. Watanabe, T., T.A. Manz, and D.S. Sholl, Accurate Treatment of Electrostatics during Molecular Adsorption in Nanoporous Crystals without Assigning Point Charges to Framework Atoms, The Journal of Physical Chemistry C, 115 (2011), 4824-4836.
72. Bae, T.-H., J.S. Lee, W. Qiu, W.J. Koros, C.W. Jones, and S. Nair, A High-Performance Gas-Separation Membrane Containing Submicrometer-Sized Metal–Organic Framework Crystals, Angewandte Chemie International Edition, 49 (2010), 9863-9866.
73. Chen, E.-Y., Y.-C. Liu, M. Zhou, L. Zhang, and Q. Wang, Effects of structure on hydrogen adsorption in zeolitic imidazolate frameworks, Chemical Engineering Science, 71 (2012), 178-184.
74. Frenkel, D. and B. Smit, Understanding Molecular Simulation: From Algorithms to Applications, Academic Press, (2002).
75. Ungerer, P., B. Tavitian, and A. Boutin, Applications of Molecular Simulation in the Oil and Gas Industry: Monte Carlo Methods, Editions Technip, (2005).
76. Keskin, S., Recent Advances in Molecular Dynamics Simulations of Gas Diffusion in Metal Organic Frameworks, Molecular Dynamics-Theoretical Developments and Applications in Nanotechnology and Energy, (2012), 255-280.
77. Sanborn, M.J. and R.Q. Snurr, Diffusion of binary mixtures of CF_4 and n-alkanes in faujasite, Separation and Purification Technology, 20 (2000), 1-13.
78. Ackerman, D.M., A.I. Skoulidas, D.S. Sholl, and J. Karl Johnson, Diffusivities of Ar and Ne in Carbon Nanotubes, Molecular Simulation, 29 (2003), 677-684.
79. Keil, F.J., R. Krishna, and M.O. Coppens, Modeling of diffusion in zeolites, Reviews in Chemical Engineering, 16 (2000), 71-197.
80. Kärger, J. and D. Ruthven, Diffusion in Zeolites and Other Microporous Materials, John Wiley & Sons, New York, (1992).
81. Myers, A.L. and J.M. Prausnitz, Thermodynamics of Mixed-Gas Adsorption, AIChE Journal, 11 (1965), 121-125.
82. Chen, H. and D.S. Sholl, Efficient simulation of binary adsorption isotherms using Transition Matrix Monte Carlo, Langmuir, 22 (2006), 709-716.
83. Krishna, R. and D. Paschek, Self-diffusivities in multicomponent mixtures in zeolites, Physical Chemistry Chemical Physics, 4 (2002), 1891-1898.

84. Krishna, R. and J.M. van Baten, Describing binary mixture diffusion in carbon nanotubes with the Maxwell-Stefan equations. An investigation using molecular dynamics simulations, Industrial & Engineering Chemistry Research, 45 (2006), 2084-2093.
85. Skoulidas, A.I., D.S. Sholl, and R. Krishna, Correlation effects in diffusion of CH_4/CF_4 mixtures in MFI zeolite. A study linking MD simulations with the Maxwell-Stefan formulation, Langmuir, 19 (2003), 7977-7988.
86. Keskin, S., J. Liu, J.K. Johnson, and D.S. Sholl, Testing the Accuracy of Correlations for Multicomponent Mass Transport of Adsorbed Gases in Metal−Organic Frameworks: Diffusion of H_2/CH_4 Mixtures in CuBTC, Langmuir, 24 (2008), 8254-8261.
87. Keskin, S. and D.S. Sholl, Efficient Methods for Screening of Metal Organic Framework Membranes for Gas Separations using Atomically-detailed Models, Langmuir, 25 (2009), 11786-11795.
88. Krishna, R. and J.M. van Baten, Using molecular simulations for screening of zeolites for separation of CO_2/CH_4 mixtures, Chemical Engineering Journal, 133 (2007), 121-131.
89. Krishna, R. and J.M. van Baten, In silica screening of zeolite membranes for CO_2 Capture, Journal of Membrane Science, 360 (2010), 323-333.
90. Sholl, D.S., Understanding macroscopic diffusion of adsorbed molecules in crystalline nanoporous materials via atomistic simulations, Accounts of Chemical Research, 39 (2006), 403-411.
91. Wesselingh, J.A. and R. Krishna, Mass Transfer in Multicomponent Mixtures, Delft University Press, Delft, (2000).
92. Keskin, S. and D.S. Sholl, Screening Metal-Organic Framework Materials for Membrane-based Methane/Carbon Dioxide Separations, The Journal of Physical Chemistry C, 111 (2007), 14055-14059.
93. Keskin, S. and D.S. Sholl, Assessment of a Metal-Organic Framework Membrane for Gas Separations Using Atomically Detailed Calculations: CO_2, CH_4, N_2, H_2 mixtures in MOF-5, Industrial and Engineering Chemistry Research, 48 (2009), 914-922.
94. Kesting, R.E. and A.K. Fritzsche, Polymeric Gas Separation Membranes, John Wiley & Sons, Inc., New York, (1993).
95. Maxwell, J.C., A Treatise on Electricity and Magnetism Dover Publications, New York, (1954).
96. McCarthy, M.C., V. Varela-Guerrero, G.V. Barnett, and H.-K. Jeong, Synthesis of Zeolitic Imidazolate Framework Films and Membranes with Controlled Microstructures, Langmuir, 26 (2010), 14636-14641.

97. Hertäg, L., H. Bux, J. Caro, C. Chmelik, T. Remsungnen, M. Knauth, and S. Fritzsche, Diffusion of CH_4 and H_2 in ZIF-8, Journal of Membrane Science, 377 (2011), 36-41.
98. Watanabe, T., S. Keskin, S. Nair, and D.S. Sholl, Computational identification of a metal organic framework for high selectivity membrane-based CO2/CH4 separations: Cu(hfipbb)$(H_2$hfipbb$)_{0.5}$, Physical Chemistry Chemical Physics, 11 (2009), 11389-11394.
99. Haldoupis, E., S. Nair, and D.S. Sholl, Efficient Calculation of Diffusion Limitations in Metal Organic Framework Materials: A Tool for Identifying Materials for Kinetic Separations, Journal of the American Chemical Society, 132 (2010), 7528-7539.
100. Newsome, D.A. and D.S. Sholl, Predictive Assessment of Surface Resistances in Zeolite Membranes Using Atomically Detailed Models, The Journal of Physical Chemistry B, 109 (2005), 7237-7244.
101. Belmabkhout, Y., G. Pirngruber, E. Jolimaitre, and A. Methivier, A complete experimental approach for synthesis gas separation studies using static gravimetric and column breakthrough experiments, Adsorption, 13 (2007), 341-349.
102. Yang, R.T., Gas Separation by Adsorption Processes, Butterworths, Boston, (1987).
103. Keskin, S., Adsorption, Diffusion, and Separation of CH_4/H_2 Mixtures in Covalent Organic Frameworks: Molecular Simulations and Theoretical Predictions, The Journal of Physical Chemistry C, 116 (2011), 1772-1779.
104. Skoulidas, A.I., D.M. Ackerman, J.K. Johnson, and D.S. Sholl, Rapid Transport of Gases in Carbon Nanotubes, Physical Review Letters, 89 (2002), 185901.
105. Holt, J.K., H.G. Park, Y. Wang, M. Stadermann, A.B. Artyukhin, C.P. Grigoropoulos, A. Noy, and O. Bakajin, Fast Mass Transport Through Sub-2-Nanometer Carbon Nanotubes, Science, 312 (2006), 1034-1037.
106. Li, S., J.L. Falconer, R.D. Noble, and R. Krishna, Interpreting Unary, Binary, and Ternary Mixture Permeation Across a SAPO-34 Membrane with Loading-Dependent Maxwell−Stefan Diffusivities, The Journal of Physical Chemistry C, 111 (2007), 5075-5082.
107. Jee, S.E. and D.S. Sholl, Carbon Dioxide and Methane Transport in DDR Zeolite: Insights from Molecular Simulations into Carbon Dioxide Separations in Small Pore Zeolites, Journal of the American Chemical Society, 131 (2009), 7896-7904.
108. Yang, Q. and C. Zhong, Molecular simulation of carbon dioxide/methane/hydrogen mixture adsorption in metal-organic frameworks, The Journal of Physical Chemistry B, 110 (2006), 17776-17783.
109. Erucar, I. and S. Keskin, Separation of CO_2 Mixtures Using Zn(bdc)$(ted)_{0.5}$ Membranes and Composites: A Molecular Simulation Study, The Journal of Physical Chemistry C, 15 (2011), 13637-13644.

110. Keskin, S., J. Liu, J.K. Johnson, and D.S. Sholl, Atomically-detailed models of gas mixture diffusion through CuBTC membranes, Microporous Mesoporous Material, 125 (2009), 101-106.
111. Ferey, G. and C. Serre, Large breathing effects in three-dimensional porous hybrid matter: facts, analyses, rules and consequences, Chemical Society Reviews, 38 (2009), 1380-1399.
112. Sloot, P., Computational Science-ICCS 2002: International Conference, Amsterdam, The Netherlands, April 21-24, 2002 : Proceedings Springer, (2002).

APPENDIX

Appendix-A: Unit Cell Representation of ZIFs

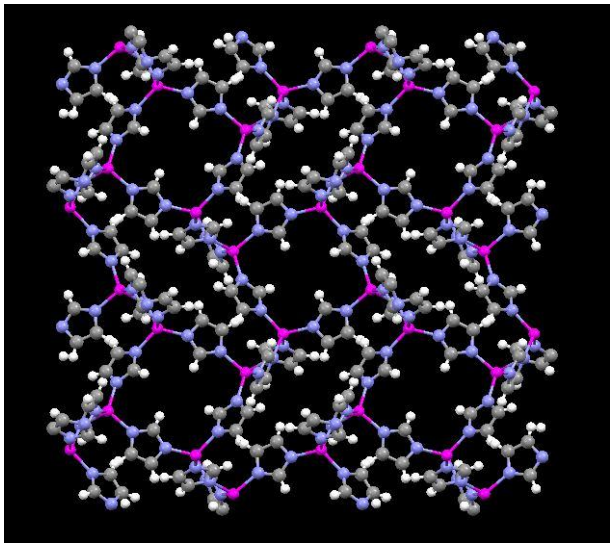

Figure A1: ZIF-1 (a)

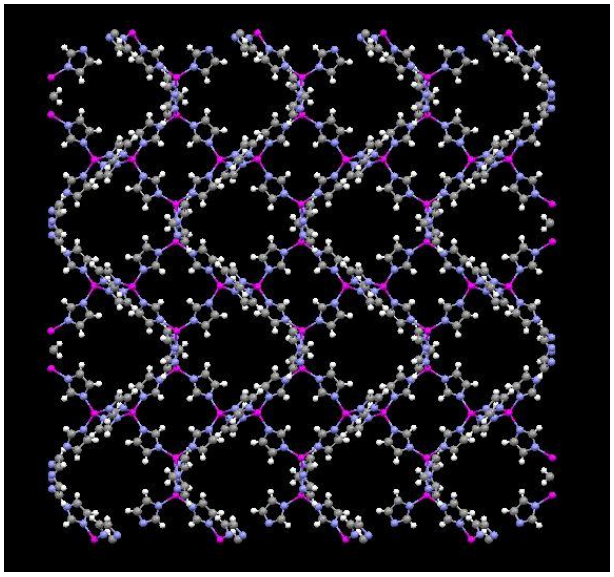

Figure A2: ZIF-2 (a)

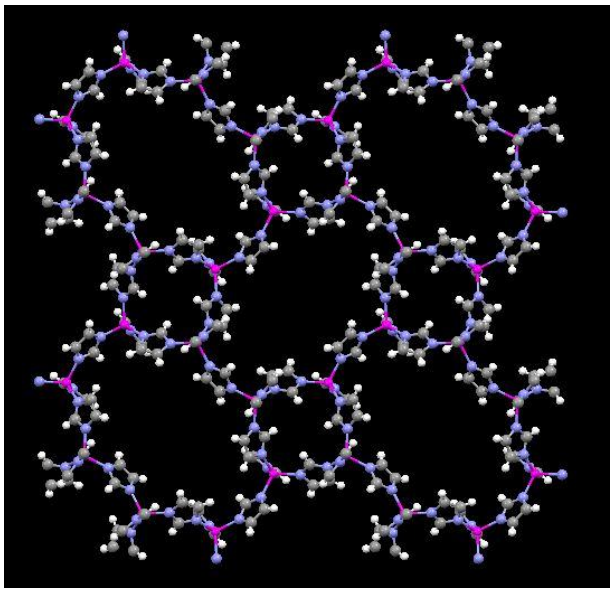

Figure A3: ZIF-3 (c)

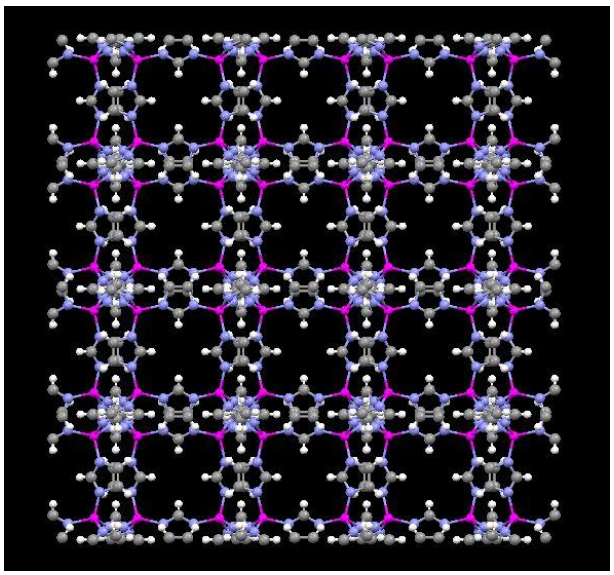

Figure A4: ZIF-6 (c)

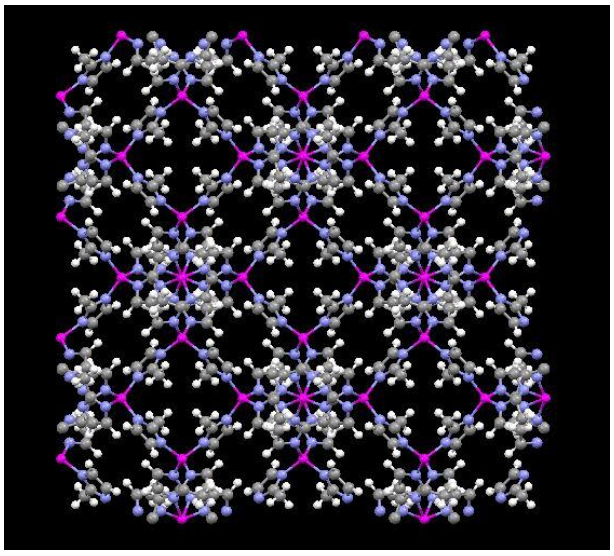

Figure A5: ZIF-8 (a)

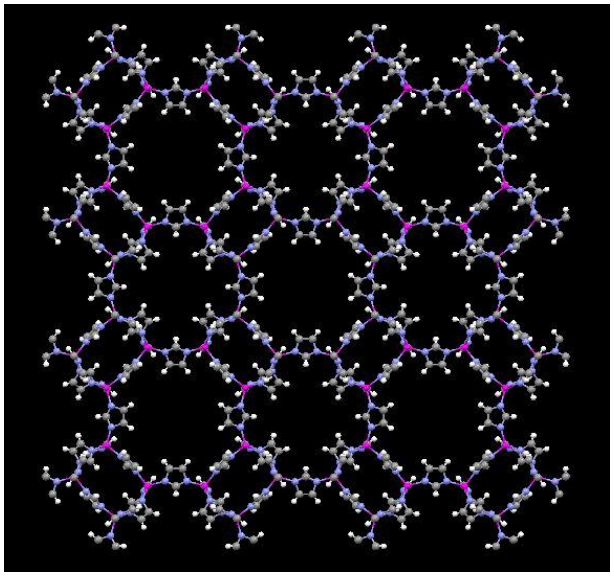

Figure A6: ZIF-10 (c)

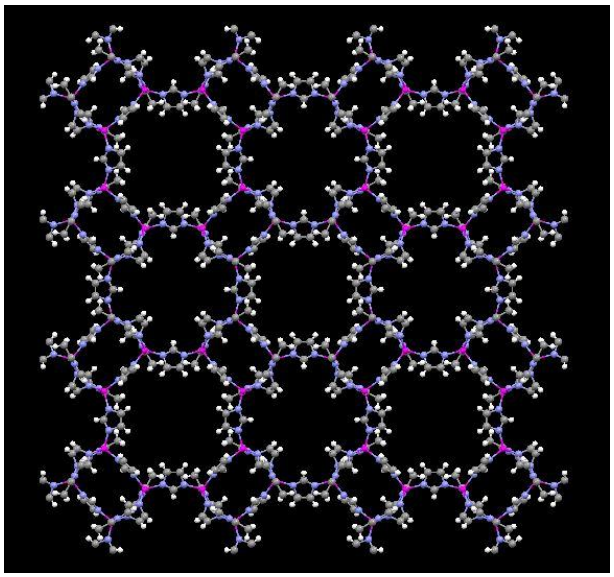

Figure A7: ZIF-60 (c)

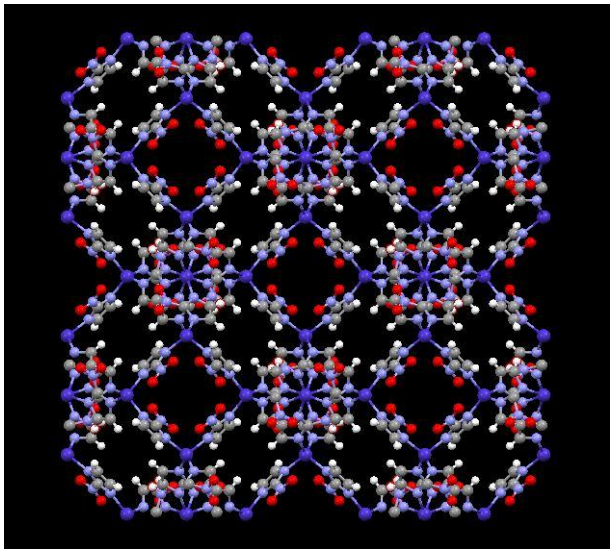

Figure A8: ZIF-65 (a)

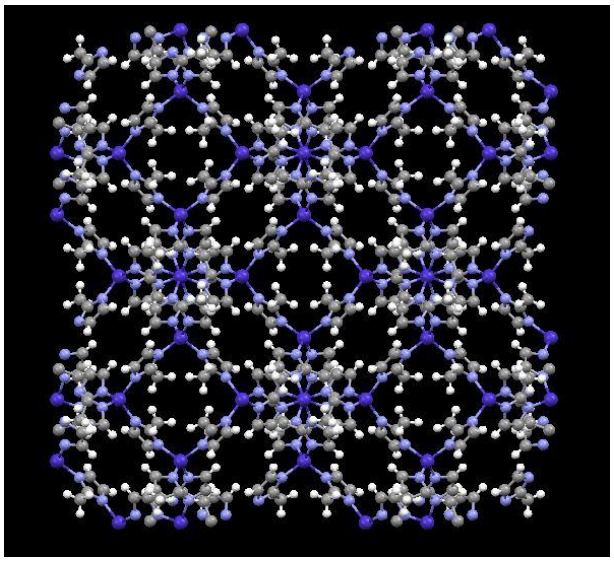

Figure A9: ZIF-67 (a)

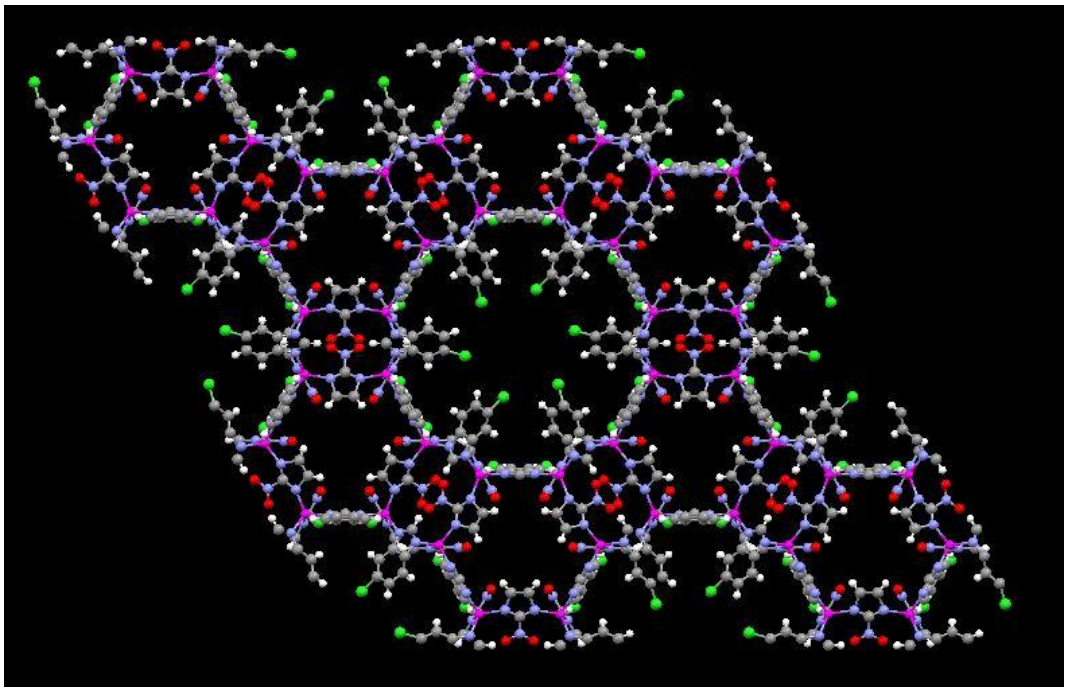

Figure A10: ZIF-69 (c)

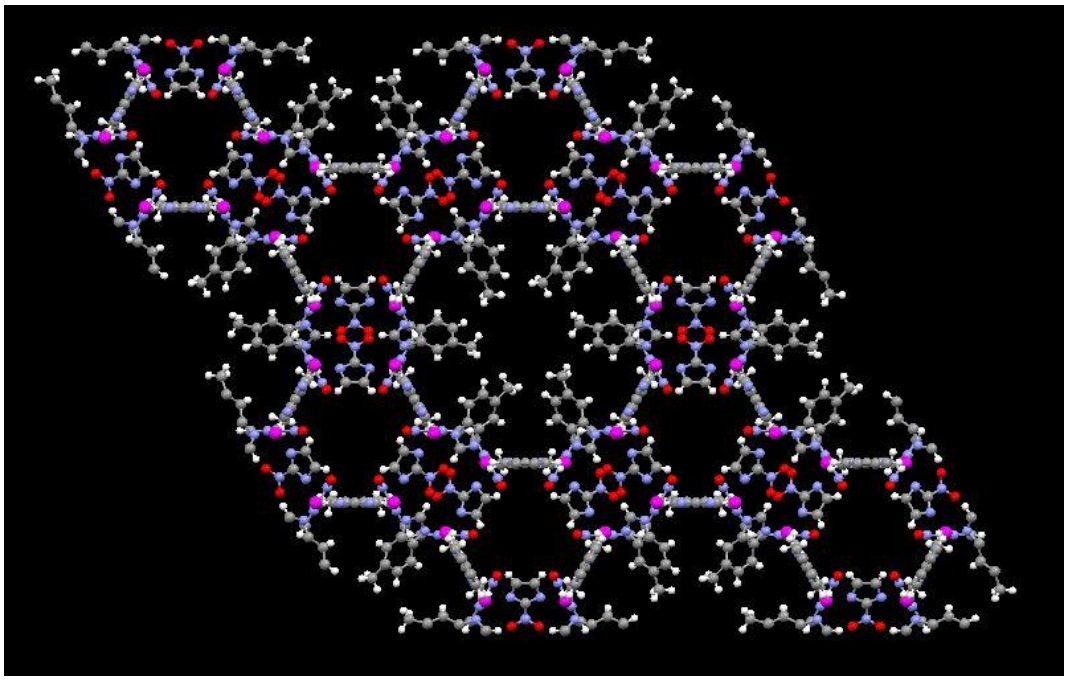

Figure A11: ZIF-79 (c)

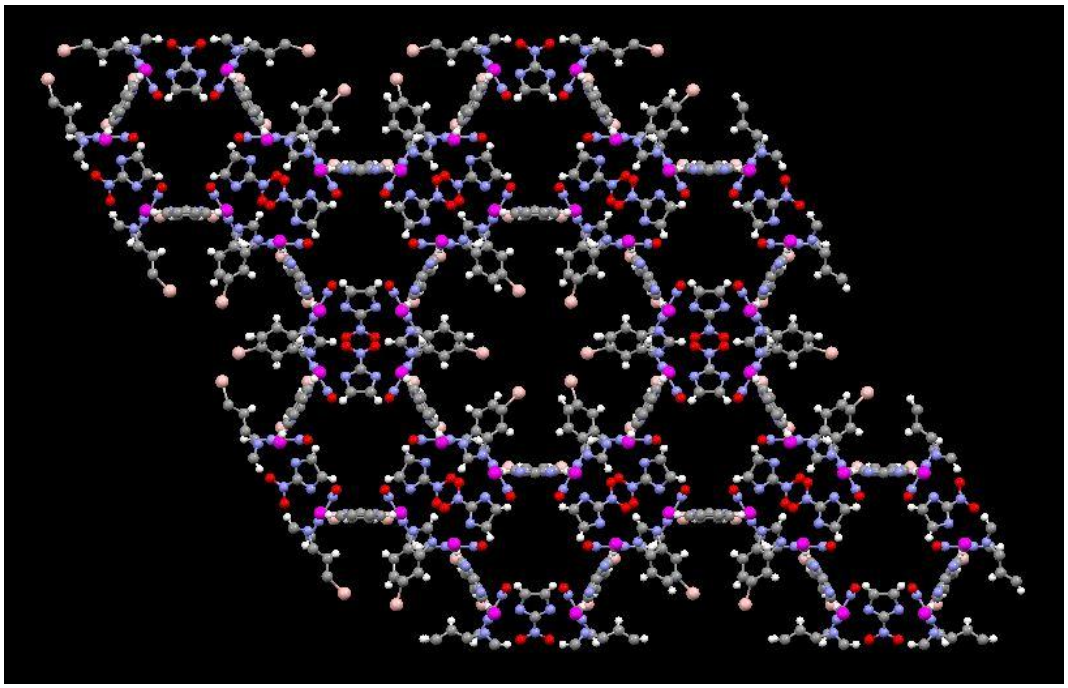

Figure A12: ZIF-81 (c)

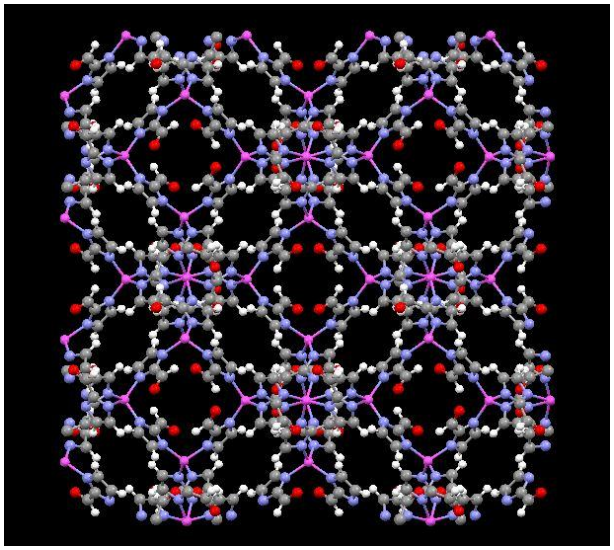

Figure A13: ZIF-90 (a)

Gray: C, white: H, pink: Zn, purple: N, blue: Co, red: O, green: Cl, orange: Br. (a), (b), (c) notations in the captions describe the view directions.

Appendix-B: Single Component and Mixture Self Diffusivities of Gases in ZIFs

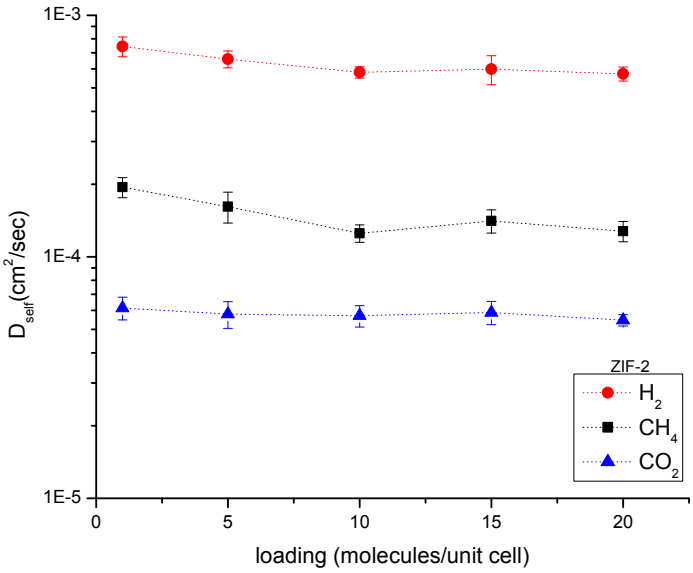

Figure B1: Single component self diffusivity of H_2, CH_4, and CO_2 in ZIF-2.

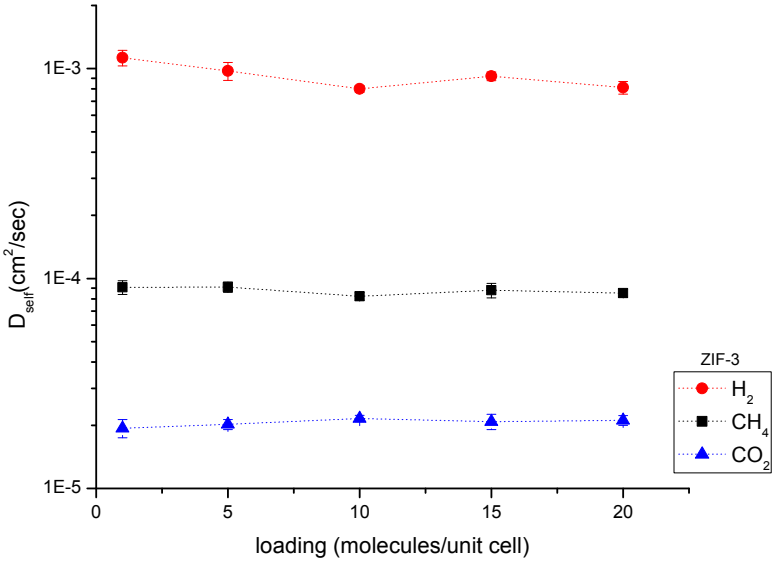

Figure B2: Single component self diffusivity of H_2, CH_4, and CO_2 in ZIF-3.

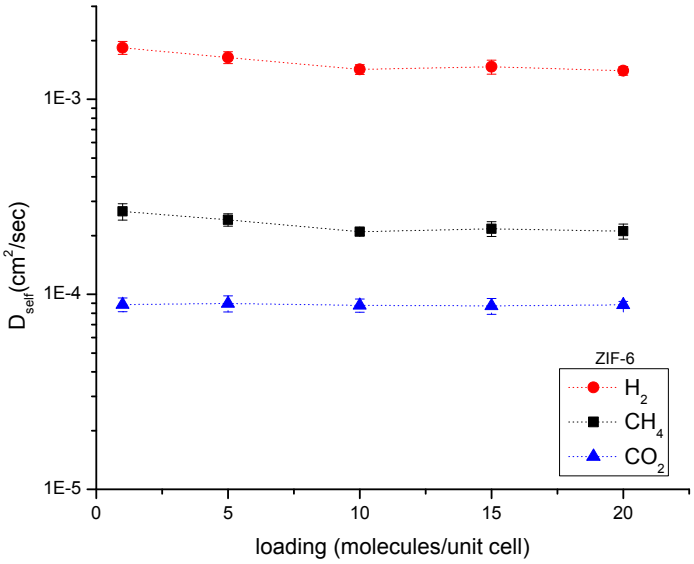

Figure B3: Single component self diffusivity of H_2, CH_4, and CO_2 in ZIF-6.

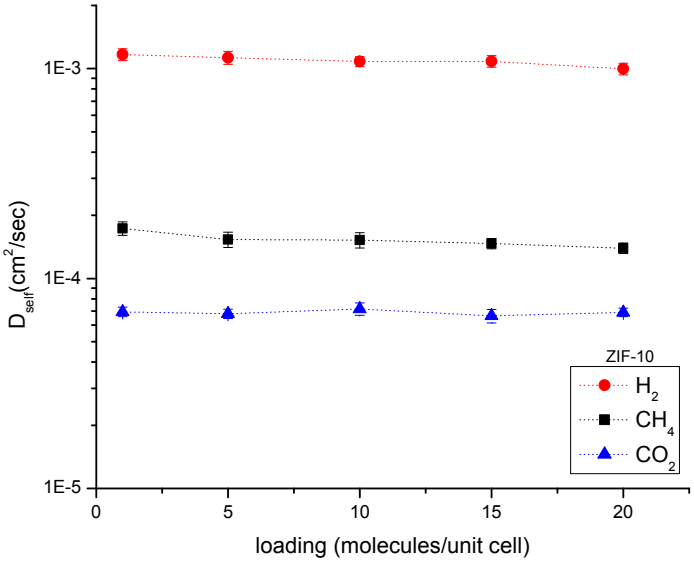

Figure B4: Single component self diffusivity of H_2, CH_4, and CO_2 in ZIF-10.

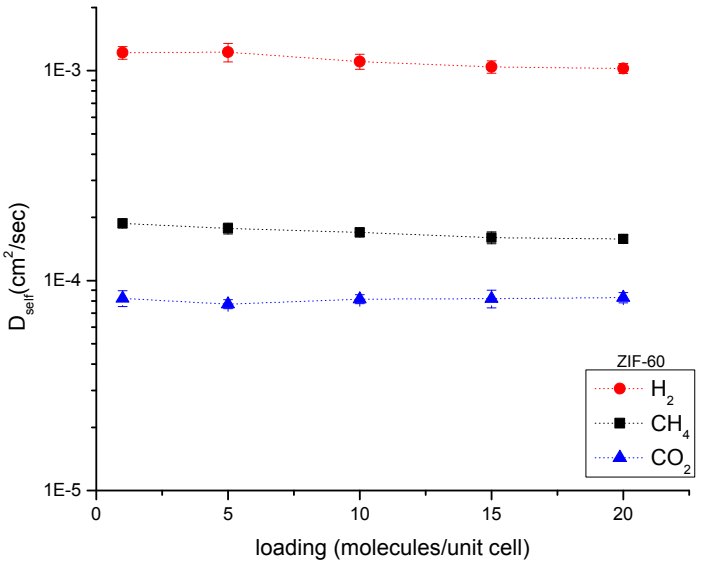

Figure B5: Single component self diffusivity of H_2, CH_4, and CO_2 in ZIF-60.

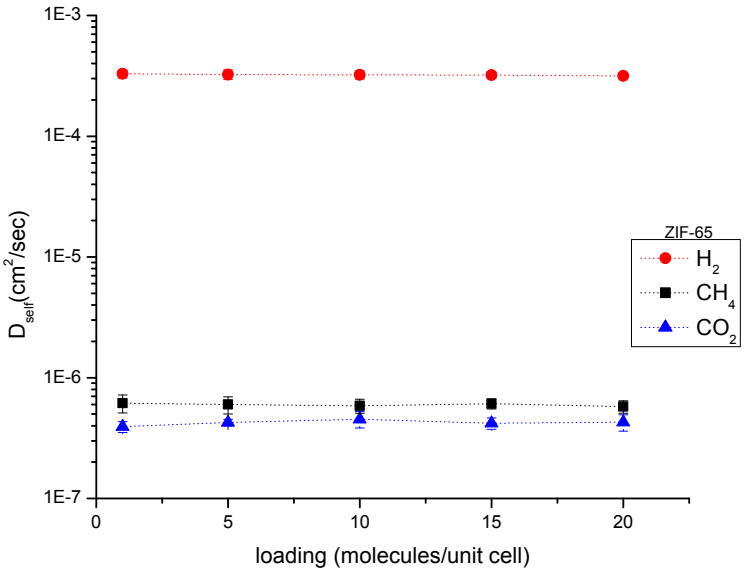

Figure B6: Single component self diffusivity of H_2, CH_4, and CO_2 in ZIF-65.

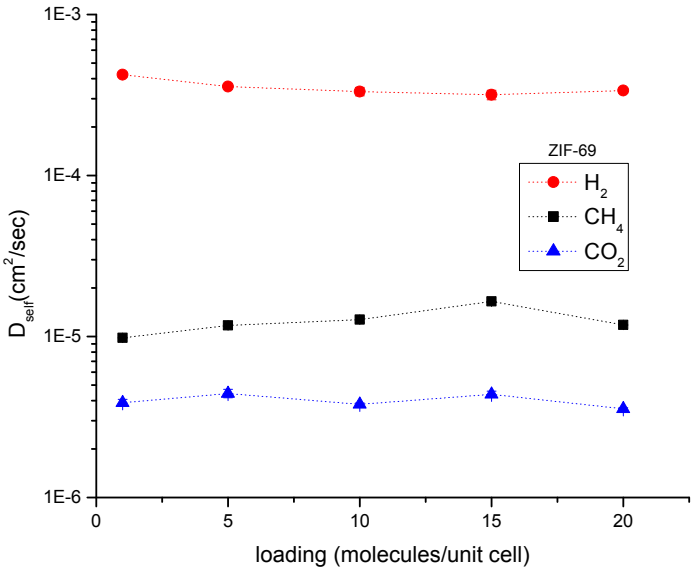

Figure B7: Single component self diffusivity of H_2, CH_4, and CO_2 in ZIF-69.

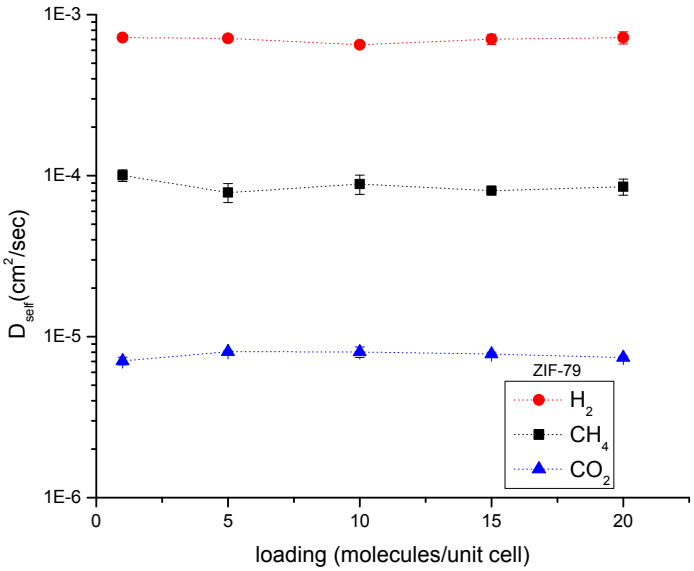

Figure B8: Single component self diffusivity of H_2, CH_4, and CO_2 in ZIF-79.

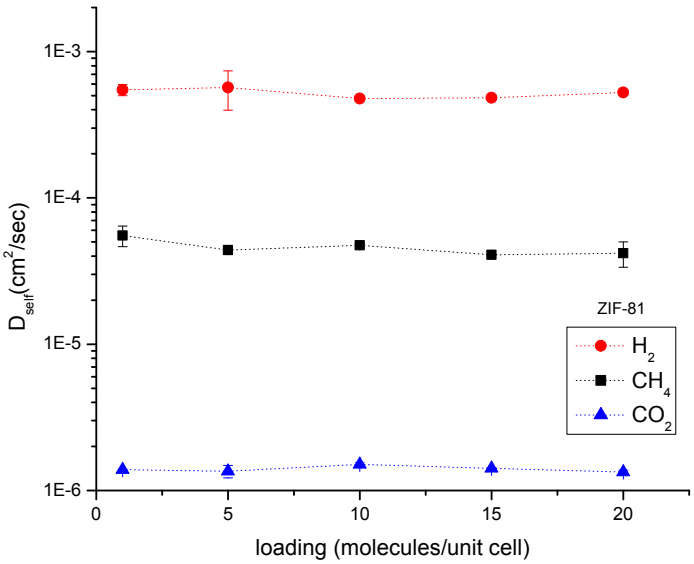

Figure B9: Single component self diffusivity of H_2, CH_4, and CO_2 in ZIF-81.

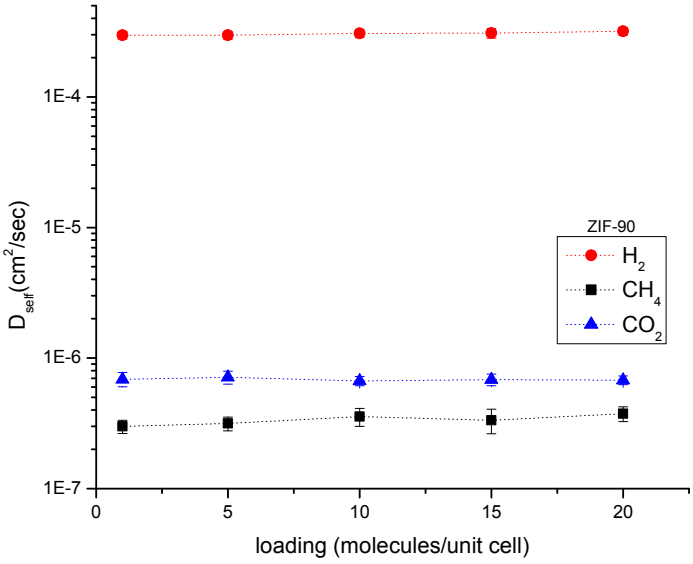

Figure B10: Single component self diffusivity of H_2, CH_4, and CO_2 in ZIF-90.

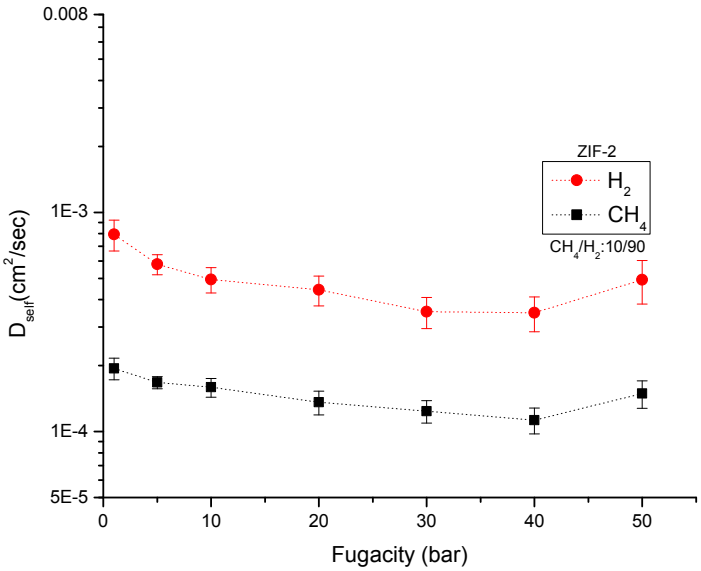

Figure B11: Mixture self diffusivities of H_2 and CH_4 in ZIF-2.

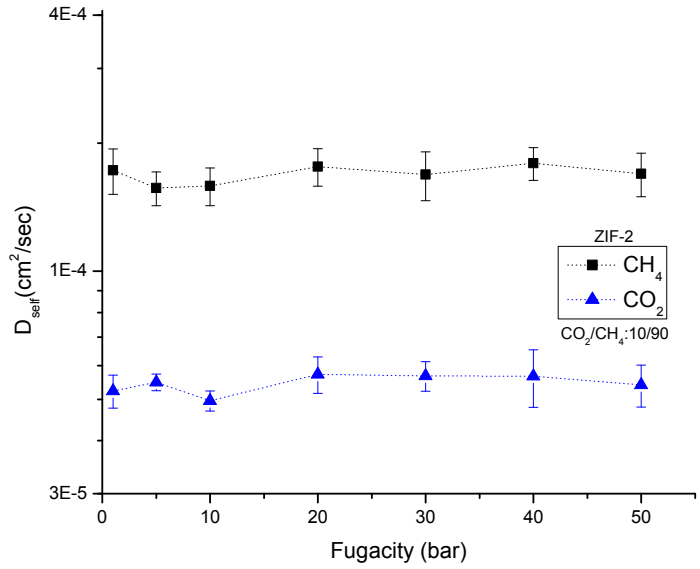

Figure B12: Mixture self diffusivities of CO_2 and CH_4 in ZIF-2.

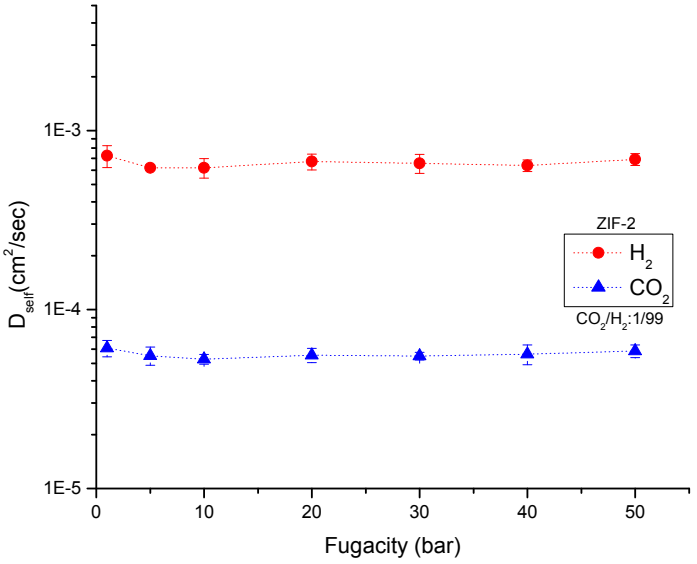

Figure B13: Mixture self diffusivities of CO_2 and H_2 in ZIF-2.

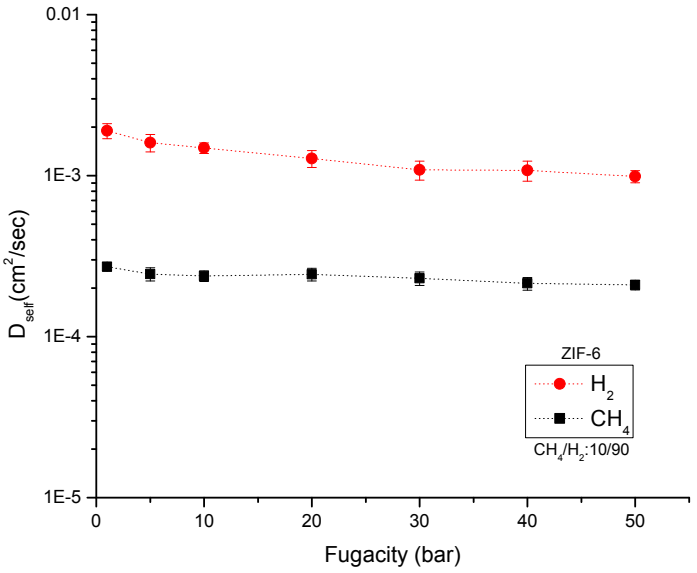

Figure B14: Mixture self diffusivities of CH_4 and H_2 in ZIF-6.

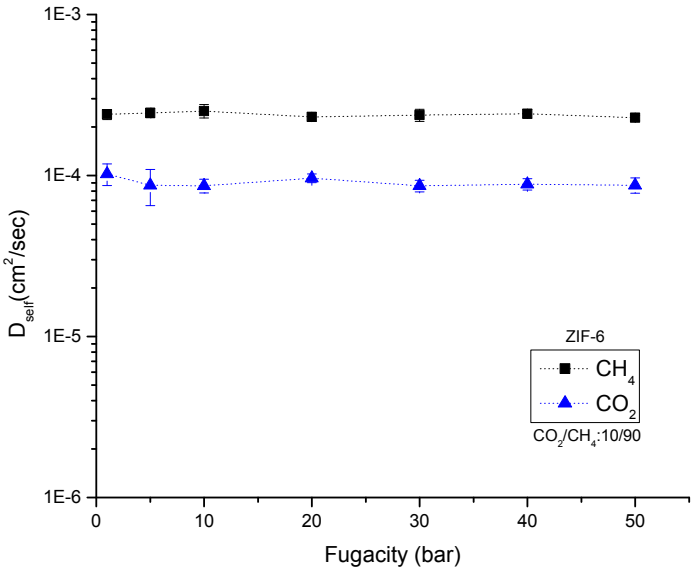

Figure B15: Mixture self diffusivities of CH_4 and CO_2 in ZIF-6.

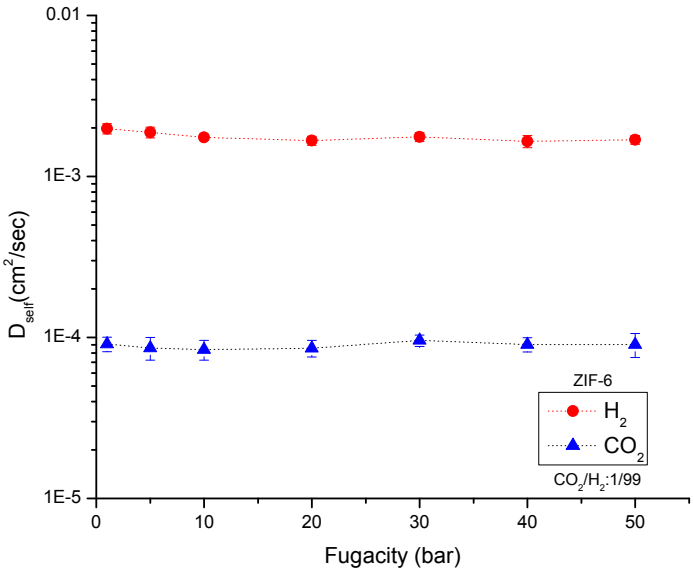

Figure B16: Mixture self diffusivities of CO_2 and H_2 in ZIF-6.

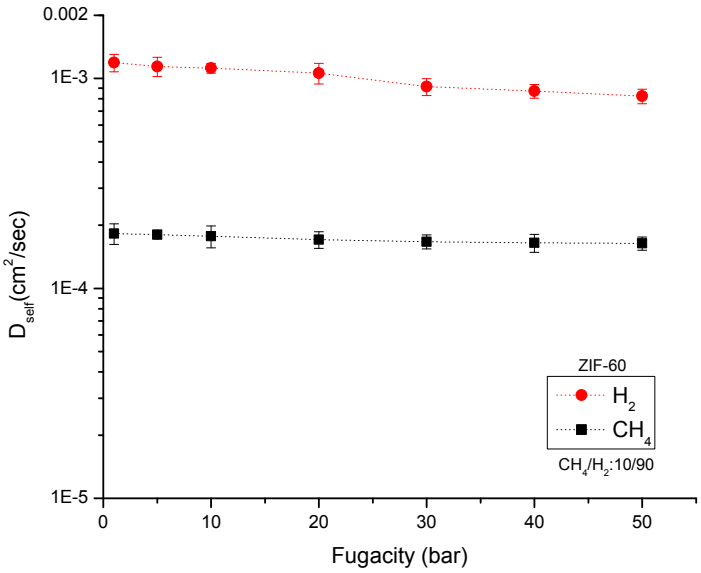

Figure B17: Mixture self diffusivities of CH_4 and H_2 in ZIF-60.

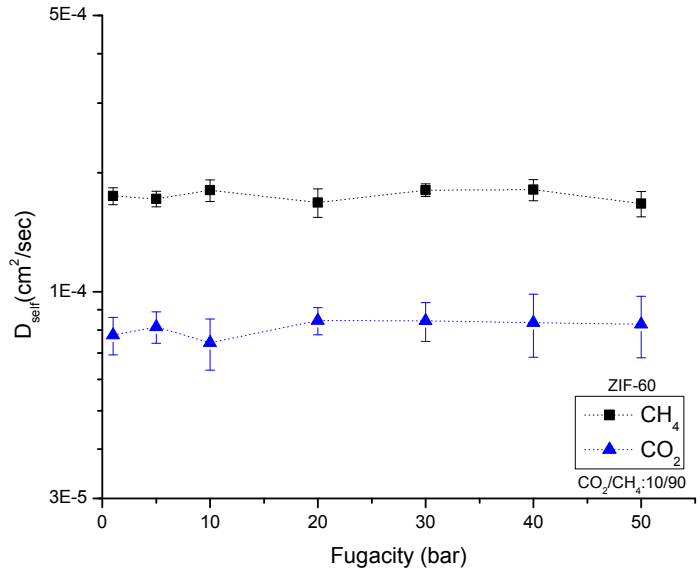

Figure B18: Mixture self diffusivities of CH_4 and CO_2 in ZIF-60.

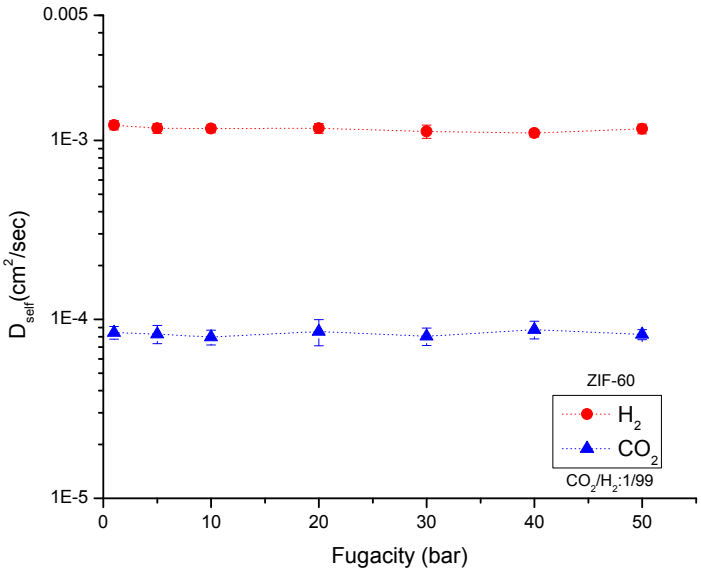

Figure B19: Mixture self diffusivities of CO_2 and H_2 in ZIF-60.

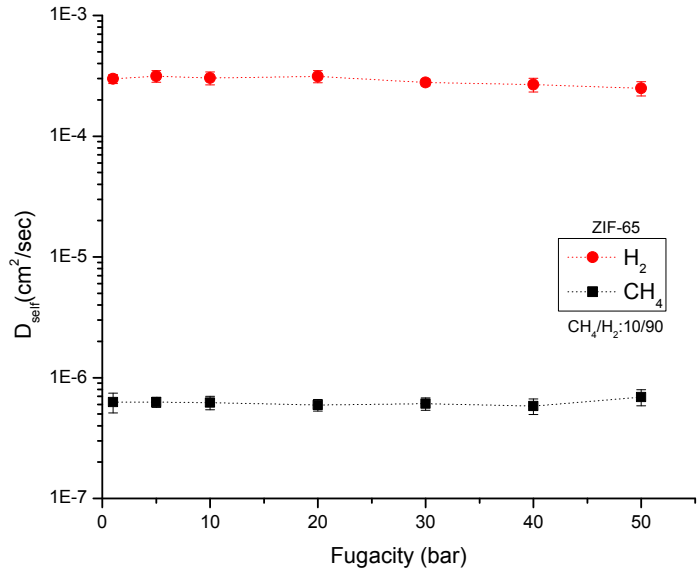

Figure B20: Mixture self diffusivities of CH_4 and H_2 in ZIF-65.

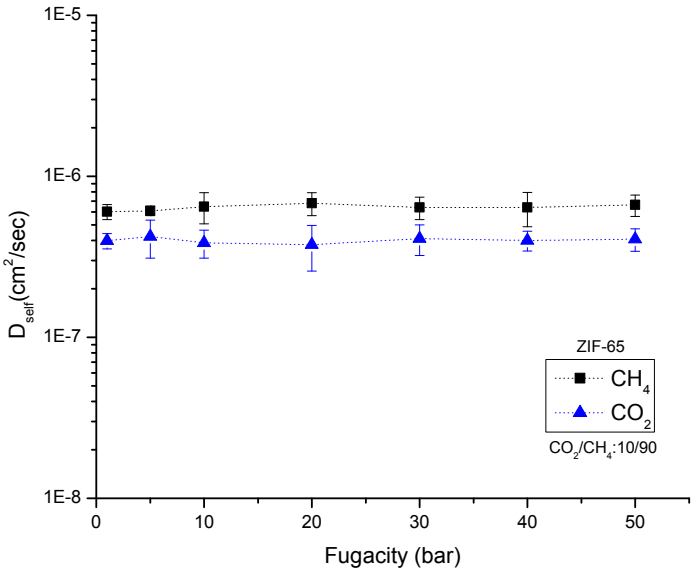

Figure B21: Mixture self diffusivities of CH_4 and CO_2 in ZIF-65.

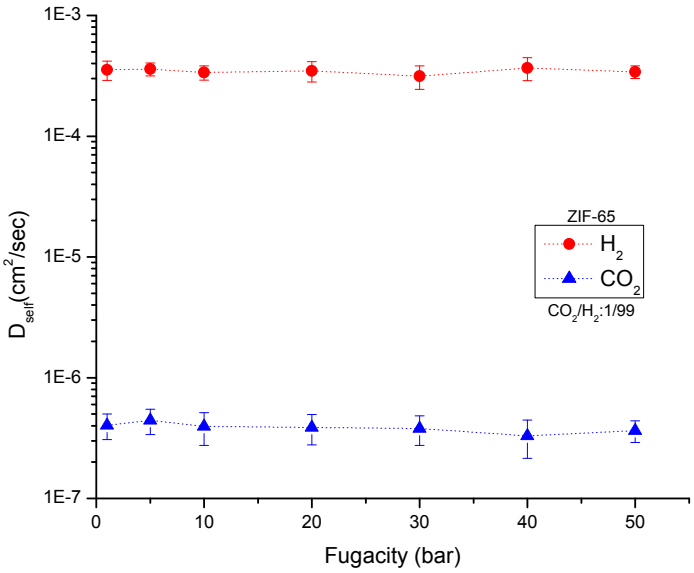

Figure B22: Mixture self diffusivities of CO_2 and H_2 in ZIF-65.

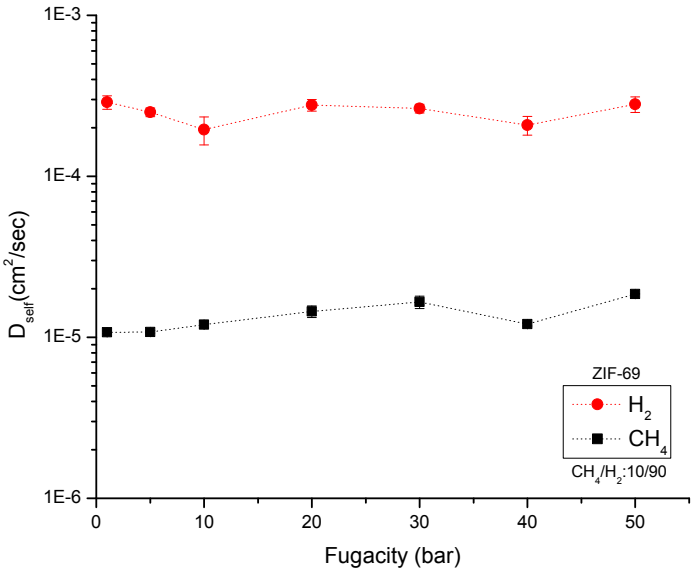

Figure B23: Mixture self diffusivities of CH_4 and H_2 in ZIF-69.

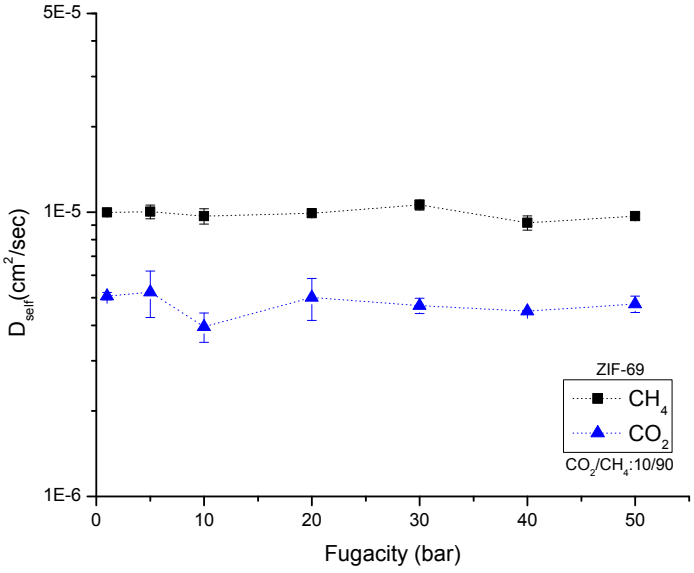

Figure B24: Mixture self diffusivities of CH_4 and CO_2 in ZIF-69.

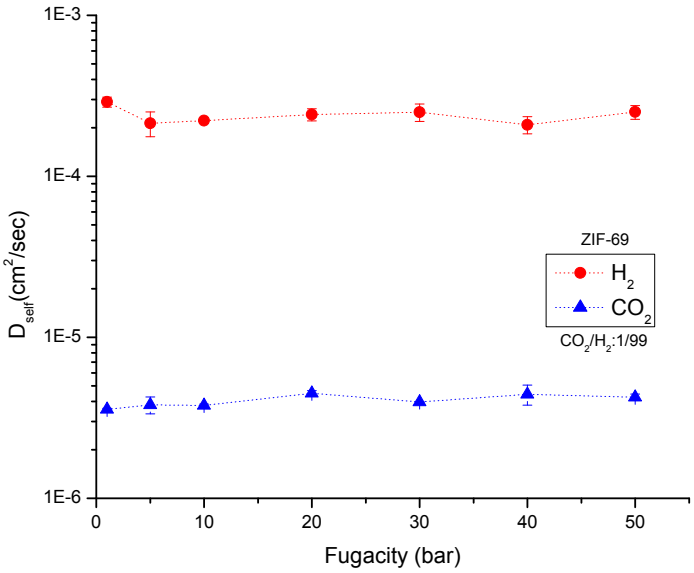

Figure B25: Mixture self diffusivities of CO_2 and H_2 in ZIF-69.

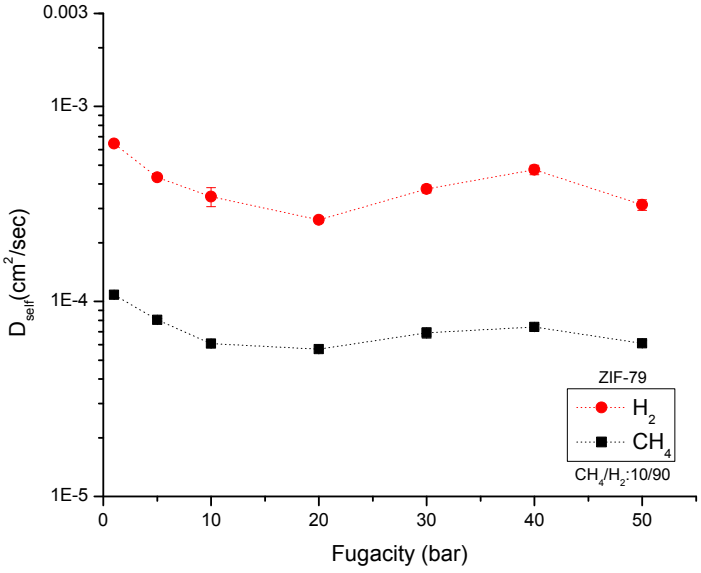

Figure B26: Mixture self diffusivities of CH_4 and H_2 in ZIF-79.

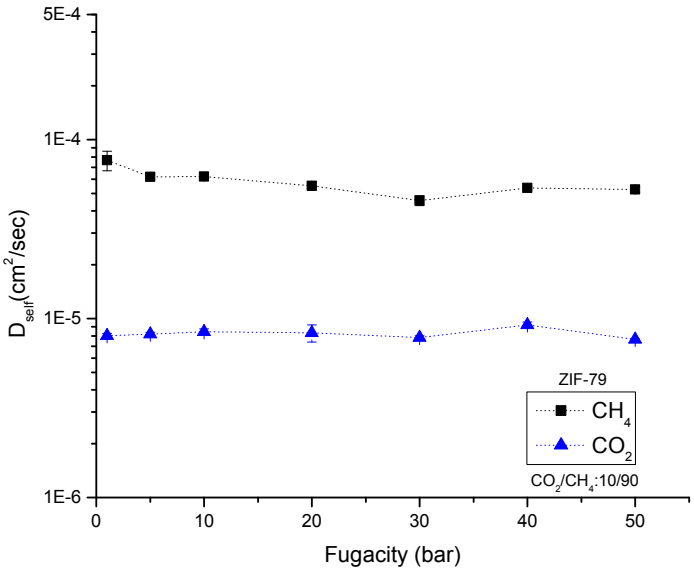

Figure B27: Mixture self diffusivities of CH_4 and CO_2 in ZIF-79.

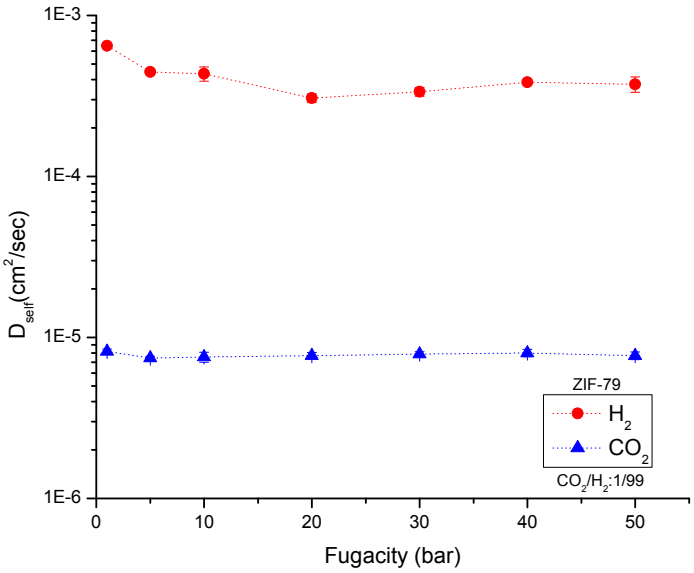

Figure B28: Mixture self diffusivities of CO_2 and H_2 in ZIF-79.

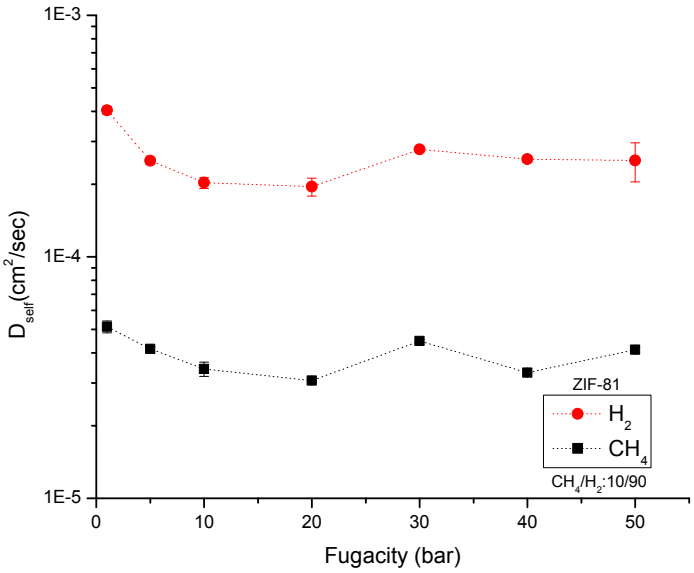

Figure B29: Mixture self diffusivities of CH_4 and H_2 in ZIF-81.

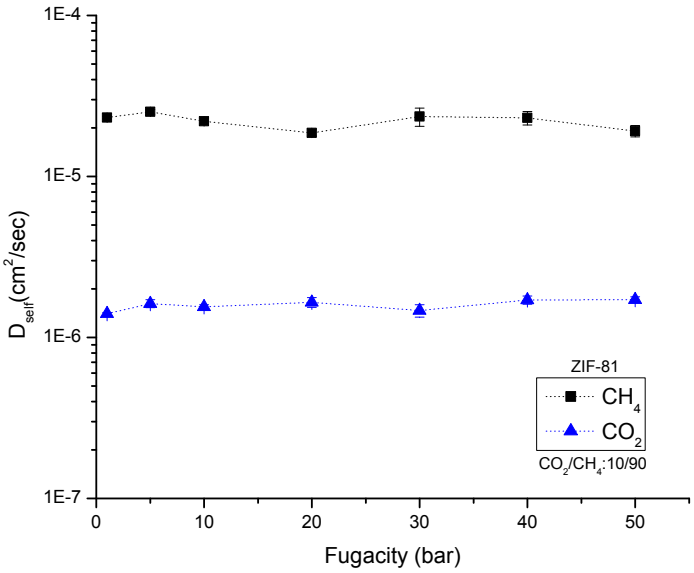

Figure B30: Mixture self diffusivities of CO_2 and CH_4 in ZIF-81.

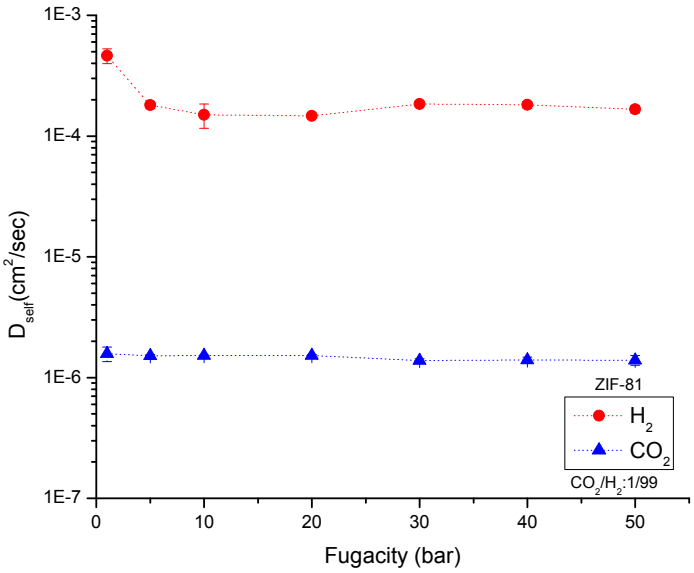

Figure B31: Mixture self diffusivities of CO_2 and H_2 in ZIF-81.

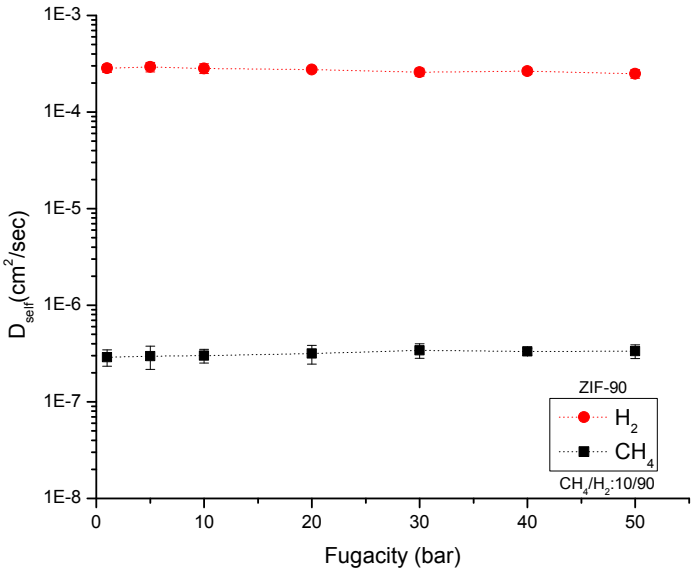

Figure B32: Mixture self diffusivities of CH_4 and H_2 in ZIF-90.

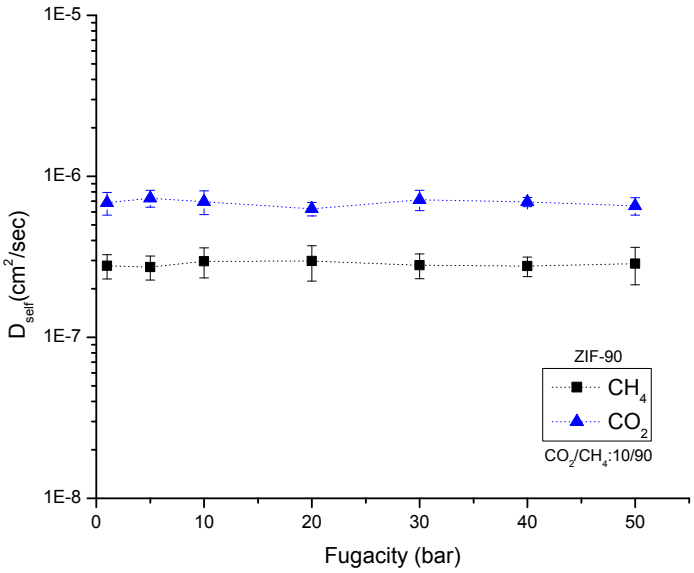

Figure B33: Mixture self diffusivities of CH_4 and CO_2 in ZIF-90.

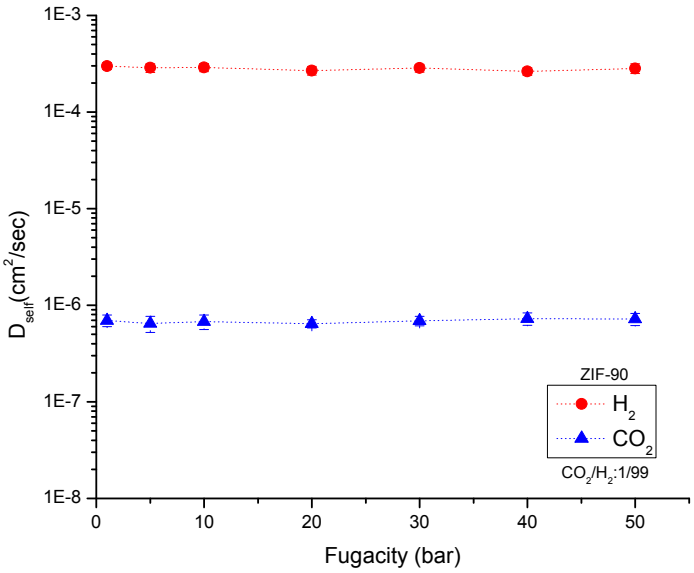

Figure B34: Mixture self diffusivities of CO_2 and H_2 in ZIF-90.

Appendix-C: Adsorption Selectivity, Diffusion Selectivity and Permeation Selectivity of CH_4/H_2, CO_2/CH_4 and CO_2/H_2 Mixtures in ZIFs

Table C1: Adsorption-based, diffusion-based and permeation-based selectivities of ZIFs at 10 bar and 298 K for CH_4/H_2:10/90 mixtures.

Material	S_{ads} (CH_4/H_2)	D_{self} CH_4	D_{self} H_2	S_{diff} (CH_4/H_2)	$S_{permeation}$ (CH_4/H_2)
ZIF-2	33.01	1.59E-04	4.94E-04	0.32	10.63
ZIF-79	52.17	6.07E-05	3.45E-04	0.18	9.19
ZIF-81	40.09	3.43E-05	2.03E-04	0.17	6.78
ZIF-3	29.06	8.77E-05	8.49E-04	0.10	3.00
ZIF-69	39.23	1.20E-05	1.95E-04	0.06	2.41
ZIF-6	13.69	2.38E-04	1.49E-03	0.16	2.19
ZIF-60	10.93	1.77E-04	1.12E-03	0.16	1.73
ZIF-10	11.05	1.57E-04	1.05E-03	0.15	1.64
ZIF-65	14.46	6.22E-07	3.03E-04	0.002	0.03
ZIF-90	15.16	3.00E-07	2.83E-04	0.001	0.02

Table C2: Adsorption-based, diffusion-based and permeation-based selectivities of ZIFs at 10 bar and 298 K for CO_2/CH_4:10/90 mixtures.

Material	S_{ads} (CO_2/CH_4)	D_{self} CO_2	D_{self} CH_4	S_{diff} (CO_2/CH_4)	$S_{permeation}$ (CO_2/CH_4)
ZIF-90	9.53	6.95E-07	2.97E-07	2.34	22.31
ZIF-65	7.67	3.86E-07	6.49E-07	0.60	4.56
ZIF-69	6.64	3.95E-06	9.68E-06	0.41	2.71
ZIF-3	4.73	2.96E-05	5.68E-05	0.52	2.47
ZIF-2	5.22	4.96E-05	1.59E-04	0.31	1.63
ZIF-10	2.86	6.13E-05	1.22E-04	0.50	1.43
ZIF-60	3.32	7.43E-05	1.81E-04	0.41	1.37
ZIF-6	2.87	8.63E-05	2.52E-04	0.34	0.98
ZIF-79	4.62	8.44E-06	6.21E-05	0.14	0.63
ZIF-81	6.73	1.55E-06	2.20E-05	0.07	0.47

Table C3: Adsorption-based, diffusion-based and permeation-based selectivities at 10 bar and 298 K for CO_2/H_2:1/99 mixtures.

Material	**S_{ads} (CO_2/H_2)**	**D_{self} CO_2**	**D_{self} H_2**	**S_{diff} (CO_2/H_2)**	**$S_{permeation}$ (CO_2/H_2)**
ZIF-2	160.87	5.28E-05	6.20E-04	0.09	13.71
ZIF-3	176.43	2.04E-05	8.36E-04	0.02	4.30
ZIF-69	240.07	3.78E-06	2.22E-04	0.02	4.09
ZIF-79	195.94	7.56E-06	4.34E-04	0.02	3.41
ZIF-67	43.48	5.25E-06	8.82E-05	0.06	2.59
ZIF-81	235.91	1.53E-06	1.50E-04	0.01	2.40
ZIF-60	31.21	7.95E-05	1.16E-03	0.07	2.13
ZIF-10	27.55	7.11E-05	1.15E-03	0.06	1.70
ZIF-6	34.68	8.42E-05	1.75E-03	0.05	1.67
ZIF-8	34.89	4.41E-06	1.11E-04	0.04	1.39
ZIF-90	137.44	6.77E-07	2.90E-04	0.002	0.32
ZIF-65	102.08	3.95E-07	3.37E-04	0.001	0.12

Appendix-D: Single Component and Mixture Self Diffusivities of H_2 and CO_2 in ZIF-90 and ZIF-65

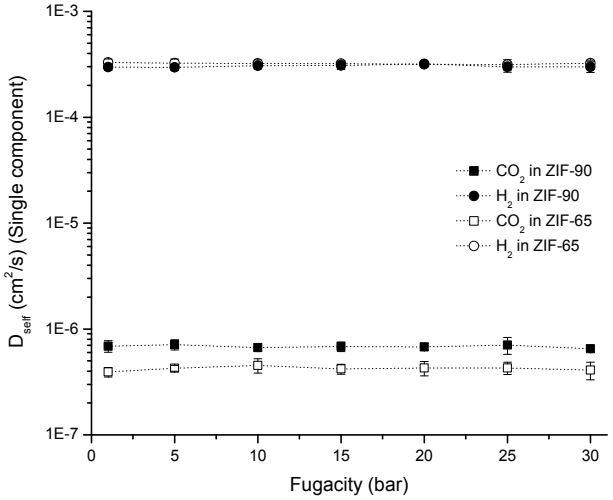

Figure D1: Single component self diffusivities of H_2 and CO_2 in ZIF-65 and ZIF-90 at 25°C.

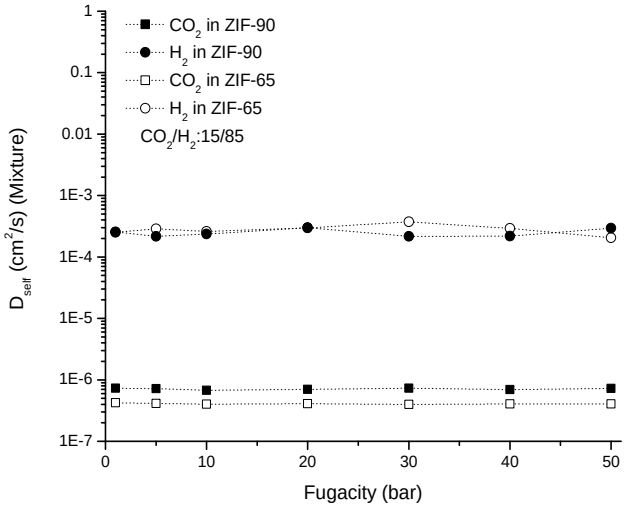

Figure D2: Self diffusivities of H_2 and CO_2 in a binary mixture in ZIF-65 and ZIF-90 at 25°C.

Appendix-E: Partial charges of ZIF-90 and ZIF-65 structures

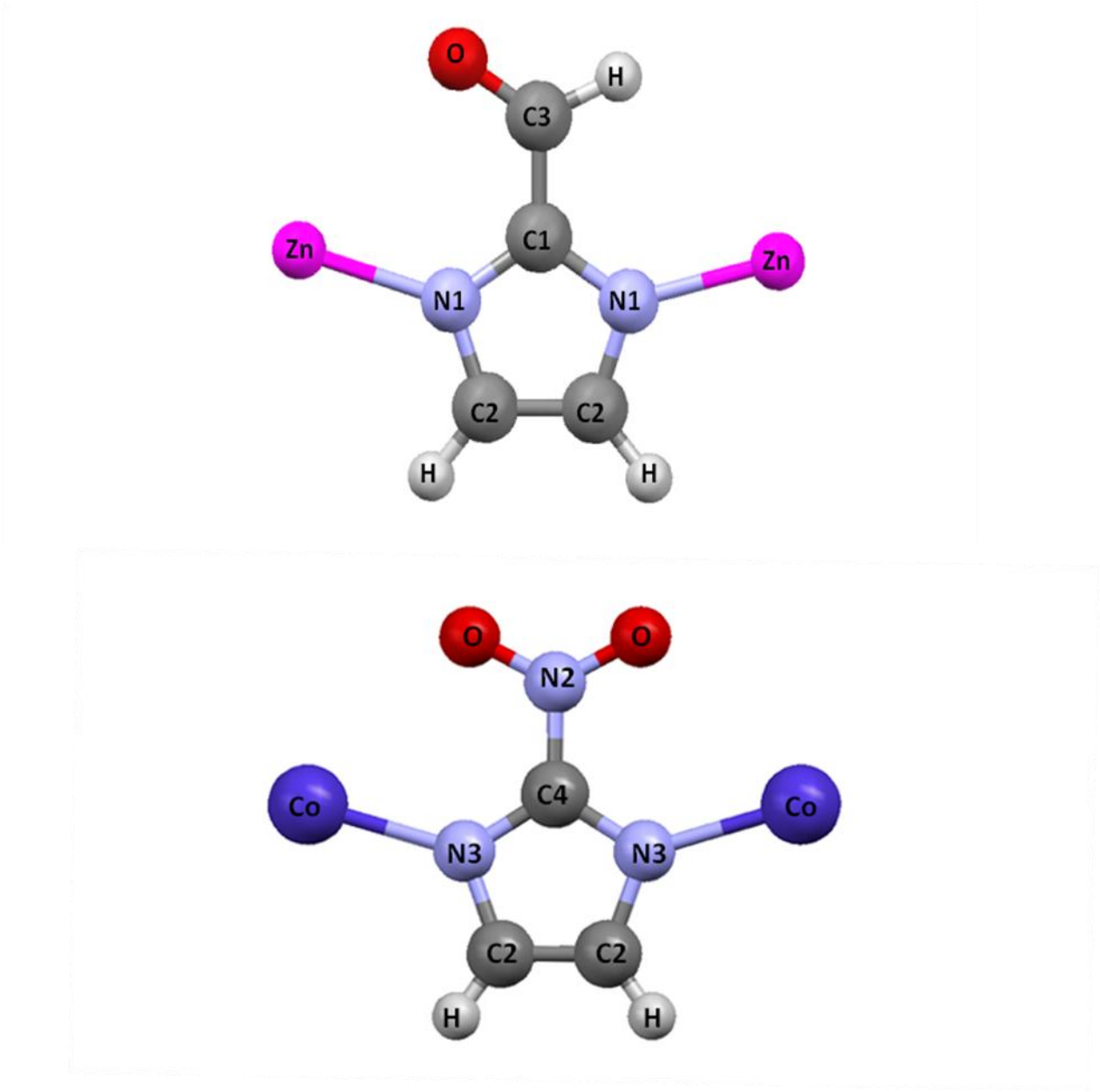

Figure E1: Atomic representations of ZIF-90 (top) and ZIF-65 (bottom).

Table E1: Partial charges of ZIF-65 and ZIF-90 structures.

Atoms	q(e)
C1	0.523
C2	-0.103
C3	0.069
C4	0.293
O1	-0.358
O2	-0.500
N1	-0.343
N2	0.733
N3	-0.440
Zn	0.590
Co	1.636
H	0.121

VITA

Erhan Atcı was born in Amasya, Turkey in 1987. After high school education in Denizli Mehmet Akif Ersoy Lisesi (Denizli Mehmet Akif Ersoy High School), he received the B.Sc. degree in chemical engineering from İzmir Institute of Technology, İzmir, Turkey in June 2010. He received M.Sc. degree in chemical and biological engineering from Koç University, İstanbul, Turkey in July 2012. He will start Ph.D. study at Georgia Institute of Technology on August 2012. His current research interests are gas adsorption and diffusion in zeolite-like nanoporous materials.